University of Genoa

School of Mathematical, Physical and Natural Sciences

Physics and Nanoscience Doctorate

XXXIV Cycle

Assessment of toxicity of particulate matter in the sub-micrometric range by an Atmospheric Simulation Chamber

Scientific – disciplinary sector: FIS/07

Candidate: **Virginia VERNOCCHI**

Supervisors: Prof. Paolo Prati (University of Genoa)

Dott. Dario Massabò (University of Genoa)

PhD scholarships granted by Regione Liguria – "Alta Formazione" projects, Programma Operativo Regione Liguria FSE 2014-2020, ASSE 3 "Education and training" - PhD Course in Physics and Nanoscience - Project "Environmental and health effects of nanoparticles and bio-aerosol dispersed in the atmosphere" - ARGE17-992/3/2

Contents

Introduction

Atmospheric pollution is a current argument of debate. Among pollutants, atmospheric aerosols (or Particulate Matter, PM) play an important role in human health and global climate changes, being a central topic in atmospheric physics and chemistry. PM consists of solid and liquid particles suspended in the atmosphere, with high variability in size, composition, concentration, shape, life-time and sources (Maynard and Howard, 1999; Seinfeld, 1986; Singh, 1995). Aerosols impact on climate and environment by modifying the radiative forcing of Earth – atmosphere system and altering structure and functions of ecosystems (Houghton et al., 2001; Pöschl, 2005). PM impact on human health depends on the level of penetration into the human body. Particles can enter not only the respiratory system but also the circulatory, lymphatic and central nervous systems (Bernstein et al., 2004; Brown et al., 2013).

Aerosols properties are typically investigated by field experiments, that means by directly analizying real PM. This type of analysis is representative of real situations but it is affected by difficulties in controlling parameters and distinguishing specific processes. In opposition to field measurements, there are laboratory experiments that allow control of operative conditions but they suffer from limitations in number of reproducible parameter and in duration. The best experimental compromise are experiments performed in Atmospheric Simulation Chambers (ASCs), as they allow to study atmospheric processes under realistic but controlled conditions, for long enough time periods to reproduce realistic environments, without the complication of typical field measurements. My PhD took place in the Laboratory for Environmental Physics at the Physics Department of the University of Genoa, where I performed ASC experiments with the only atmospheric simulation chamber installed in Italy, ChAMBRe (Massabò et al., 2018).

Among PM constituents, carbonaceous compounds cover a substantial fraction. My thesis focuses on soot particles that are carbonaceous particles generated as by-products of incomplete combustion of hydrocarbon fuels (Moore et al., 2014; Nordmann et al., 2013). Soot particles are responsible of negative impacts, both on climate and health (Ackerman et al., 2000; Bond et al., 2013; Ramanathan and Carmichael, 2008; Segersson et al., 2017).

Therefore, it is necessary to investigate their properties and behaviour in the atmosphere in order to fully understand their adverse effects. The employ of a stable source of soot particles is useful to perform experiments concerning them. In this context, soot generators are introduced. They generate particles with controlled and known properties, similar to the real atmospheric ones. During my PhD, the Mini-Inverted Soot Generator "MISG" was used, fuelled with both ethylene and propane and varying the oxygen-fuel ratio.

Soot particles generated with controlled and known properties can mimic the real atmospheric soot particles and can be used to perform experiments in atmospheric simulation chambers. The main objective of this thesis was to develop an experimental setup and a procedure that allow to perform systematic studies on soot particles exposed and maintained in different conditions thus investigating their properties, effects and interactions with the other atmospheric pollutants. Firstly combustion conditions and resulting flame shapes were classified, then a deep characterization of MISG exhaust, in connection to ChAMBRe, was performed in terms of concentration of emitted particles and gases, particle size distribution, composition and optical properties. The comprehensive characterization of the MISG soot particles is an important piece of information to design the subsequent experiments. Well-characterized soot particles could be used to investigate the effects that atmospheric parameters can have on soot particles, and to study the interactions between soot particles and other pollutants. During my PhD work, preliminary studies on the soot oxidative potential and toxicological effects as well on interactions between soot particles and bio-aerosols were performed.

Thesis Layout

In ***Chapter 1***, the main characteristics of atmospheric aerosols are described, in conjunction with their effects on climate, environment and health. Details about the carbonaceous fraction of aerosol are reported, focusing on soot particles. Overviews on bio-aerosol, oxidative potential and toxicological assays are given. ***Chapter 2*** describes experimental setup and procedures. The atmospheric simulation chamber and its instrumentation, soot generator and offline instruments are detailed. In ***Chapter 3***, the characterization of soot particles is given, by comparing ethylene and propane combustion exhausts. ***Chapter 4*** shows preliminary applications of characterized soot particles, in particular studies on their interactions with bacteria and on their toxicology.

CHAPTER 1

Atmospheric Aerosols

1.1 Overview

Atmospheric aerosols are a complex system of solid and liquid particles suspended in the atmosphere, usually referred as Particulate Matter (PM). Particles have high variability in size, composition, concentration, shape, life-time and sources (Maynard and Howard, 1999; Seinfeld, 1986; Singh, 1995). Particle size ranges between few nm to tens µm (Seinfeld, 1986). Particulate Matter mainly contains carbonaceous compounds and usually also nitrates, sulphates, mineral dust, heavy metal traces (Cu, Cd, Ni, Pb, Zn), traces of other elements (i.e., Ca, K, Mg, S). Liquid particles usually are considered spherical while solid particles have irregular shapes or they are crystals. There are several aerosol sources that can be distinguished as natural (i.e., fires, dust, volcanic eruption, sea salt, biological materials, etc.) or anthropogenic (i.e., urban and naval traffic emissions, heating systems, industries, etc.). In particular, particles are classified as "primary" or "secondary" depending on their origin. Primary particles are directly emitted in the atmosphere from specific sources. Typical sources are biomass burning, incomplete fossil fuel combustion and anthropic activities. Secondary particles result from gas-to-particle processes (i.e., nucleation and condensation) and are formed in the atmosphere.

Particles suspended in the atmosphere are the result of balance between different and competing processes: emission by sources, transport and deposition (Whitby and Cantrell, 1976). In the troposphere, for dry conditions, aerosols have bimodal distribution: most of the mass is confined in two separate modes or fractions, the *fine* and the *coarse* (Johansson et al., 1995). Formation of particles smaller than 0.1 µm (i.e., ultrafine) generally is by nucleation (i.e., condensation of low vapour-pressure substance or by chemical reactions in the atmosphere to form new particles) and subsequent rapid growth by coagulation (i.e., combination of two or more particles to form a larger particle) or by condensation (i.e., condensation of gas or vapour molecules on the surface of existing particles). Particles do not grow by coagulation or condensation beyond approximately 2 - 3 µm. Particles smaller than 0.1 µm are removed by diffusion. The range 0.1 – 1 µm (i.e., fine) is called "accumulation range" because particles with these sizes tend to accumulate;

their life-time in atmosphere is up to 10 days so they can travel long distances. For wet conditions, particles in that range are removed being incorporated into clouds. When clouds incorporate acidic aerosols, acidic fog and acid rain can occur (Johansson et al., 1995). Formation of particles larger than 2 µm (i.e., coarse) is mechanical, by breaking-up larger solid particles. This fraction includes wind-blown dust, road-dust re-suspended by traffic, sea spray particles, pollens and spores. The removal of coarse fraction is usually by settling and the life-time is of the order of hours.

1.1.1 PM classification

Since aerodynamic properties determine particle life-time in the air, particles can be classified by their aerodynamic diameter (D_ae). D_ae is the size of a unit-density sphere with the same aerodynamic characteristics of the particle under study (Marple and Willeke, 1976). This parameter is used as size to describe particles and sampling, both in scientific and law fields (Nemmar et al., 2002; Oberdörster et al., 2005). Formally, three classes of PM are distinguished:

PM10: mass concentration of particles with D_ae < 10 µm,

PM2.5: mass concentration of particles with D_ae < 2.5 µm,

PM1: mass concentration of particles with D_ae < 1 µm.

The totality of solid matter observed in the atmosphere is referred as total suspended particulate (TSP). PM fractions and their mass distribution are depicted in Fig. 1.1.

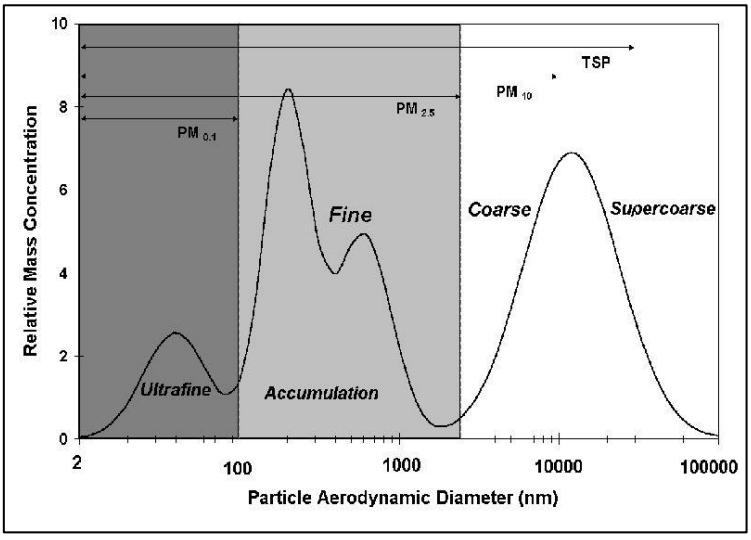

Figure 1.1: Typical mass distribution of PM in function of D_ae. Also shown the most used definitions of aerosol fractions (Slezakova et al., 2013).

Properties and effects of PM10 and PM2.5 are relatively well known: limits on the levels of PM10 and PM2.5 are set to preserve the air quality (concentration limits set by legislation in accordance with the European Directive 2008/50/EC) but aerosol grains with aerodynamic smaller diameter are still little studied. While health and environmental risk dues to the diffusion of fine PM is growing, specific monitoring techniques are still missing and the scientific understanding of phenomena and effects is therefore scarce. Sub-micrometric particles have a high surface/volume ratio and consequently they are very reactive: studies to understand how they interact with other pollutants and atmosphere's compounds (i.e., NO_x and O_3) are definitively needed.
My PhD work focuses on PM1 or on the fine fraction.

1.2 Carbonaceous Aerosol

Carbonaceous compounds often are the main fraction of PM and exhibit a wide range of molecular structures. Since they cover up to 50 % of atmospheric aerosol mass in urban areas, they strongly influence physicochemical, biological, climate and health related properties, and effects of atmospheric aerosols (Finlayson-Pitts and Pitts, 2000; Gelencsér, 2004; Henning et al., 2005; Kanakidou et al., 2005; Kulmala et al., 2004; Seinfeld et al., 1998).
Total Carbon (TC) of PM is defined as the sum of all the carbon contained in aerosol particles, with the exception of carbonates (Pöschl, 2005). TC is conventionally divided into two main fractions: Elemental or Black Carbon (EC or BC) and Organic Carbon (OC). These are operative definitions, depending on the analytical techniques used to determine them. When investigated by optical techniques, the inorganic fraction is generally referred as Black Carbon, BC (Petzold et al., 2013), while the result of thermal-optical characterizations is referred as Elemental Carbon, EC (Bond and Bergstrom, 2006). However, both BC and EC are operative terms that do not identify the same compounds (Massabò and Prati, 2021) and often produce non-negligible differences in concentration values. However, as first approximation, EC and BC are often assumed as equivalent.
Determination of carbonaceous compounds is usually performed by optical and/or thermal-optical methods, due to their different properties. By the optical point of view, EC is the most absorptive aerosol in the IR-VIS and near-UV range (Pöschl, 2003); OC is

assumed to have a neutral optical behaviour. By the thermal point of view (i.e., refractoriness), EC degradation and volatilization requires temperature higher than 550°C and oxidative atmosphere, it is the graphitic and refractory fraction of TC. OC decomposes and volatilizes in a temperature range of 200 – 350 °C, with both inert and oxidative atmosphere (Huntzicker et al., 1982). However, there is a continuous decrease of thermo-chemical refractoriness and specific optical absorption going from graphite-like structures to non-refractive and colourless organic compounds, respectively (Pöschl, 2003), as shown in Fig. 1.2. An additional fraction with intermediate properties has been defined as Brown Carbon (BrC). BrC is an organic fraction that resists in inert atmosphere up to 400 – 450 °C and it also absorbs IR-VIS radiation. Peculiarity of Brown Carbon is the dependence of light absorption on wavelength: absorption increases when λ decreases, thus it is more relevant in the blue-UV range (λ < 550 nm) and lends to a yellow/brown colouration from which the name Brown Carbon. Absorption of BC is predominant for λ > 550 nm (Andreae and Gelencsér, 2006).

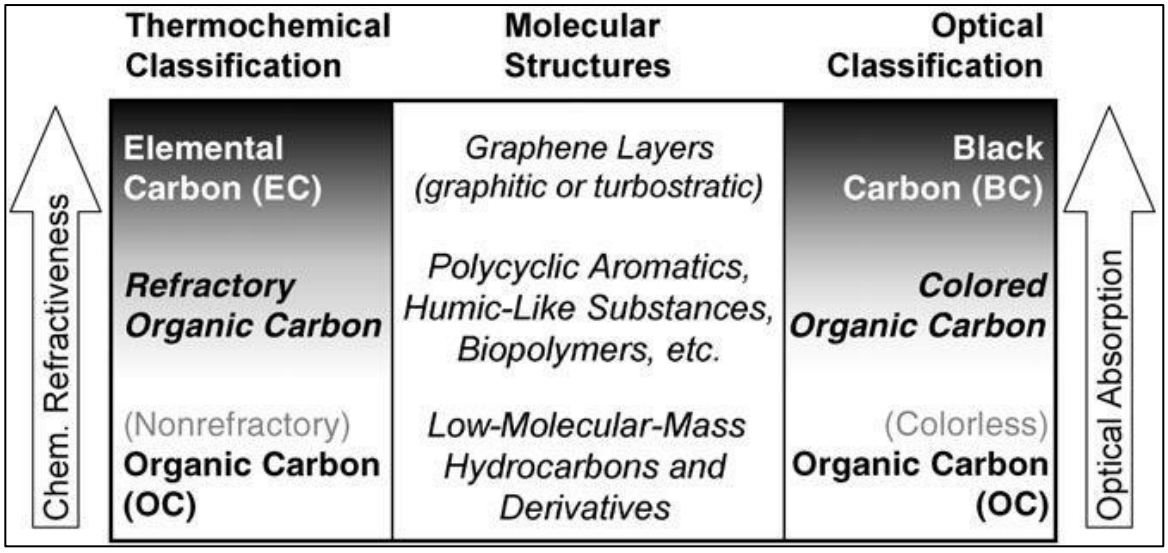

Figure 1.2: Thermal and optical classification of EC/OC and BC/OC (Pöschl, 2003).

EC/BC is produced by fuel-lean combustion or by hydrocarbon pyrolysis; BrC is generated by biomass (i.e., biodegradable fraction of biological products) burning (Kirchstetter et al., 2004; Pöschl, 2003); OC results from sources similar to EC/BC and BrC as biomass burning and traffic, but also from secondary production (Saarikoski et al., 2008), and biogenic emission (Favez et al., 2010).

1.2.1 Focus on soot particles

My thesis investigated properties of soot particles. Soot particles are carbonaceous particles generated as by-products of incomplete combustion or pyrolysis of hydrocarbon fuels and more generally of fossil fuels and/or biomass burning (Moore et al., 2014; Nordmann et al., 2013), the terms also indicates particles emitted from a flame and into the exhaust stream or outlet from a reactor (Michelsen et al., 2020).

There are still significant lacks in knowledge on soot particles formation and their evolution during combustion (DOE, 2006) due to a shortage in measurement techniques and computational limitations in simulation models (Michelsen, 2017). Anyway, some basic and fundamental steps in soot formation can be identified (Fig. 1.3). Firstly, a gas phase chemistry occurs and soot precursor species (i.e., the molecular building blocks of soot particles) are formed by the reaction of fuel and air (i.e., O_2). Soot precursors are molecular gas-phase species; they can be ions, radicals (i.e., OH, O, CH, CH_2), polycyclic aromatic hydrocarbon (PAH) and oxygenated hydrocarbons (Bockhorn, 1994; Calcote, 1981; Frenklach, 2002; Homann, 1998; McEnally et al., 2006; Richter and Howard, 2000; Wang, 2011). Precursors activity (i.e., they nucleate, react and combine, or grow) generates incipient soot particles by a gas-to-condensed-phase conversion, termed soot inception (Michelsen et al., 2020). Incipient soot particles grow by coagulation and then agglomerate in more or less ordered structures, depending on the air:fuel combustion ratio. Growing particles undergo dehydrogenation, through a high-temperature carbonization process, and solidify, thus resulting in a graphitic random rotated layers aggregation (Michelsen, 2017). This is the coalescence and agglomeration phase. As consequence of the carbonization process of particles, their optical properties evolve and they become able to absorb and emit light in the visible and near-infrared spectral regions (Michelsen et al., 2020). Loosely bound agglomerates of quasi-spherical primary particles are formed by particle collisions, they eventually become firmly bound, branched-chain aggregates of primary particles (Michelsen et al., 2020). Aggregates become oxidized and particle size decreases during oxidation (Megaridis, 1989; Puri et al., 1993). The oxidation and fragmentation is the last phase.

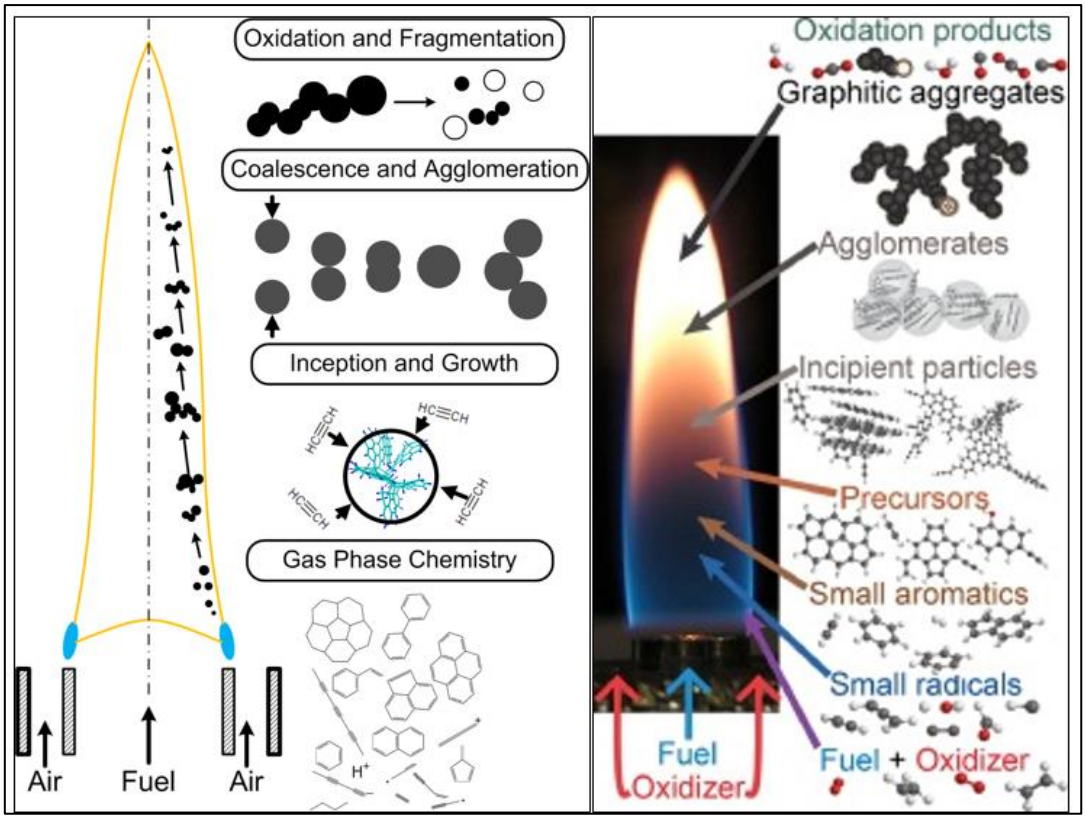

Figure 1.3: Scheme of soot formation (Michelsen, 2017; Propulsion and Clean Energy Research Group).

Soot particles constitute an important fraction of anthropogenic particulate matter (PM) especially in urban environments (Weijers et al., 2011), and are emitted by traffic, domestic stoves, industrial chimneys and by any incomplete combustion process. Soot highly absorbs in the IR-VIS range and does not volatilize at low temperature (T < 550°C) and in inert atmosphere. This means that soot particles are included in the definition of EC/BC.

The understanding of properties and behaviour of soot particles when they are suspended in the atmosphere is thus necessary to fully assess their adverse effects and the use of proxies with controlled and known properties can be useful.

1.3 Effects on climate and environment

Particulate Matter impacts on climate because it modifies the radiative forcing of Earth – atmosphere system. Radiative forcing is the change in energy fluxes of solar radiation (incoming energy, maximum intensity in the spectral range of visible light) and terrestrial radiation (outgoing energy, maximum intensity in the infrared spectral range) in the

atmosphere; it can be induced by anthropogenic or natural changes in atmospheric composition, Earth surface properties, or solar activity. Variations of atmospheric composition and terrestrial surface properties cause alteration of optical properties (i.e., absorption and scattering of radiation) thus impacting on the radiative forcing. Negative forcings, such as scattering and reflection of solar radiation by aerosols and clouds, tend to cool the Earth's surface; positive forcings, such as the absorption of terrestrial radiation by greenhouse gases and clouds, tend to warm it (Houghton et al., 2001). Absorption and scattering of radiation by aerosol particles are classified as direct effects, while indirect effects are the influence on clouds and precipitation, on trace gas emissions and transformation. Properties relevant for both direct and indirect effects are determined by aerosol particle size, structure, and chemical composition. In addition, effects are strongly influenced by atmospheric processes as coagulation, chemical transformation and different kind of interactions (i.e., water, solar and terrestrial radiation). A schematization of PM effects on the radiative forcing of Earth – atmosphere system is given in Fig. 1.4.

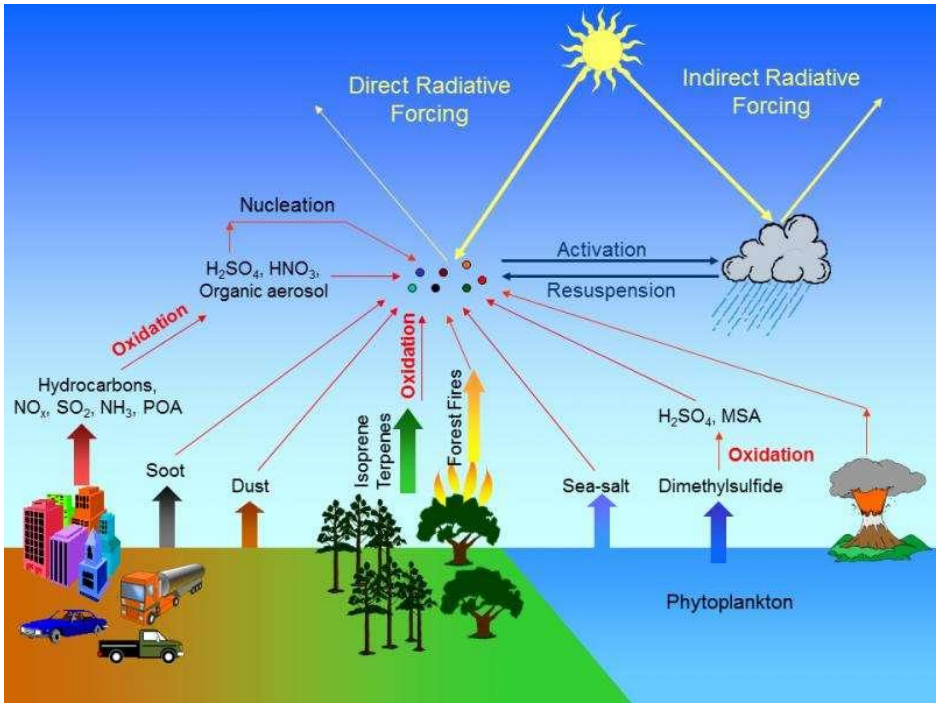

Figure 1.4: Schematization of PM effects on the radiative forcing of Earth – atmosphere system (Kelly, 2016).

Furthermore, PM can alter structure and functions of aquatic and terrestrial ecosystems; for example, aerosol deposition on plant's surface can cause direct or indirect effects if

particles remain on the leaf for a long time or if they are transferred to the ground. The main environmental impact occurs when compounds contained in the aerosol reach the ground and vary its chemical composition by wet or dry deposition processes. This can lead to an increase in soil acidity with effects on bacteria and fungi growth, on biochemical cycles and on vegetation growth (Pöschl, 2005).

1.3.1 Focus on climate and environment effects of soot particles

Among PM constituents, the carbonaceous fraction is one of the most contributing to the effects on climate and environment, as several works state (Ackerman et al., 2000; Bond et al., 2013; Menon et al., 2002; Quinn et al., 2008; Ramanathan and Carmichael, 2008). From the climatic point of view, soot particles absorb the solar radiation, causing a positive radiative forcing and climate warming. BC is considered one of the most significant radiative forcing agent, second only to CO_2 (Bond et al., 2013; Ramanathan and Carmichael, 2008). Another positive effect on radiative forcing is related to the darkening of glaciers surface due to the deposition of carbonaceous particulate matter whose consequences are the decrease of the planetary albedo and the speed-up of ice melting (Skiles et al., 2018). Soot contributes to air pollution also via reactions with NO_2 (Al-Abadleh and Grassian, 2000; Finlayson-Pitts and Pitts, 2000; Kirchner et al., 2000; Nienow and Roberts, 2006; Stanmore et al., 2008), SO_2 (Finlayson-Pitts and Pitts, 2000; Koehler et al., 1999; Nienow and Roberts, 2006), and O_3 (Antiñolo et al., 2015; Browne et al., 2015; Lelièvre et al., 2004; Nienow and Roberts, 2006).

1.4 Health effects

The impact on human health is clearly connected with the different capacity of the particles to penetrate into the respiratory system. The level of penetration depends on several factors such as airways size and structure, inhaled aerosol flow and volume (i.e., the breathing pattern, it depends on human factors such as age and sex) and particle size (Brown et al., 2013). Particles with D_ae > 10 µm are stopped in the first part of the respiratory system and then easily expelled while particles with D_ae < 10 µm are able to penetrate into the respiratory system (inhalable particulate) (Hagens et al., 2007). Penetration level is related to particle size: as D_ae decreases they are able to reach the

bronchial tract (thoracic particulate) and alveoli (breathable particulate), as reported in Fig. 1.5.

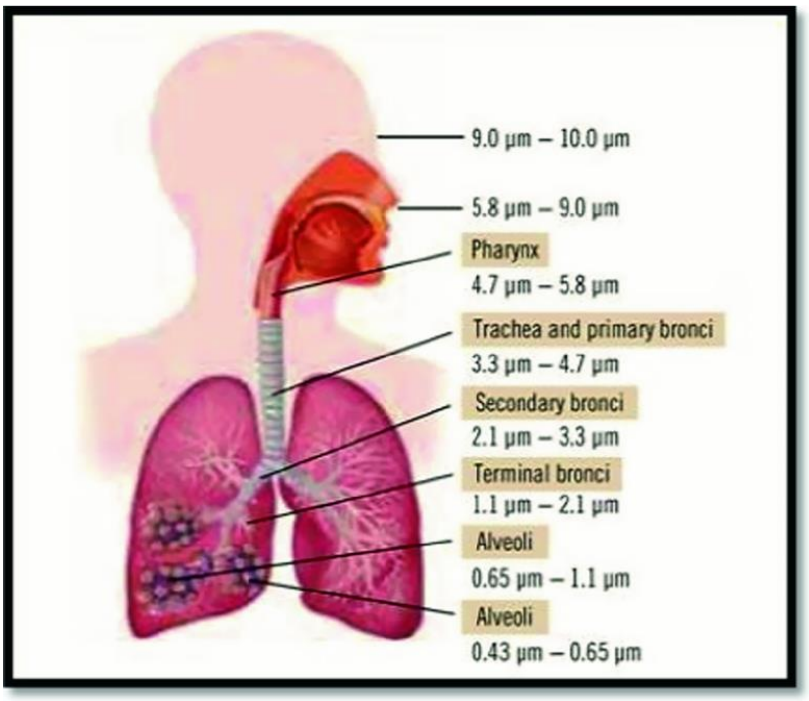

Figure 1.5: Penetration of respiratory system vs. particle size (Satsangi and Agarwal, 2019).

The behaviour after the deposition depends on the type of particle. It is clear which physical and chemical particle properties (particle size, structure, number, mass concentration, solubility, chemical composition, and individual components, etc.) determine their adverse health effects. For example, soluble particles are dissolved while insoluble particles move to other sites. In addition, another important factor contributing to toxicity seems to be the surface area (Tran et al., 2000) because it determines how much toxic gaseous species can be absorbed on particles (Wang et al., 2005). Also particle morphology is relevant, it determines interactions between deposited particles and cells (Oberdörster et al., 1994).

Removal efficiency could depend on particle size (Forbe et al., 2011; Oberdörster et al., 2005). The removal of thoracic fraction usually is by swallowing while the removal of breathable fraction occurs through the blood stream, which is generally more hazardous than through the respiratory system (Bernstein et al., 2004).

Obviously, characteristics of the specific person determine the rate of every process.

Diseases caused by inhaled particles do not concern only respiratory system, as pulmonary inflammations. Indeed, smaller particles are able to enter in the circulatory and lymphatic system by absorption across the lung epithelium. Absorbed particles can reach cells in the bone marrow, lymph nodes, spleen, and heart causing several problems such as heart attacks or cardiac-rhythm disturbances (Forbe et al., 2011; Nel et al., 2006; Oberdörster et al., 2005). Some particles can also penetrate the central nervous system and move in the olfactory nerves up to the brain by translocation (Gilmour et al., 2004; Hagens et al., 2007; Oberdörster et al., 2004). In addition, particles with D_ae < 0.1 µm can reach other organs through the gastrointestinal system; it seems that smaller particles pass through intestinal wall easier than the larger ones (Behrens et al., 2002).

Summarizing, numerous epidemiological studies show that fine air particulate matter and traffic-related air pollution are correlated with severe health effects, including enhanced mortality, cardiovascular, respiratory, and allergic diseases (Bernstein et al., 2004; Gauderman et al., 2004; Pope et al., 2004; Samet et al., 2005).

1.4.1 Focus on health effects of soot particles

Soot particles contribute to PM impact on human health; some effects are shared with other components but some works (Costabile et al., 2017; Fuzzi et al., 2015; Olstrup et al., 2016; Segersson et al., 2017) hypotize that there may be other specific impacts. Although, on the possible specific health effect a comprehensive and firm picture is still largely missing.

Anyway, several works state adverse effects of soot on health (Anenberg et al., 2010; Cassee et al., 2013; Gan et al., 2011; Lelieveld et al., 2015; Pope et al., 2002), which include cardiopulmonary morbidity and mortality (Janssen et al., 2012). Typical size range of soot particles is the fine fraction that in this field means breathable particulate. Thus these particles are suspected to be particularly hazardous to human health, because they are sufficiently small to penetrate the membranes of the respiratory tract and enter the blood circulation or be transported along olfactory nerves into the brain (Nemmar et al., 2002; Oberdörster et al., 2005).

1.5 Overview on bio-aerosol

Another relevant component of the atmosphere is the atmospheric aerosol of biological origin or primary biologic aerosol particles (PBAP or in brief “bio-aerosol”). PBAP, a mix of vital and non-vital bacteria and other kinds of biologic material, is a reactive fraction of aerosol particles. Bio-aerosols also seem to play an important role in the reactivity of particulate matter: they can modify PM toxicity due to their ability to modulate the oxidative potential of toxic chemicals present in it (Jones and Harrison, 2004; Samake et al., 2017).

Among PBAP, bacteria have a crucial role (Bowers et al., 2011); they are part of the atmospheric ecosystem (Fig. 1.6) and can impact the equilibrium of other ecosystems, human health (Ghosh et al., 2015; Pearson et al., 2015; Sala Ferré et al., 2008) and the formation of ice and cloud condensation nuclei (Amato et al., 2015; Bauer et al., 2003; Deguillaume et al., 2008). Airborne bacteria are highly diverse, with complex variations in their species diversity (Burrows et al., 2009; Gandolfi et al., 2013). PBAP composition depends on many factors among them seasonality, meteorological factors, anthropogenic influence and sources. Anyway, it is believed that bacteria suspended in the air often are typical soil bacteria (Després et al., 2012). Their size are in the order of few micrometres and concentration in the outdoor atmosphere ranges from 10^4 to 10^6 cells m^{-3} (Lighthart, 2000).

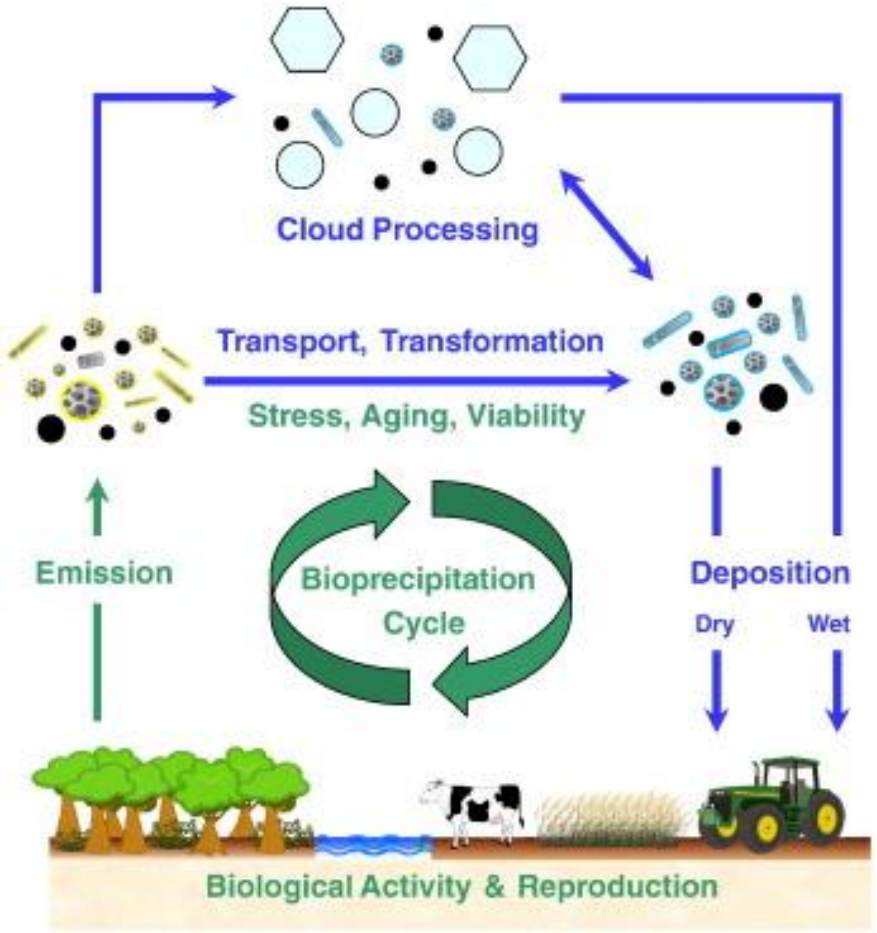

Figure 1.6: Bio-aerosol cycling in the Earth system (Fröhlich-Nowoisky et al., 2016).

Bacterial viability (Tang, 2009) depends on the interaction between bacteria and other organic and inorganic atmospheric constituents (Brotto et al., 2015; Deguillaume et al., 2008; Hussey et al., 2017; Noda et al., 2021, 2019). Some pollutants as NO_x and soot particles are suspected to enhance bacteria viability by preventing from degradation processes, for example during UV irradiation, or inducing structural changes in their survival strategies (Hussey et al., 2017). However, soot particles can have a primary toxic effect on bacteria (Noda et al., 2021, 2019). Therefore it is clear that such interplay is still far from a satisfactory understanding (Jones and Harrison, 2004; Kellogg and Griffin, 2006) and systematic studies are needed.

In this thesis, preliminary studies on interactions between soot particles and two bacteria strains are discussed: bacteria are exposed to soot particles generated by propane combustion, with the aim of investigating how this affect the bacteria viability.

1.6 Overview on oxidative potential and toxicological assays

The existing link between PM and many adverse health effects, such as cardiovascular and respiratory diseases, is already established (Delfino et al., 2013; Hamanaka and Mutlu, 2018; Lim and Thurston, 2019; Rajper et al., 2018; Rao et al., 2018), as well as the dependence of PM induced biological effects from PM properties such as composition and size (Dergham et al., 2012; Dieme et al., 2012; Oh et al., 2011; Peacock et al., 2011). Even if the effect of PM on health is scientifically recognised, mechanisms by which this occur are still under research (Abbas et al., 2013; Billet et al., 2007; Garçon et al., 2006; Sun et al., 2012). However, these adverse effects are supposed to be caused by the oxidative activity of PM. In particular, the interaction between PM and epithelial cells produces reactive oxygen species (ROS) (Rao et al., 2020). ROS have high reactivity due to unpaired electrons. PM can induce ROS in the human body by depositing oxidant species, which are on the surface or contained in the particles. Another way of PM to induce ROS is the stimulation of cells to produce higher concentrations of ROS by the interaction between some chemical/biochemical compounds (Bates et al., 2019; Chen et al., 2019). This happens because toxic pollutants absorbed on particle can enter the human respiratory system (Badyda et al., 2013; Chuang et al., 2013; Wang et al., 2013) up to the lung alveoli (Boublil et al., 2012; X. Li et al., 2013). In general, oxidative stress actives redox-sensitive mechanisms that can lead even to inflammation and cell death: this is how air pollution damages human health through inhalation (Lodovici and Bigagli, 2011). Inflammation is the first response to the negative stress, it is a protective mechanism whose goal is to induce cell killing. This means that at the beginning oxidant stress is responsible of stress defence genes transcription and not of cell damage. Negative effects of oxidation stress occur when ROS formation and individual antioxidant activity become unbalanced. Damages can regard, for example, macromolecules (i.e., DNA and RNA), lipids or proteins (Risom et al., 2005). Defence against ROS starts in lungs with antioxidants (Kelly and Tetley, 1997). Composition and quantity of these antioxidants are critical for the individual responsiveness to air pollutants (Behndig et al., 2006). Anyway, it seems that the ability to upregulate protective scavenging systems determines the susceptibility of the lung to oxidative stress.

One way to investigate the toxicity of PM is the determination of oxidative potential (OP) caused by PM. OP is defined as the ability of PM to oxidize molecules, that means ROS generation and antioxidants depletion activated by inhaled PM (Bates et al., 2019; Leni et al., 2020). Therefore, OP can be used as metric for PM toxicity (Øvrevik, 2019), representing the acute PM health effects (Weichenthal et al., 2016). These kind of studies can be performed, but not only, by chemical (i.e., acellular) assays. Several chemical assays exist and they differ in sensitivity to different PM characteristics (i.e., composition and size distribution); PM composition and particle sizes lead to different OP results in various assays (Bates et al., 2019; Rao et al., 2020). In addition, methods are also specific for fractions of ROS or ROS-inducers and a standard method to determine the OP of PM does not exist (Weber et al., 2018). Thus, the combined application of different assays on the same PM sample is often considered advantageous in providing insightful assessment of particles OP (Ayres et al., 2008; Frezzini et al., 2022, 2019; Lin and Yu, 2020; Manigrasso et al., 2020). Some of the wider used assays are the ascorbic acid assay (AA assay), the dithiothreitol assay (DTT assay) and the dichlorofluorescin assay (DCFH assay). Briefly, AA assay measures the loss of endogenous antioxidant species; AA is one of the detoxifying acid encountered by inspired particulate matter (Yang et al., 2014). OP of PM is reported in terms of depletion rate of AA caused by the permanence with PM. DTT is a redox active compound so DTT assay measures the loss of a proxy of cellular reductants. Here, OP represents the depletion of relevant antioxidants by PM (Xiong et al., 2017). In DCFH assay, the fluorescence intensity is used, since DCFH fluoresces when oxidized. The fluorescence signal is then converted into equivalent H_2O_2 concentration (Venkatachari et al., 2005). DCFH assay exists also as cellular assay, to evaluate the oxidative stress induced by ROS on cells.

Several studies report that atmospheric particles also contain genotoxic chemicals able to react with cell genetic material causing changes and alterations (Aammi et al., 2017; Dhawan et al., 2009; Traversi et al., 2015). In particular, PM exposure can induce higher level of DNA strand breaks, DNA adducts formation, and increased mutation frequency and genetic rearrangement (André et al., 2011; Lepers et al., 2014). It is clear that to deeper investigate PM impact on health, genotoxicity analysis are needed (Aammi et al., 2017). Study of DNA damage at the chromosome level is an essential part of genetic toxicology. Among sources of genotoxic effects, there are mechanical interferences with

cellular components (Daniel et al., 1995) that could lead to cell division dysfunction and disturbed cellular trafficking. These effects are evaluated by the MicroNucleus assay (MN assay). MN is a genotoxic assay considered a marker of cytogenetics damages (Kirsch-Volders et al., 2003), verifying if a particular pollutant induces MN formation. Micronucleus, also known as Howell–Jolly bodies, are fragments of nuclear material expelled from the main nucleus; they can derive from double strand DNA breaks or chromosome malsegregation (Fenech, 2000; Kirsch-Volders et al., 2002).

A significant assay to evaluate cytotoxicity is the 3-(4,5-dimethylthiazol-2-yl)-2,5-diphenyl tetrazolium bromide assay (MTT assay). MTT assay estimates the metabolic activity of living cells by the spectrophotometric determination of the enzymatic reduction of the lightly coloured tetrazolium salt to its formazan of intense purple-blue colour. The measured absorbance value is proportional to the number of living cells (Grela et al., 2018).

In general, toxicity indicates the degree to which a substance can cause a negative effect on a living organism at biochemical, physiological or behavioural level (Lionetto et al., 2019). Information about biological effects of PM, provided by toxicological assays, are complementary to physical-chemical characterizations.

During my PhD, preliminary studies on soot particles toxicological effects and dose-response relationship were carried out. Laboratories at the University of Milan and Rome performed OP and toxicological analysis on samples produced during the thesis work.

CHAPTER 2

Experimental setup and methods

2.1 Soot Generator

The emission of soot particles is often simulated by combustion-based aerosol generators, that are burners using gaseous fuels (Kazemimanesh et al., 2019). They are stable sources of soot: emitted particles have controlled and known properties and are similar to airborne soot particles. Because of their characteristics, soot generators are used in laboratory activities to mimic soot particles and to study their behaviour in the atmosphere.

I used the Mini-Inverted Soot Generator "MISG" (Argonaut Scientific Corp., Edmonton, AB, Canada, Model MISG–2, Fig. 2.1) that is a combustion-based soot generator working as inverted-flame burner (Stipe et al., 2005), introduced by (Kazemimanesh et al., 2019).

Figure 2.1: The Mini-Inverted Soot Generator (Argonaut Scientific).

An inverted-flame burner uses air and fuel flowing in an opposite way to the buoyancy force of the hot exhaust gases, resulting in a co-flow diffusion flame. This configuration leads to a better flame stability by reducing flame tip flickering (Kirchstetter and Novakov, 2007; Stipe et al., 2005), and consequently to a more stable soot particle generation.

Specific cylinders of air and fuel fed the MISG. Gas flow rates to the inlet were controlled by two mass flow controllers (MFCs, Bronkhorst High-Tech B.V., Ruurlo, Netherlands, Models F-201CV-10K-MGD-22-V and FG-201CV-MGD-22-V-AA-000 respectively) operated via a homemade National Instruments LabVIEW code. MFCs allow adjusting air flow rate in the range 0 - 12 lpm and fuel flow rate in the range 0 - 200 mlpm. The gas control system (i.e., MFCs choice and user interface creation) was developed within this thesis work.

Different air and fuel flow rates lead to variation in concentration and size of the generated particles. The maximum reachable concentration is about 10^7 particles cm^{-3} (Argonaut Scientific), while size can range from few tens to few hundreds of nm, depending on burning conditions.

The MISG differs from other commercial generators by the fact that its operation does not require an additional carrier gas (i.e., N_2), since the air flow is internally split between combustion and dilution of exhaust product. As consequence, the comburent:fuel is the only adjustable ratio, while the comburent:carrier gas ratio is determined by the instrument operation.

2.1.1 Global equivalence ratio

A generic combustion requests a fuel and a comburent: during my thesis both ethylene and propane were used as fuel while air always was the comburent. Ethylene and propane are fuels with a well-known capability of producing soot. The efficiency of combustion process can be described by the global equivalence ratio, starting from the air-to-fuel ratio (AFR):

$$\mathrm{AFR} = \frac{m_A}{m_F} = \frac{n_A * M_A}{n_F * M_F} \qquad \text{Eq. 2.1}$$

m_A: air mass;

m_F: fuel mass;

n_A: number of moles of air;

n_F: number of moles of fuel;

M_A: molecular weight of air;

M_F: molecular weight of fuel.

The stoichiometric AFR value for propane is 15.64 m^3/m^3 (inverse value = 0.064 m^3/m^3) and for ethylene is 14.75 m^3/m^3 (inverse value = 0.068 m^3/m^3). The ratio between stoichiometric and actual AFR corresponds to the global equivalence ratio:

$$\phi = \frac{(m_F/m_A)}{(m_F/m_A)_{st}} \quad \text{Eq. 2.2}$$

(m_F/m_A): inverse of actual AFR;

$(m_F/m_A)_{st}$: inverse of stoichiometric AFR.

If $\phi > 1$, the resulting flame is fuel-rich, it leads to an additional mode in the nucleation size range (i.e., 10 - 30 nm) (Moore et al., 2014) and generates semi-volatile organics (Mamakos et al., 2013). If $\phi < 1$, the flame is fuel-lean, it produces soot particles with larger mode diameter (about 100 - 200 nm) (Moore et al., 2014) and generates particles with a large fraction of EC (Mamakos et al., 2013).
During my PhD, since the interest was on soot particles, I focused on fuel-lean conditions.

2.1.2 Flame shapes

Combustion processes produce flames with different shapes and characteristics, that can be distinguished (Kazemimanesh et al., 2019; Moallemi et al., 2019) as:
- *Closed tip* flames (Fig. 2.2.a), which generate low concentrations of soot particles (i.e., around 10^3 particle cm^{-3}) and usually form particle aggregates at the nozzle of the MISG.
- *Partially Open tip* flames (Fig. 2.2.b), which are the transition between *Open* and *Closed tip*.
- *Open tip* flames (Fig. 2.2.c), which generate high concentrations of soot particles (i.e., > 10^5 particle cm^{-3}).
- Asymmetric flames, which show a large variability (very short, flickering, etc.) and can form particle aggregates at the nozzle of MISG.
- *Curled Base* flames (Fig. 2.2.d), which is a particular shape of asymmetric flames that could also form particles aggregates at the nozzle of MISG.

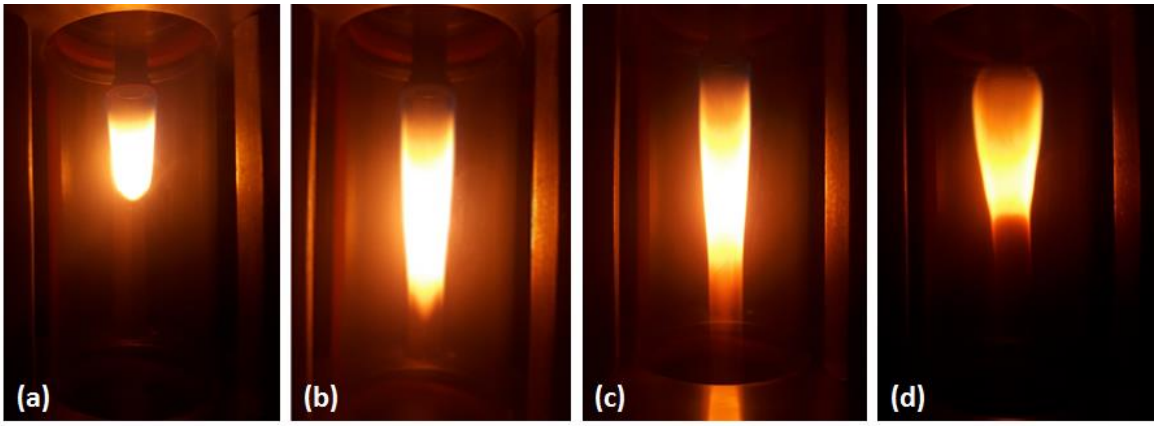

Figure 2.2: Examples of different flame shapes. (a) Closed tip; (b) Open tip; (c) Partially Open tip; (d) Curled base.

In the thesis work, I investigated combustion conditions with the air flow rate in the range 2 - 10 lpm, by 0.5 lpm steps, and the fuel flow rate in the range 30 - 100 mlpm, by 5 mlpm steps.

2.1.3 Combustion parameters

The characterization of the flame shapes was used to select the more interesting combustion conditions to perform the subsequent experiments. *Open tip* flames were considered since they produce higher soot particle concentration than other flames; some *Partially Open tip* flames were also considered, in order to retrieve possible differences.
One of the objective of my thesis was to compare the exhausts of ethylene and propane combustion. First of all, as comparable as possible combustion conditions for both the fuels were selected. Once picked the operative conditions for propane experiments, those for ethylene were established by keeping fixed air flow rates and global equivalence ratios of propane, and consequently adjusting fuel flow rates; this supposing that a certain air flow was split into combustion and carrier operations with the same ratio, regardless of which gas was used for combustion.
Operating conditions selected for propane and ethylene are reported in Table 2.1 and 2.2, respectively.

Table 2.1: Combustion parameters and corresponding flame shapes selected for propane.

PROPANE			
AIR flow [lpm]	FUEL flow [mlpm]	Global Equivalence Ratio	Flame shape
7	70	0.244	Partially Open Tip
7	75	0.261	Open Tip
7	80	0.278	Open Tip
7	85	0.296	Open Tip
8	70	0.213	Partially Open Tip
8	75	0.228	Open Tip
8	80	0.244	Open Tip
8	85	0.259	Open Tip

Table 2.2: Combustion parameters and corresponding flame shapes selected for ethylene.

ETHYLENE			
AIR flow [lpm]	FUEL flow [mlpm]	Global Equivalence Ratio	Flame shape
7	118	0.244	Partially Open Tip
7	127	0.261	Open Tip
7	135	0.278	Open Tip
7	144	0.296	Open Tip
8	118	0.213	Partially Open Tip
8	127	0.228	Open Tip
8	135	0.244	Open Tip
8	144	0.259	Open Tip

2.2 Atmospheric Simulation Chambers

Atmospheric Simulation Chambers (ASCs) are exploratory platforms which allow to study atmospheric processes under realistic but controlled conditions. Inside an ASC, atmospheric conditions (i.e., both chemical and physical parameters) can be maintained

and monitored in real time for periods long enough to reproduce realistic environments and to study interactions among their constituents (Finlayson-Pitts and Pitts, 2000).

ASC experiments merge advantages of both field and laboratory approaches. Field experiments are representative because all the atmospheric constituents are involved in the system; however, the system is very complex and does not allow to isolate and study a single phenomenon or a specific process. In addition, working parameters are not controllable but they depend on atmospheric conditions at the site of observation. Instead, during laboratory experiments, operation conditions can be managed but on a limited number of parameters only. Also limitations on timescale of observable processes occur. ASC experiments are performed under controlled but realistic scenarios where the complicated effects typical of field experiments are reduced.

The atmospheric simulation chamber ChAMBRe - Chamber for Aerosol Modelling and Bio-aerosol Research - (Massabò et al., 2018) is installed at the Physics Department of the University of Genoa, in collaboration with INFN. All the experiments performed during my PhD took place in ChAMBRe. The chamber and its equipment is described in the following paragraphs.

2.2.1 ChAMBRe: Chamber for Aerosol Modelling and Bio-aerosol Research

ChAMBRe (Danelli et al., 2021; Massabò et al., 2018) is built in stainless steel, it has a cylindrical shape with total volume of about 2.2 m^3; the body is made up of two domed cylinders connected by a central ring (see Fig. 2.3). Scattered all over the main body, there are ISO-K flanges, with different diameter, which permit the access to the inner volume. On one side, there is a movable shelf, hosted in a smaller horizontal cylinder connected through a pneumatic valve to ChAMBRe, used to move specific samples inside the chamber.

ChAMBRe was specifically designed for the research on atmospheric bio-aerosol (i.e., bacterial viability vs. air quality level) but the high versatility of the facility allows to cover several fields of atmospheric science.

Figure 2.3: ChAMBRe full view (a) and details on some connected instruments (b).

Connected to ChAMBRe, several instruments and online monitors complete the facility. The whole set-up is managed by a custom NI LabVIEW SCADA (Supervisory Control And Data Acquisition): sensors and instruments are connected and controlled by a remote Ethernet connection and a NI Compact-RIO acquisition module (based on the NI cRIO-9064 controller).

In the follow paragraphs, the equipment of ChAMBRe are presented. The most relevant instruments for my thesis are described in sections 2.3, 2.4 and 2.5.

Pressure, Temperature and Relative Humidity

A HMT334 Vaisala® Humicap® monitors temperature and relative humidity (RH) inside the chamber. The atmospheric pressure is measured both inside and outside ChAMBRe, using a set of two pressure gauges. A MKS Instruments 910 DualTrans™ transducer measures the internal pressure, with a measuring range of $5*10^{-4}$ to $2*10^{3}$ mbar. A Vaisala BAROCAP® Barometer PTB110 measures the pressure outside the chamber, with a measuring range of $5*10^{2}$ to $1.1*10^{3}$ mbar. In Table 2.3 are listed the accuracy values of the sensors.

Table 2.3: Accuracy values of sensors.

Instruments	Measured quantity	Accuracy	Operative range
HMT334 Vaisala® Humicap® transmitter	Relative Humidity	1 % 1.7 %	0 – 90 %RH 90 – 100 %RH
	Temperature	0.2 °C	15 - 25 °C
Pressure Gauges MKS 910 Dual-Trans™	Inner pressure	0.75 % 5 % 10 %	15 – 1000 mbar 10^{-3} – 15 mbar $5*10^{-4}$ – $2*10^{-3}$ mbar
Vaisala BAROCAP® PTB110	Outer pressure	0.3 mbar	$5*10^{2}$ to $1.1*10^{3}$ mbar

Gas monitors

Gas analysers, manufactured by Environnement SA, continuously monitor gas concentrations inside the chamber or, alternatively, in the laboratory of: O_3 (O342e), $NO/NO_2/NO_x$ (AC32e), CO/CO_2 (CO12e), SO_2 (AF22e) and BTEX (VOC72M). Detection limits of the monitors are defined in Table 2.4.

Table 2.4: Detection limits of gas monitors.

Instruments	Measured quantity	LDL
Envea AC32e	NO_x (NO_2)	0.2 ppb
Envea O342e	O_3	0.2 ppb
Envea AF22e	SO_2	0.4 ppb
Envea VOC72M	BTEX	0.02 ppb
Envea CO12e	CO/CO_2	0.05 ppm

Mixing fan

A fan installed in the bottom of the structure favours the mixing of gas and aerosol species in the chamber volume. The fan has four metallic arms of 25 cm length each connected to an external engine through a rotating shaft, whose speed can be regulated by an external controller and varied between 0.0 and 50 Hz in steps of 0.1 Hz (0 to 3000 rpm, in

steps of 6 rpm). Mixing time for gaseous species is of about 180 s when the fan rotates at about 1.6 revolutions per second.

Vacuum system

A composite pumping system is connected to ChAMBRe and it can evacuate the total volume down to 10^{-5} mbar in about 15 minutes. The system consists of a rotary pump (model TRIVAC® D65B, Leybold Vacuum), followed by a root pump (model RUVAC WAU 251, Leybold Vacuum) and a turbo pump (Leybold Turbovac 1000). Between the pumping system and ChAMBRe is collocated a safety valve (Leycon Secuvac DN 63, Oerlikon Leybold Vacuum) as a gate to prevent possible backwashes of the pumps oil inside the chamber.

This system is used to clean up the chamber at the end of each experiment, to avoid possible contamination in the further tests. Reached the needed vacuum level, ChAMBRe can be re-filled with clean air and it returns to atmospheric pressure. To do this, pure N_2 from a compressed gas cylinder is flushed in up to 5 mbar and then ambient air enters the chamber through an absolute HEPA filter (model: PFIHE842, NW25/40 Inlet/Outlet – 25/55 SCFM, 99.97 % efficient at 0.3 μm) and several pollutant traps (including a HEPA filter and zeolite traps).

Lamps

The ChAMBRe equipment includes two different UV lamps. The first, with an 85W radiation at $\lambda = 253.7$ nm (UV-STYLO-F, Light Progress srl), is used to sterilize the chamber volume without producing ozone. The second lamp (BHK Incorporated, Analamp models) irradiates at $\lambda < 240$ nm and works to the ozone generation via photoreaction.

Nebulization system

To inject particles into the chamber, there are three different nebulizer available. A Blaustein Atomizer (BLAM, single-jet model, CH Technologies), connected to the facility by a curved stainless-steel tube (length = 50 cm, diameter = 1.5 cm) can be used to spray both bacteria and inorganic species. A Sparging Liquid Aerosol Generator (SLAG - CH Technologies), directly connected to the chamber, can be used to nebulized bacteria due

to its gently action. A Collison nebulizer (CH Technologies) is used to spray inorganic particles inside ChAMBRe.

2.2.2 Soot experiments

The Mini Inverted Soot Generator was warmed for about 45 minutes before injecting soot particles inside ChAMBRe, the exhaust was directed to the waste line. A three-way valve selects the soot flow direction. Injection of soot particles inside ChAMBRe lasted 2 or 3 minutes, depending on the soot concentration required for the specific experiment. All the connections (i.e., MISG-tubes and tubes-ChAMBRe) were made by Swagelok adaptors or ISO-K flanges to avoid any possible leak. Some fluid-dynamic evaluations were performed with the Particle Loss Calculator (PLC) software tool (von der Weiden et al., 2009): the geometry of the experimental setup, combined with particle size and used flow rates, results in particle losses lower than 0.1 % in the dimensional range of 80 - 2000 nm. The ChAMBRe setup to perform soot experiments is sketched in Fig. 2.4.

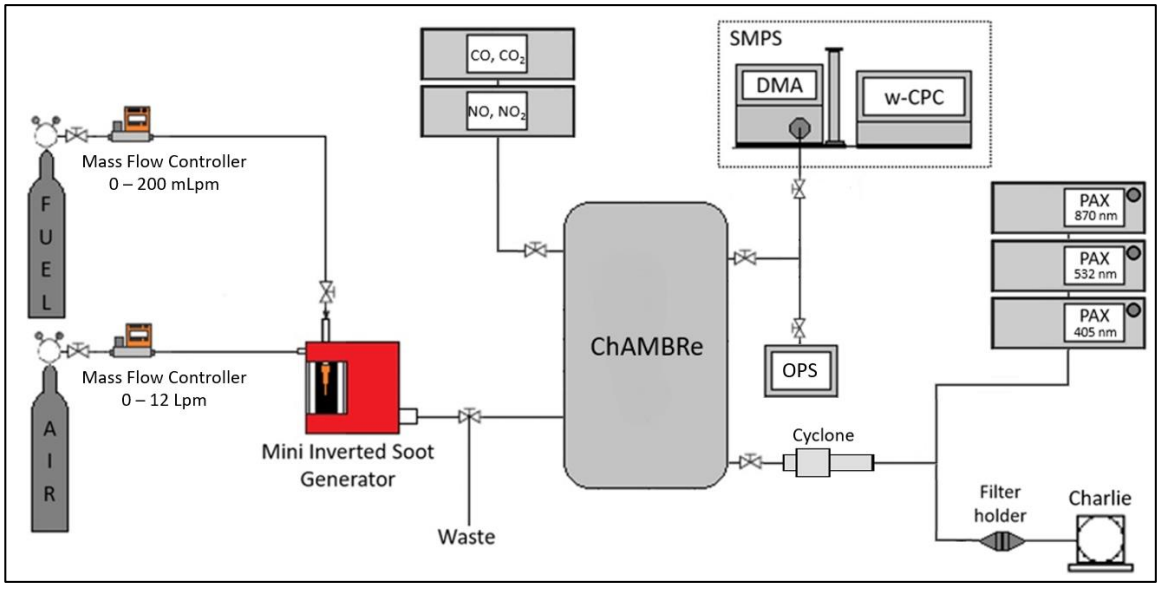

Figure 2.4: ChAMBRe setup for experiments with the soot generator.

2.3 Size distribution

Particle concentration and size distribution inside the chamber are measured continuously by two different instruments: a Scanning Mobility Particle Sizer (SMPS, TSI

Inc., Shoreview, MN, USA, Model 3938) and an Optical Particle Sizer (OPS, TSI Inc., Shoreview, MN, USA, Model 3330).

SMPS classifies particles with diameter < 1 μm, the size range of interest for this thesis work.

2.3.1 SMPS: Scanning Mobility Particle Sizer spectrometer

SMPS is a scanning system to measure the size distribution of aerosol particles. Its operation is based on the relationship between electrical mobility and particle size with singly charged particles. Briefly, the system takes an air sample by a pump; an inertial impactor is set at the inlet to prevent particles larger than a known size enter inside the instrument. In this way risk of contamination and soiling of the internal parts are avoided. The impactor has an orifice of 0.0508 cm, resulting in cut-off capability at 50 % of 940 nm. Firstly, air sample flows throughout a soft X-ray (< 9.5 KeV) neutralizer that leads the aerosol to a known charge distribution. The following step is the electrostatic classifier, connected to the differential mobility analyzer (DMA), which divided particles by their electric properties. Finally, selected particles are counted by the condensation particle counter (CPC). Summarizing, the SMPS system is made up of three parts:

- Charge neutralizer by soft X-Ray: Advanced Aerosol Neutralizer (TSI model 3088)
- Electrostatic classifier: flow controller and Differential Mobility Analyzer (DMA, TSI model 3081A Long DMA or TSI model 3085A Nano DMA)
- Water based Condensation Particle Counter (wCPC, TSI model 3789).

The instrument operates in the particle size range between 2.2 nm and 1000 nm. Its sensitivity is 1 % at 100 nm, the maximum concentration is 10^7 particles cm^{-3} and the minimum scanning time is 10 seconds. Working flows range between 0.2 and 1.5 lpm. During the experiments described in the following, the SMPS was set to measure particles having diameter from 34 nm to 649 nm; aerosol sample and sheath airflow rates were fixed at 0.17 lpm and 1.60 lpm, respectively, while the scanning period for each cycle was 70 s.

Advanced Aerosol Neutralizer

The SMPS particle sizing operation is based on particles having a well-defined charge level as a function of particle size; this charge distribution is reached by a bipolar diffusion

charging process (Reischl et al., 1996). The neutralizer produces high concentrations of both positive and negative ions by a low-energy soft X-ray (< 9.5keV) source that ionizes air molecules. Sample particles through the neutralizer attract oppositely charged ions. In this way, neutralization of excess charges occurs (Liu and Pui, 1974). Ion-particle interactions of charges exchanging are driven by diffusion processes (Reischl et al., 1996).

DMA: Differential Mobility Analyzer

The SMPS mounted a Long DMA 3081A that classifies particles having size between 10 and 1000 nm. Long DMA, schematized in Fig. 2.5, separates particles by an electrostatic way, using the motion generated by the electric force on the charged particles and the movement due to the transport in the airflow. In particular, inside the DMA, particles are separated on according to their electrical mobility, a parameter that is proportional to number of charges on the particles and inversely proportional to particle size.

On the top of Long DMA there are two inlets, one for the aerosol sample and another for the sheath flow (i.e., particle-free air keeping sample centred to avoid wall-losses): the resulting flow goes axially downward through the classifier region. Long DMA is made up of two concentric cylindrical electrodes resulting in an internal electric field; the inner cylinder has a negative voltage while the outer is electrically grounded thus creating an electric field between the two cylinders. Negative charge particles are attracted by the external electrode and positive charge particles are attracted radially by the inner electrode while are flowing with the sheath flow. Neutral particles are removed with the excess flow. In particular, the position to which a particle precipitates along the collector rod depends on the particle electrical mobility: particles with higher mobility are collected along the upper portion of the rod while particles with lower mobility along the lower portion of the rod.

Monodisperse aerosol, composed by particles with quite the same electrical mobility, exits the DMA from holes at the bottom of the inner electrode.

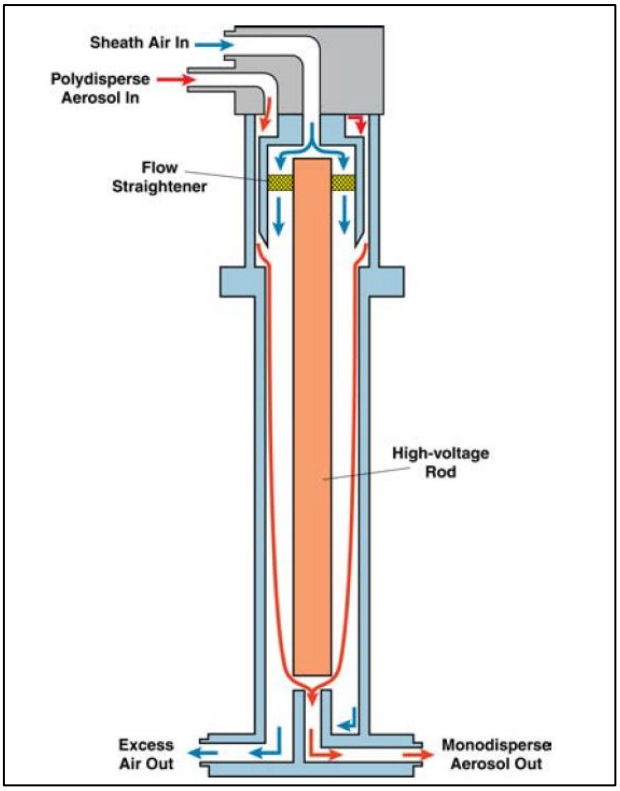

Figure 2.5: Long DMA scheme, extracted from (TSI Inc., 2009).

Particles classified by their electric mobility diameter exit from DMA and enter a Condensation Particle Counter (CPC) where their concentration is measured.

wCPC: water-based Condensation Particle Counter

The wCPC (see Fig. 2.6) is a water-based condensation particle counter. It measures number concentration (i.e., particles cm^{-3}) of sub-micrometric airborne particles. To improve the detection process, particles are grown up to be droplets by condensation of vapour onto them: wCPC uses deionized water as condensing fluid. In particular, this unit is filled with technical demineralized water (Conductivity (20°C), max. 1.5 µS/cm; VWR Chemicals INTERNATIONAL S.R.L.). After being grown, particles are detected by an optical counting system. The instrument can measure particles with a diameter between about 2 nm and 1000 nm, in concentration up to $2*10^5$ particles cm^{-3}.

Sub-micrometric particles are continuously sampled (inlet flow rate is 0.6 lpm). Two flows are derived from the inlet flow: the aerosol sample flow (flow rate is 0.3 lpm) and the sheath flow, after filtering the particles. Aerosol sample flows first through a cooled conditioner and then through a heated condenser (growth tube); sheath flow keeps

sample centred. In the growth tube, particles are enlarged into micro-metric droplets by heterogeneous condensation of a supersaturated water vapour. A vapour surrounding particles begins to condense onto them when it reaches a certain degree of super-saturation (Keady et al., 1986). Vapour pressure is raised by heating wetted walls; supersaturated conditions are due to water vapour diffusion to the centre of sample. Exhaust water resulting from the condensation process is removed via the exhaust port and collected in a dedicated bottle. Enlarged particles are optically detected. They enter by a nozzle into a lighted viewing volume. Here, a laser beam illuminates particles that scatter light. Scattered light pulses are collected by a photodiode, converted into electrical signal and finally counted leading to the measure of particles concentration. The number concentration is calculated following the formula:

$$C = \frac{N}{Q * t} \qquad \text{Eq. 2.3}$$

N = number of particles counted

Q = Sample flow rate [$cm^3\ s^{-1}$]

t = actual sample time [s]

Number concentration information merged with the diameter information from DMA, gives the aerosol size distribution.

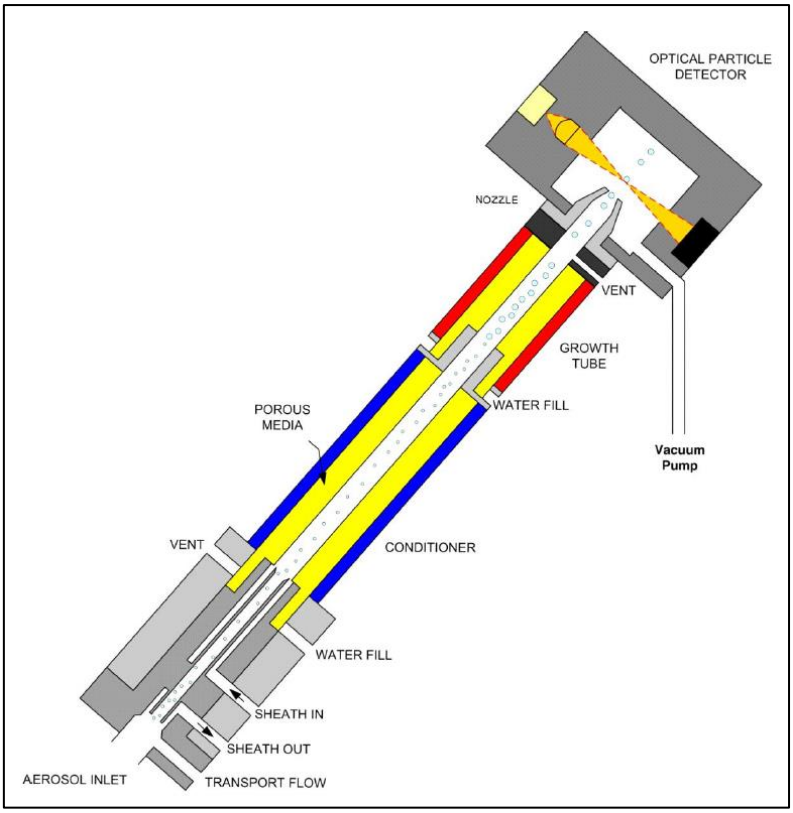

Figure 2.6: wCPC scheme, extracted from (TSI Inc., 2019).

The SMPS has an automatic flow control: air pressure and temperature are continuously monitored and integrated in the input air flow control, to ensure the correct air flow even if air conditions are not stable. Pressure and temperature are included in the calculation of the size distribution and both parameters are recorded in a data file.

2.3.2 OPS: Optical Particle Sizer spectrometer

The OPS (see Fig. 2.7) uses the principle of optical scattering from single particles to count and classify particles by their size. The size measurement range goes from 300 nm to 10 µm, overlapping the SMPS in the range 300 nm – 1 µm. Particles bigger than 10 µm are only counted, not sized.

Particles throughout a sensing volume are illuminated by a thin laser beam (λ = 660 nm). Every particle passing through the laser beam scatters light: a flow of particles result in pulses that are counted and sized. Scattered light is collected by an elliptical mirror and focused to a photodetector where the electronic process the signal. Pulse intensity is proportional to the optical particle size: by a calibration with monodispersed spherical

particles every pulse intensity is related to a particle size. Measurement is binned on 16 channels. Optical parameters (i.e., refractive index) and density of particles under analysis can be set by the operator.

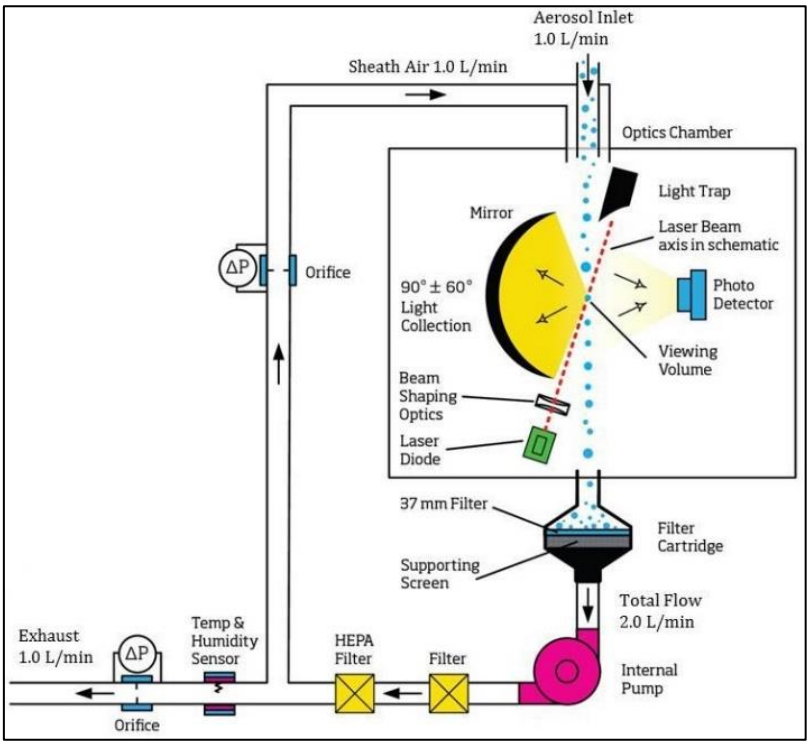

Figure 2.7: OPS scheme, extracted from (TSI Inc., 2011).

The number concentration of particles at size channel *i* is determined by the following equation:

$$C_i = \frac{N_i}{Q * t} \qquad \text{Eq. 2.4}$$

N_i = number of particles counted at size channel *i*

Q = Sample flow rate [$cm^3\ s^{-1}$]

t = actual sample time [s]

While the concentration measured by the instrument depends on the flow rate, the flow is maintained at 1.0 lpm ± 5 % by measuring the pressure drop across orifices. Particles are kept in the sensing volume by an independent sheath flow of 1.0 lpm: this flow is recirculating inside the instruments after being filtered by a HEPA filter to avoid

contaminations. Both flows are measured, pump voltage is consequently modified to maintain these flows stable.

2.4 Optical properties

Optical properties depend both on composition and aging of particles; the absorption capability of aerosols is described by the absorption coefficient (b_abs).
Carbonaceous compounds (see. Par 1.2) are a significant constituent of PM and the inorganic fraction (i.e., Black Carbon) is the most efficient light-absorbing aerosol species in the VIS range (Lindberg et al., 1993; Rosen et al., 1978). Thus, the measurement of b_abs in the VIS range is strongly correlated to the measurement of BC. The absorption coefficient can be correlated with BC concentration by the following relationship:

$$b_{abs} = C_{BC} \cdot MAC \qquad \text{Eq. 2.5}$$

b_abs: absorption coefficient [Mm^{-1}],

C_{BC}: BC concentration, [$\mu g\ m^{-3}$],

MAC: Mass Absorption Coefficient, [$m^2\ g^{-1}$].

Due to the variability in particle composition, different MAC values are reported in literature (Bond and Bergstrom, 2006; Fuller et al., 1999; Horvath, 1993; Reche et al., 2011).

2.4.1 PAX: Photoacoustic extinctiometer

Values of b_abs for soot particles suspended inside ChAMBRe are determined online by three photoacoustic extinctiometers (PAXs, Droplet Measurement Technologies, Boulder, CO, USA), working at λ = 870, 532 and 405 nm. PAX is made up of two distinct measurement cells, the sample inlet is placed between them and the sample flow (inlet flow rate is 1.0 lpm) is split towards both cells. The beam of a modulated laser diode crosses the whole cells path. The operation scheme is reported in Fig. 2.8.
Absorption properties are determined by an acoustic detector: as particles absorb light they heat up and, quickly release heat to the surrounding air resulting in acoustic waves

(Moosmuller et al., 2009). An ultra-sensitive microphone receives the signal which intensity is interpreted to infer the particle absorption coefficient. Value of b_abs is calculated by the instrument as follows:

$$b_{abs} = \frac{P_{mic} \cdot A_{res} \cdot \pi^2 \cdot f_{res}}{P_L \cdot (\gamma - 1) \cdot Q} \cdot \cos(\Phi) \qquad \text{Eq. 2.6}$$

P_{mic}: microphone pressure at f_{res},

A_{res}: cross-sectional area of the resonator,

f_{res}: resonance frequency [Hz],

P_L: laser power,

γ: ratio of isobaric and isochoric specific heat,

Q: resonator quality factor,

ϕ: phase of b_abs signal.

Scattering properties are measured by using a wide-angle reciprocal nephelometer. A nephelometer is made up of a laser diode, generating a beam, and a photodiode set at 90° with respect to the beam. Sampled particles reflect the incident radiation that is detected by the photodiode. Value of scattering coefficient (b_scat) is calculated by the instrument as follows:

$$b_{scat} = \frac{P_{scat}}{P_L} \qquad \text{Eq. 2.7}$$

P_{scat}: calibrate readings from the photomultiplier tube,

P_L: laser power.

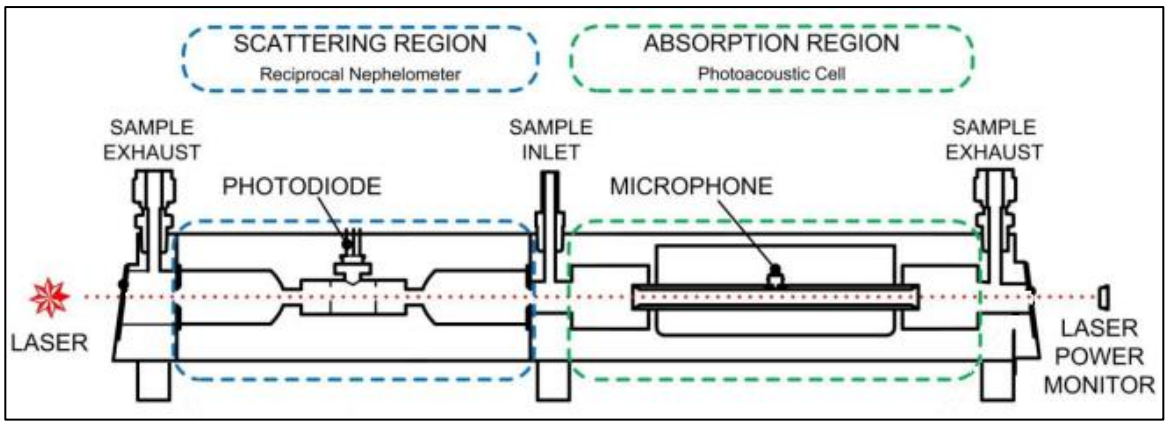

Figure 2.8: Operational scheme of PAXs, extracted from (Droplet Measurement Technologies, LLC, 2020).

With very high concentration of soot particle inside ChAMBRe, a diluter (eDiluter Pro, Dekati Ltd., Kangasala, Finland) was introduced before the PAXs inlet. Aerosol sampled from ChAMBRe was diluted by dry air from a cylinder, with dilution factor of 1:100. No significant discrepancy was observed in the results of experiments performed without and with the diluter.

2.5 Sampling and offline analysis

During each experiment, soot particles inside ChAMBRe were also collected on dedicated media to be analysed offline at a later time. I used, quartz fibre filters (Pallflex Tissuquartz 2500 QAO-UP, diameter of 47 mm). Quartz fibre filters are classified as *depth-filter*, which means they trap particles in their matrix. The material of these filters is recommended for thermal-optical analysis due to its capability of resisting high temperature. Filters were held in a stainless-steel holder and operated at a fixed and stable sampling flow rate (i.e., 10 lpm or 13.7 depending on the experiment) by an electronically controlled flow rate sampler (TECORA – Charlie). For each experiments, three filters with different volumes of sampled air were collected.

2.5.1 Cyclone

To investigate the influence of particle size on particle properties, a series of experiments was performed with a size cut. During such experiments, a cyclone (PM1 Sharp Cut Cyclone - SCC 2.229, MesaLabs, Lakewood, CO, USA) was inserted upstream the PAXs and

the filters sampler (Fig. 2.4). Cyclone operation is based on the inertial classification of particles as function of their aerodynamic diameter. The cyclone used in this work has a cut point at particle diameter of 1.0 µm with a nominal flow of 16.7 lpm (Gussman et al., 2002), this means that the 50 % of particles with diameter of 1 µm are removed from the sample flow.

The cyclone is composed of a chamber in which sample flow enters tangentially, and follows a certain rotary motion. Particles are separated from the air flow according to their inertia. Particles larger than the cut-off are collected on the walls, while particles smaller than the cut-off follow the air flow towards the subsequent stages (i.e., instruments and/or samplers). In Fig. 2.9 a cyclone is schematized.

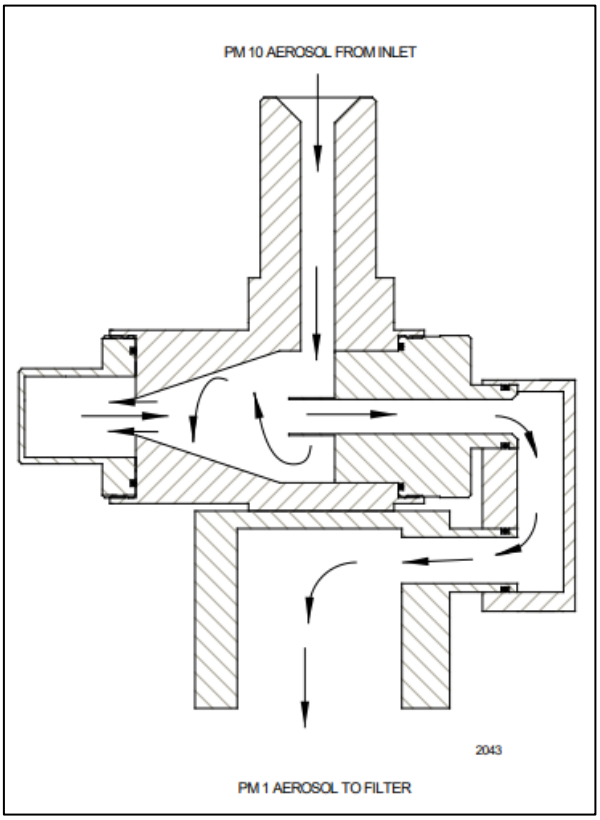

Figure 2.9: Cyclone scheme, extracted from (Mesa Labs, 2001).

2.5.2 Optical analysis: Multi Wavelength Absorbance Analyzer

The MWAA (Multi Wavelength Absorbance Analyzer, Fig. 2.10.a) is an optical analyser designed and built at the Environmental Physics laboratory of the Department of Physics (University of Genoa and INFN), for the non-destructive analysis of PM samples collected

on filters (Massabò et al., 2015, 2013). MWAA operation is based on the light absorption and scattering by PM components and provides information on the carbonaceous fraction in the sample (Massabò et al., 2015, 2013).

The MWAA exploits five laser diodes (WSTech products, Fig. 2.10.b) covering the visible spectrum, from IR to UV: infrared, λ = 870 nm; red, λ = 635 nm; green, λ = 532 nm; blue, λ = 405 nm; ultraviolet, λ = 375 nm. One at time, a different laser beam is collimated to illuminate a sample area of about 1 mm^2. Filter samples are located on an aluminium wheel (Fig. 2.10.c) with the sampled surface exposed to the laser beam. They are analysed one at time. A stepper motor automatically moves the wheel changing the sample in analysis; two translational motors allow the scanning of filter surface by 1 mm steps. Filter partially transmits and partially scatters the incident laser beam: three photodiodes situated at 0°, 125° and 165°, (Thorlabs products, Fig. 2.10.d) detect transmitted and backscattered light fractions. Photodiodes, with spectral response in the range 200 – 1100 nm, detect light signal and produce an electric current whose intensity is proportional to incident beam power and wavelength. The signal of photodiodes is driven to a current to voltage converter (CVC), amplified with a selected gain and finally acquired by a multifunction device (NI USB 6002), used as A/D converter.

The whole system is managed by a home written LabVIEW™ software.

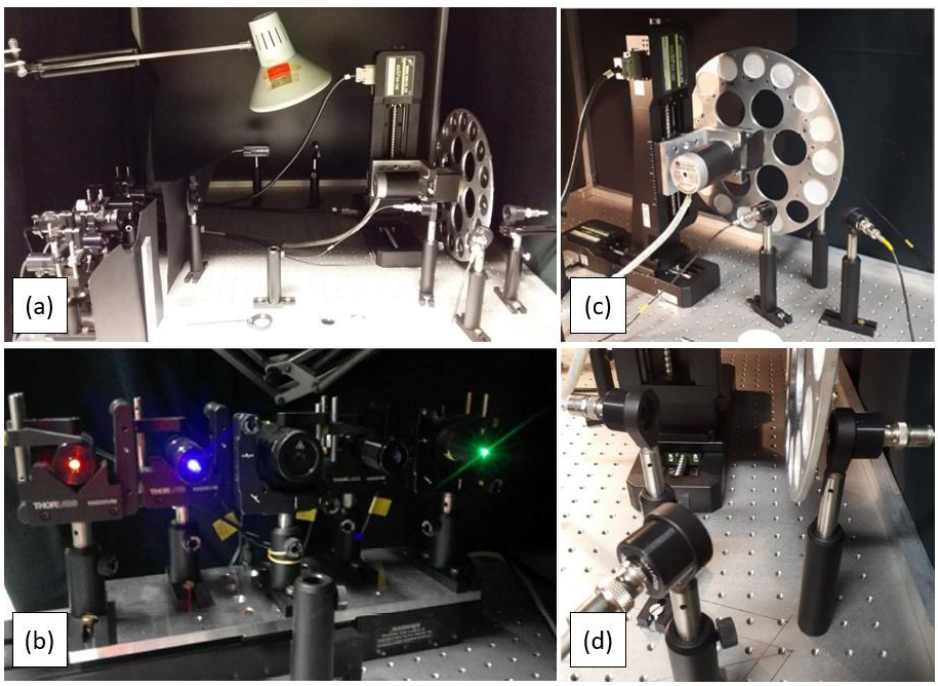

Figure 2.10: MWAA: (a) setup; (b) laser diodes; (c) sample wheel; (d) photodiodes.

The angular distribution of radiation scattered by the sample can be determined from photodiodes signal by using analytical functions described by (Petzold and Schönlinner, 2004), which retrieves absorption coefficient (b_abs) from transmission and back-scattering measurement. Transmitted light is detected by the 0° photodiode (forward hemisphere) while back-scattered radiation is detected by the 125° and 165° photodiodes (backward hemisphere).

Regarding quartz fibre filters, radiation is isotropically scattered in the forward hemisphere (scattering angles: $0° \leq \theta \leq 90$) and all the angular distribution follow the Lambertian cosine law:

$$S(\theta) \propto \cos(\theta) \qquad \text{Eq. 2.8}$$

Since angular distribution in the forward hemisphere does not depend on aerosol composition, the transmitted radiation can be revealed by only one photodiode at 0°.

In the backward hemisphere (scattering angles: $90° < \theta \leq 180$), angular distribution depends on aerosol composition and can be treated as a linear combination of the Lambertian cosine law of scattered radiation and Gaussian distribution of reflected radiation:

$$S(\theta) \propto \left(\alpha - \cos(\theta - \pi) + (1 - \alpha)\exp\left[-\frac{1}{2}\frac{(\theta-\alpha)^2}{\rho^2}\right]\right) \qquad \text{Eq. 2.9}$$

α: fraction of scattered radiation,

ρ: filter roughness, estimated ρ ≈ 0.50 (Petzold and Schönlinner, 2004)

For a totally scattered radiation α = 1 while α = 0 for complete reflected radiation.

Following the analytical approach of (Petzold and Schönlinner, 2004), only two photodiodes (in this case at 125° and 165°) are sufficient to measure diffuse radiation. Data analysis provides parameters about transmitted, diffuse and back-scattered radiation for both the blank-filter (i.e., before PM sampling) and the same loaded filter (i.e., after PM sampling). Following the data processing developed by (Hänel, 1994, 1987;

Petzold and Schönlinner, 2004), the absorbance value of each individual sample is determined:

$$ABS = \tau_{P,ABS} = (1 - \omega_P)\tau_P \quad \text{Eq. 2.10}$$

$\tau_{P, ABS}$: aerosol absorption optical thickness,

ω_P: sample single-scattering albedo (i.e, ratio of light scattering to light extinction),

τ_P: sample optical thickness

Merging absorbance value with filter geometry and sampling condition, the value of the absorption coefficient is obtained:

$$b_{abs} = ABS \cdot \frac{A}{V} \quad \text{Eq. 2.11}$$

ABS: measured absorption,

A: filter area,

V: sampled air volume.

The b_abs value is measured at each wavelength of MWAA. Dependence of b_abs on light wavelength (i.e., spectral dependence) is described by the Ångström Absorption Exponent (AAE) (Ångström, 1964) with the power law:

$$b_{abs}(\lambda) = K \cdot \lambda^{-AAE} \quad \text{Eq. 2.12}$$

AAE value depends on PM composition (Bond and Bergstrom, 2006; Kirchstetter et al., 2004). In particular, BC from fossil fuel combustion (as soot particles) leads to $0.8 \leq AAE \leq 1.1$ (Bond and Bergstrom, 2006; Kirchstetter et al., 2004; Schnaiter et al., 2005) while AAE increase up to 1.5 - 7 when BrC from biomass burning is also present in the sample (Favez et al., 2010; Hoffer et al., 2006; Sandradewi et al., 2008; Yang et al., 2009).

2.5.3 Thermal-optical analysis: Sunset EC/OC Analyzer

Thermal-Optical Transmittance (TOT) methods are widely used to separate EC/OC and quantify their concentration (Birch and Cary, 1996; Chow et al., 1993; Huntzicker et al., 1982). These methods require that PM is collected on quartz fibre filters, since they resist to high temperature (Huntzicker et al., 1982).

The Sunset EC/OC Analyzer (Sunset Laboratory Inc., Fig. 2.11.a, in the follow "Sunset") is the most widespread thermal-optical instrument. Its scheme is showed in Fig. 2.11.b. Thermal-optical analysis is destructive: it is performed on a punch with area of 1 cm^2, extracted from the filter. The punch is inserted inside a quartz oven and exposed to a controlled heating. In particular, the instrument follows a sequence of thermal steps (namely a "protocol"), characterized by specific temperature, atmosphere and duration. The EC/OC separation is based on the different thermal evolution of carbonaceous fractions and it is determined by the two phases of the analysis:

- inert phase: the first heating phase occurs in He atmosphere and the OC fraction volatilizes;
- oxidative phase: the second heating phase occurs in He - O_2 atmosphere (95 % He – 5 % O2) and the inorganic EC fraction volatilizes.

A FID (Flame Ionization Detector) quantifies OC and EC fractions. A gas-carrier (He) line is connected to the oven; heating products are fluxed through several reactive steps. Firstly, they are oxidised to CO_2 by an oxidative atmosphere and high temperature (T = 870°C, catalyst: MnO_2). Then, inside the methanator, in a reducing atmosphere of H_2 (T = 500°C), CO_2 is converted into CH_4, detected by the FID. Inside the FID, CH_4 is transformed in CH_3 radicals by a potential difference producing a current. The proportionality between the current intensity and the quantity of methane allows retrieving the initial concentration of carbonaceous compounds on the filter. The instrument is calibrated at the end of each measurement by sending to the FID a known quantity of methane.

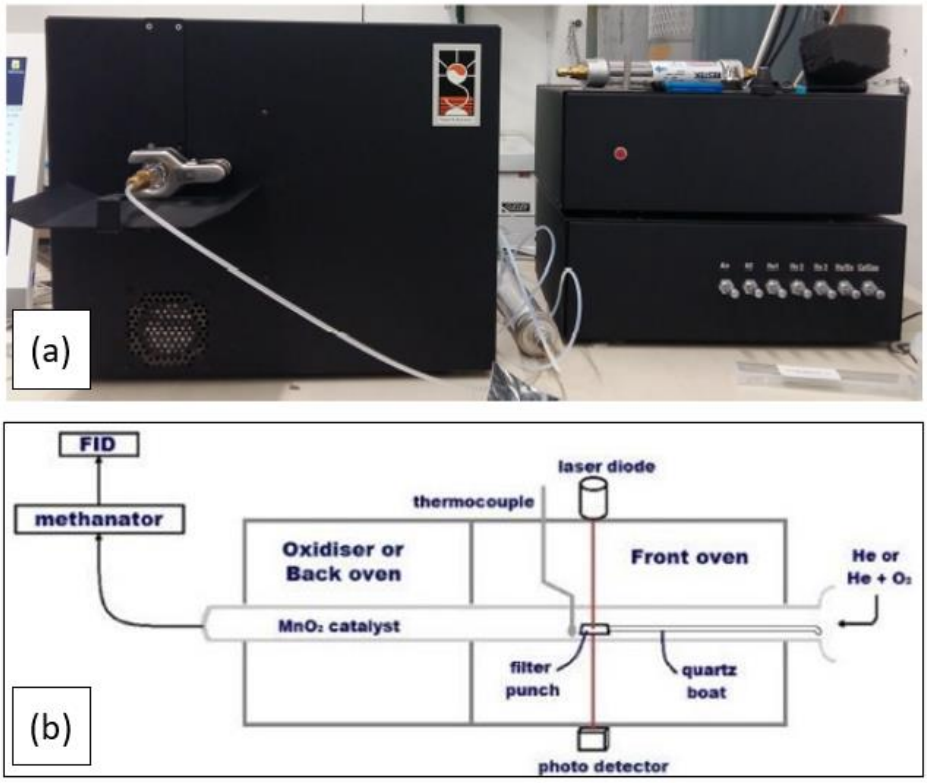

Figure 2.11: (a) Setup of Sunset EC/OC Analyzer. (b) Scheme of the instrument.

During the inert phase, a pyrolysis of the particulate deposited on the filter can occur. Part of the organic compounds could be converted into pyrolytic carbon (PYRC) by thermal energy, by a charring process. PYRC thermal properties are similar to those of EC, thus meaning that pyrolytic carbon can evolve during the oxidative phase and not during the inert phase. This can affect the EC/OC separation and resulting in an underestimation of OC and an overestimation of EC (Chow et al., 2007). To solve the artefact, an optical measurement is performed simultaneously to the thermal one. PYRC has also optical properties similar to EC: it absorbs light. By monitoring the filter transmittance with a laser diode (λ = 635 nm, see Fig. 2.11.b), the evolution of PYRC is observed. During the He-phase, as consequence of the pyrolysis, the transmittance decreases because sample turns black; during the Ox-phase, as consequence of PYRC and EC evolution, transmittance increases. A separation point between OC and EC fractions is set when the transmittance reaches the same value registered at the beginning of analysis, assuming that a quantity of EC equal to the formed PYRC has evolved in CO_2. This moment is defined as split point. As operative definition, carbonaceous compounds evolved before the split point are quantified as Organic Carbon while those converted in CO_2 after the split point are

quantified as Elemental Carbon. Fig. 2.12 shows an example of thermogram and the different phases of the analysis. Thermograms can differ depending on the protocol. Several protocol have been developed (Cavalli et al., 2010; Chow et al., 1993; Peterson and Richards, 2002), they differ in temperature set points and in the residence times at each temperature step. It is reported in literature (Massabò et al., 2019) that protocols do not affect the quantification of Total Carbon (i.e., OC + EC) but the EC/OC separation. However, during the thesis work, analysis performed using the EUSAAR_2 showed a non-negligible signal of the FID is still present during the last part of the He-Ox analysis, so basically overlapping the calibration peak, causing a non-complete combustion (and then quantification) of EC. For this reason, EUSAAR_2 results have been considered as not reliable and therefore excluded from the present work. In the last part of the oxidant phase, NIOSH reaches higher temperature than EUSAAR_2 (i.e., 940 °C for NIOSH and 850 °C for EUSAAR_2), thus all the TC on the filter evolves in CO_2 being properly quantified. All the analysis in this work were performed using the NIOSH protocol (National Institute for Occupational Safety and Health: NIOSH, 1999).

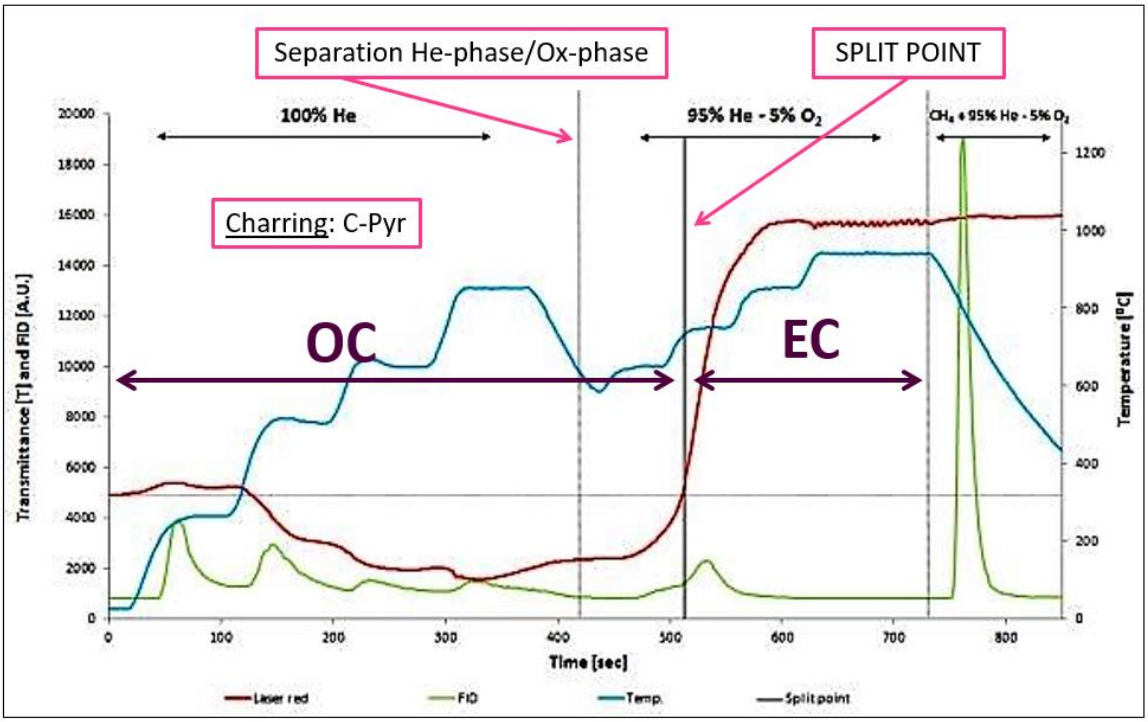

Figure 2.12: Example of thermogram: different phases of the analysis and the OC/EC separation by the split point are reported. Time evolution of temperature (blue line), transmittance (red line) and FID signal (green line) are also shown.

2.6 Bacteria and soot experiments

Some experiments were designed to investigate the possible change in bacteria viability under exposure to soot. Such experiments required dedicated instruments and protocols (Danelli et al., 2021).

Bacteria strains used to perform these experiments are *Escherichia coli* (ATCC® 25922™, Fig. 2.13) and *Bacillus subtilis* (ATCC® 6633™, Fig. 2.14). They are non-pathogen proxies of typical atmospheric bacteria, respectively Gram-negative and Gram-positive; they are extensively used as model organisms in microbiology and molecular biology fundamental and applied studies (Lee et al., 2002). *E. coli* is rod-shaped, about 1–2 µm long and about 0.25 µm in diameter. It is a common inhabitant of the gastrointestinal apparatus of warm-blooded animals, including humans. *B. subtilis* is rod-shaped with a length ranging between 2.5 and 6.5 µm. It is commonly found in soils but has been also observed in other environmental matrices such as water and air (Earl et al., 2008).

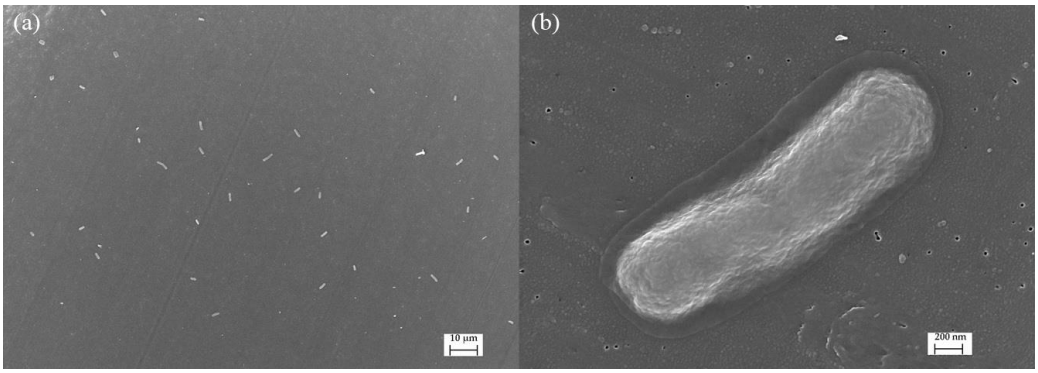

Figure 2.13: Detail of Escherichia Coli in physiological solution, magnifications 2000x in panel (a) and 100000x in panel (b) (Massabò et al., 2018).

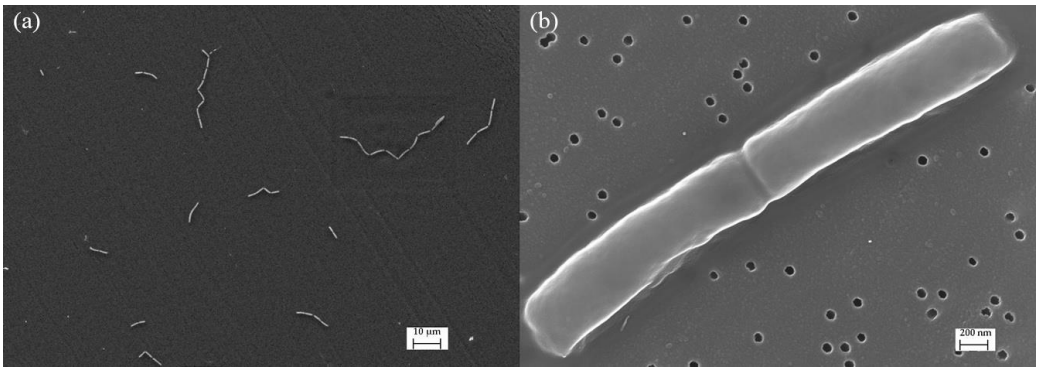

Figure 2.14: Detail of Bacillus subtilis in physiological solution, magnifications 2000x in panel (a) and 100000x in panel (b) (Massabò et al., 2018).

At ChAMBRe, bacteria concentration is monitored by a Wideband Integrated Bioaerosol Sensor (WIBS-NEO, Droplet Measurement Technologies Boulder, CO, USA). WIBS-NEO detects the fluorescent emission, due to biological fluorophores present in airborne microorganisms. Since bacteria have a typical fluorescence pattern (Hernandez et al., 2016), their signal can be distinguished from the inorganic particle background to quantify the airborne bacteria concentration.

A typical experiment proceeds as follow: bacteria are first cultivated on a non-selective Tryptic Soy Broth (TSB) until they are sufficiently grown, resuspension in sterile physiological solution (NaCl 0.9 %) and finally preparation of a suspension with an adequate concentration of CFU ml^{-1} (Colony Forming Units). The suspension is then nebulized inside ChAMBRe by using the SLAG (i.e., Sparging Liquid Aerosol Generator, by CH Technologies) nebulizer. After the bacteria, also soot particles are injected in ChAMBRe. Bacteria injection lasts 5 minutes and the concentration of injected bacteria turned out to be about 10^6 cell m^{-3} for the *E. coli* and 10^5 cell m^{-3} for the *B. subtilis* (measured by WIBS) pretty similar to the total average bacterial aerosol centration in near-surface air, over lands, which are estimated to be between 10^4 and 10^5 cell m^{-3} (Burrows et al., 2009). Soot injection lasts 1 minute and soot concentration inside chamber reaches 400 – 660 µg m^{-3} (measured by PAXs). MISG is fuelled with 70 mlpm of propane and 7 lpm of air. Experiments were at temperature in the range between 20 °C and 25 °C, atmospheric pressure and relative humidity around 60 %-70 %. This range of meteorological parameters was chosen to reproduce a suitable environment for bacteria survival, as reported in several works (Benbough, 1967; Cox, 1966; Dunklin and Puck, 1948). Injections time and atmospheric conditions inside the chamber are the same for all the experiments. Bacteria are collected by gravitational settling on four petri dishes, filled with an appropriate culture medium, placed in the bottom of the chamber through an automated shelf. The exposure time of bacteria to soot is of about 5 h, according to the lifetime in ChAMBRe of particles with diameter around 1 µm (Massabò et al., 2018). At the end of the experiment, the Petri dishes are extracted outside and incubated at 37°C overnight. The bacteria culturable fraction is determined by CFU visual counting. The gravitational settling method was adopted to minimize microbial damage (Aydogdu et al., 2010; Brotto et al., 2015; Xu and Yao, 2011). The living microorganisms in the aerosol were expected to settle down without suffering any stress apart from those related to the

permanence in the chamber atmosphere. In addition, losses due to particle bouncing were expected to be minimal due to low impaction velocity. In this way, the number of CFUs counted on a Petri dish was assumed to be proportional to the concentration of viable bacteria in ChAMBRe.

Possible effects of soot particles on bacteria viability are determined by comparison with baseline experiments performed in “clean” air, without the soot injection. These experiments are described in the PhD thesis “Assessment of the impact of atmospheric pollutants on bacteria viability by an atmospheric simulation chamber” by Silvia Giulia Danelli (cycle XXXIV, University of Genoa) so baseline results are not described here, but only cited as reference.

CHAPTER 3

Characterization of the MISG soot generator

Before the present work, a few partial characterization of the exhausts of MISG fuelled with ethylene (Kazemimanesh et al., 2019) and propane (Moallemi et al., 2019) were reported in literature. In this thesis an extensive classification of combustion conditions and resulting flame shapes was performed. The reproducibility and stability of soot emissions were investigated, focusing on number concentration and size distribution of soot particles and concentration of co-emitted gas species. Then, exhausts were characterized in terms of optical properties. Finally, optical and thermal-optical techniques were adopted to investigate particles collected on quartz fibre filters, thus determining the absorption coefficient b_abs, and their composition in terms of Elemental and Organic Carbon (EC and OC).

Most of the result discussed in this chapter were published in (Vernocchi et al., 2021).

3.1 Characterization of flame shapes

Different combustion conditions generate different flame shapes. Existing flames and investigated combustion conditions are discussed in Par. 2.1.2 and 2.1.3, here the results of flame observation are reported in Tables 3.1 and 3.2, for propane and ethylene respectively. Propane flow rates higher than 85 mlpm were not investigated due to instrumental limitation. It is noteworthy that no correlation could be found between global equivalence ratio (ϕ) and the shape of the corresponding flame. This means that the fundamental parameter describing the combustion process cannot be used to predict flame shape.

From this observation, combustion conditions to use in characterization experiments were selected (see Par. 2.1.3).

Table 3.1: Flame shapes observed for different combustion conditions of propane. Flames are identified as A – asymmetric, CB – Curled Base, CT – Closed tip, POT – Partially Open tip and OT – Open tip; FL indicates if flickering. The dash indicates that the flame does not ignite.

		FUEL flow [mlpm]											
		30	35	40	45	50	55	60	65	70	75	80	85
AIR flow [lpm]	2	A	A/FL	A	A/FL	A	CB/FL	CB/FL	CB/FL	CB/FL	CB/FL	CB/FL	CB/FL
	2.5	A/FL	A/FL	A	A/FL	A/FL	CB/FL	CB/FL	CB/FL	CB/FL	CB	CB	CB/FL
	3	A/FL	A/FL	A	A/FL	A/FL	CB/FL	CB/FL	CB/FL	CB/FL	CB/FL	CB	CB/FL
	3.5	A/FL	A	A	A	A	CB	CB	CB	CB	CB	CB	CB/FL
	4	A	A	A	A	A	CB	CB	CB/FL	CB	CB	CB	OT
	4.5	A	A	A	A	A	CB	CB	CB	CB	CB	CB	OT
	5	A	A	A	A	A	A/CB	CT	POT	OT	OT	OT	OT
	5.5	A	A	A	A	A	CT	CT	POT	OT	OT	OT	OT
	6	A	A	A	A	CT	CT	CT	CT	POT/OT	OT	OT	OT
	6.5	A	A	A	A	CT	CT	CT	CT	POT	OT	OT	OT
	7	A	A	A	A	A	CT	CT	CT	POT	POT/OT	OT	OT
	7.5	A	A	A	A	A	CT	CT	CT	POT	POT/OT	OT	OT
	8	-	-	A	A	A	CT	CT	CT	POT	POT/OT	OT	OT
	8.5	-	-	A	A	A	CT	CT	CT	POT/OT	POT/OT	OT	OT
	9	-	-	A	A	A	CT	CT	CT	CT	POT	OT	OT
	9.5	-	-	-	A	A	CT	CT	CT	CT	POT	OT	OT
	10	-	-	-	A	A	CT	CT	CT	CT	POT	OT	OT

Table 3.2: Flame shapes observed for different combustion conditions of ethylene. Flames are identified as A – asymmetric, CB – Curled Base, CT – Closed tip, POT – Partially Open tip and OT – Open tip; FL indicates if flickering.

		FUEL flow [mlpm]														
		30	35	40	45	50	55	60	65	70	75	80	85	90	95	100
AIR flow [lpm]	2	A	A	A	A	A/FL	A	A	A	CB	CB	CB	CB	CB	CB	CB
	2.5	A	A	A	A/FL	A/FL	A/FL	A	A	CB	CB	CB	CB	CB	CB	CB
	3	A	A	A	A	A/FL	A/FL	A	A	A/CB	CB	CB	CB	CB	CB	CB
	3.5	A	A	A	A	A/FL	A/FL	A	A	A/CB	CB	CB	CB	CB	CB	CB
	4	A	A	A	A	A	A	A	A	A	A/CB	CB	CB	CB	CB	CB/OT
	4.5	A	A	A	A	A	A	A	A	CB	CB	CB	CB	CB/OT	CB/OT	CB/OT
	5	A	A	A	A	A	A	A	A	CB	CB	CB	CB	CB/OT	CB/OT	CB/OT
	5.5	A	A	A	A	A	A	A	A	CB	CB/OT	CB/OT	CB/OT	CB/OT	CB/OT	CB/OT
	6	A	A	A	A	A	A	CT	CT	CT	CT/POT	CT/POT	POT	POT	OT	OT
	6.5	A	A	A	CT	CT	CT	CT	CT	CT/POT	POT	POT/OT	POT/OT	OT	OT	OT
	7	A	A	A	CT	CT	CT	CT	CT/POT	POT	POT/OT	OT	OT	OT	OT	OT
	7.5	A	A	A	A	CT	CT	CT	CT	POT	POT/OT	OT	OT	OT	OT	OT
	8	A	A	A	CT	CT	CT	CT	CT/POT	POT	POT/OT	OT	OT	OT	OT	OT
	8.5	A	A	A	CT	CT	CT	CT	CT	CT/POT	POT	OT	OT	OT	OT	OT
	9	A	A	CT	CT	CT	CT	CT	CT	POT	OT	OT	OT	OT	OT	OT
	9.5	A	A	CT	CT	CT	CT	CT	CT	CT	POT	OT	OT	OT	OT	OT
	10	A	CT	CT	CT	CT	CT	CT	CT/POT	POT	POT/OT	OT	OT	OT	OT	OT

In literature, a similar characterization for the propane-fuelled MISG is reported in (Moallemi et al., 2019). Few differences occur especially in the transition range from

Closed tip to *Open tip* flames, probably due to differences in experimental setups. Also the subjectivity of the visual determination, that is user dependent, can lead to differences.

3.2 Comparison between propane and ethylene combustion exhausts

3.2.1 Size distribution

The reproducibility of MISG emissions was investigated, in terms of number concentration and size distribution of soot particles. For each selected combustion condition, four experiments were performed and values of total particle number concentration and mode diameter were recorded. Reproducibility was calculated as percentage ratio of standard deviation and mean value of each series of repeated experiments. For propane combustion, mode reproducibility resulted equal to 6 %, while total concentration showed a 16 % of reproducibility. Ethylene combustion reproducibility was equal to 4 % and 10 %, respectively for mode and total concentration.

Mean size distributions were determined for each combustion condition. To make all the experiments comparable, curves were normalized to the same injection time (i.e., 3 minutes). Retrieved size distributions of all the four series of experiments are shown in Fig. 3.1 and 3.2, for propane and ethylene respectively.

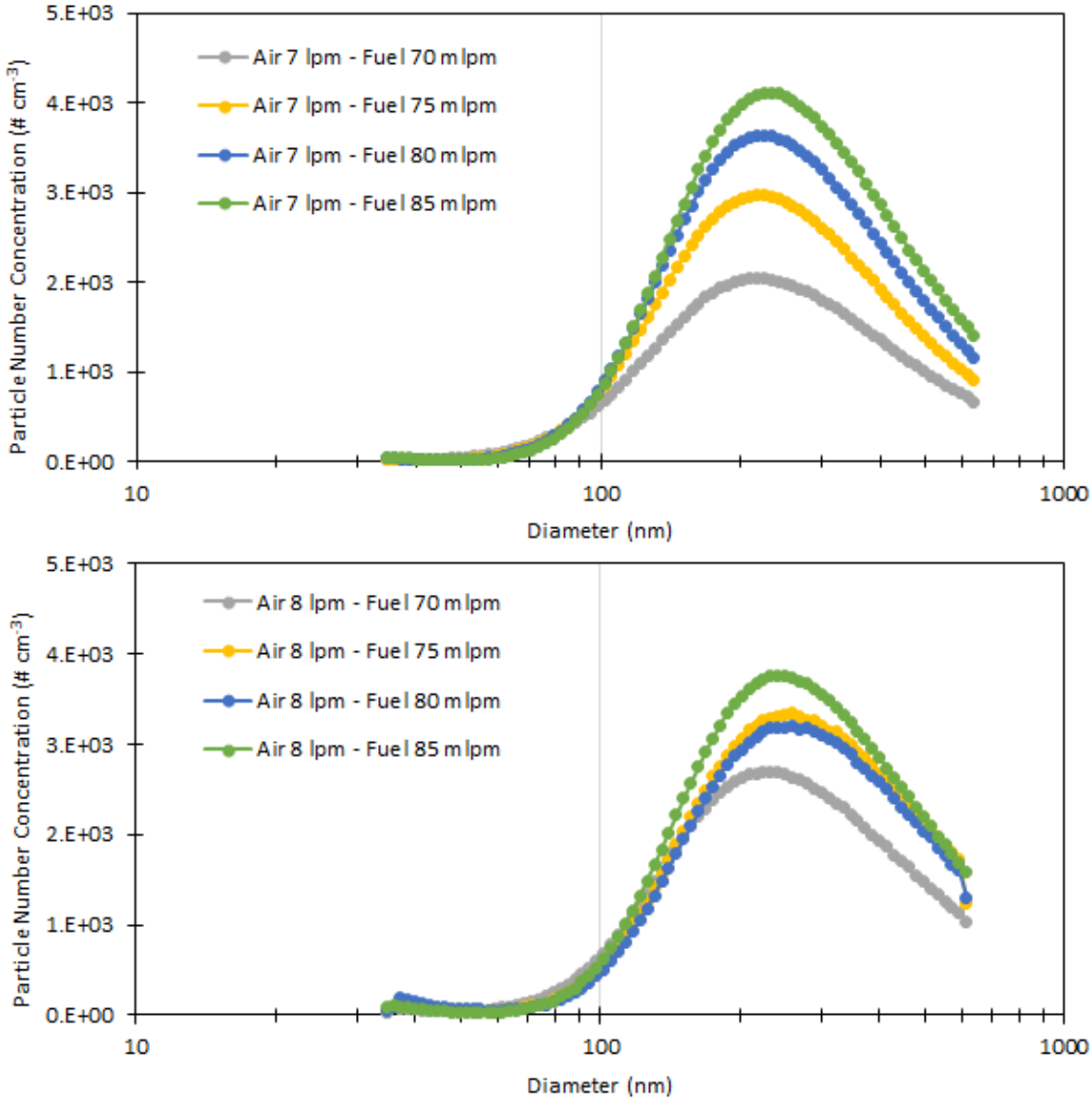

Figure 3.1: Mean size distributions measured by SMPS. MISG is fuelled with propane using air and fuel flows indicated in the plots frame.

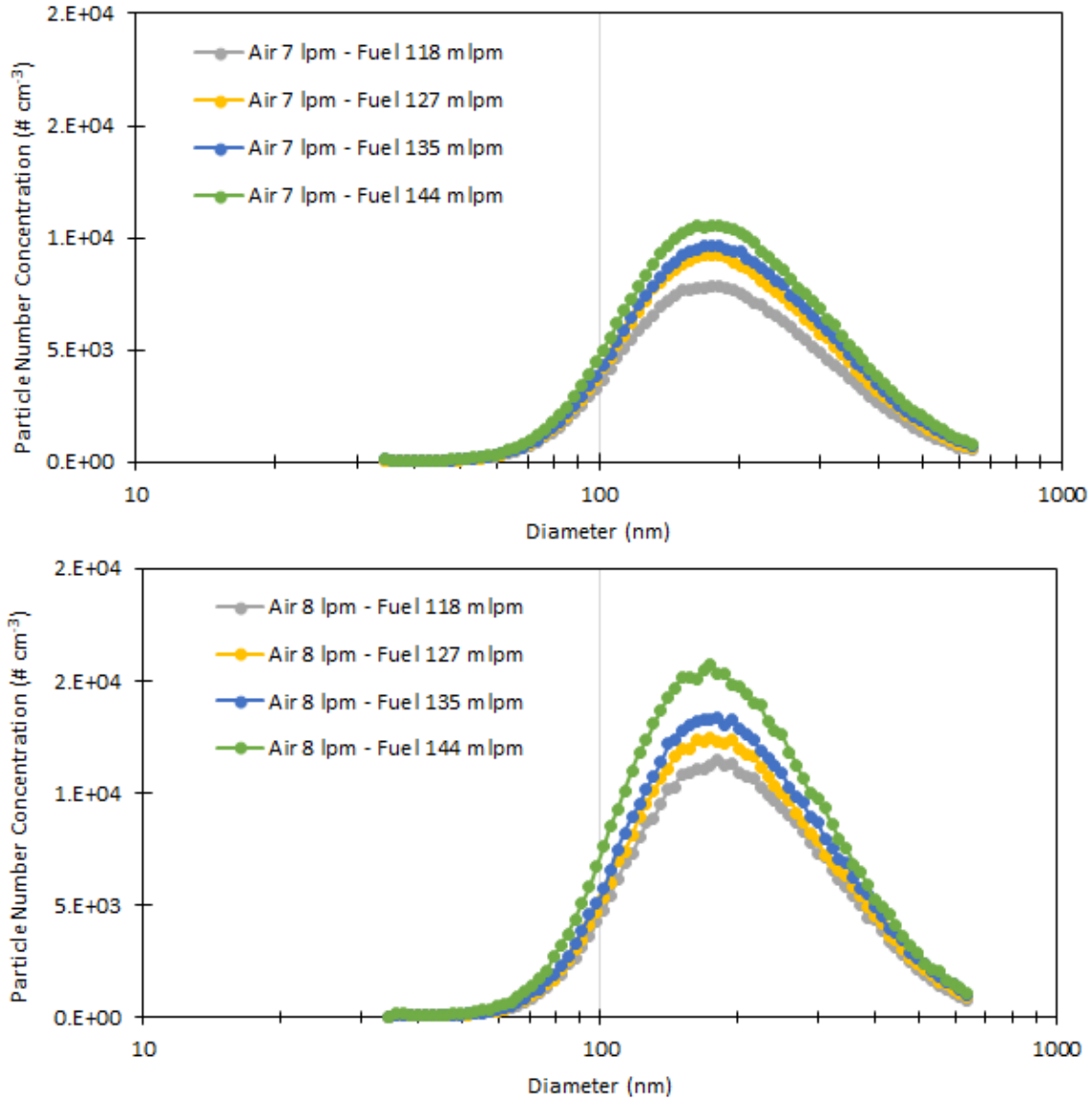

Figure 3.2: Mean size distributions measured by SMPS. MISG is fuelled with ethylene using air and fuel flows indicated in the plots frame.

Values of total particle number concentration resulted in the order of 10^5 particle cm^{-3} for both propane and ethylene. For a better comparison between different experiments, particle concentration values were normalized to the maximum value recorded during the whole set of tests; thus results vary in the 0 – 1 range. Normalized results are reported in Fig. 3.3 and can be summarized in few points:

- At fixed air flow, particle number concentration increased with fuel flow (i.e., with global equivalence ratio).

- For the same combustion conditions (i.e., same air flow and same global equivalence ratio), ethylene generated more particles than propane.

- At fixed fuel flow, particle number concentration increased with air flow, with a much larger effect on ethylene combustion.

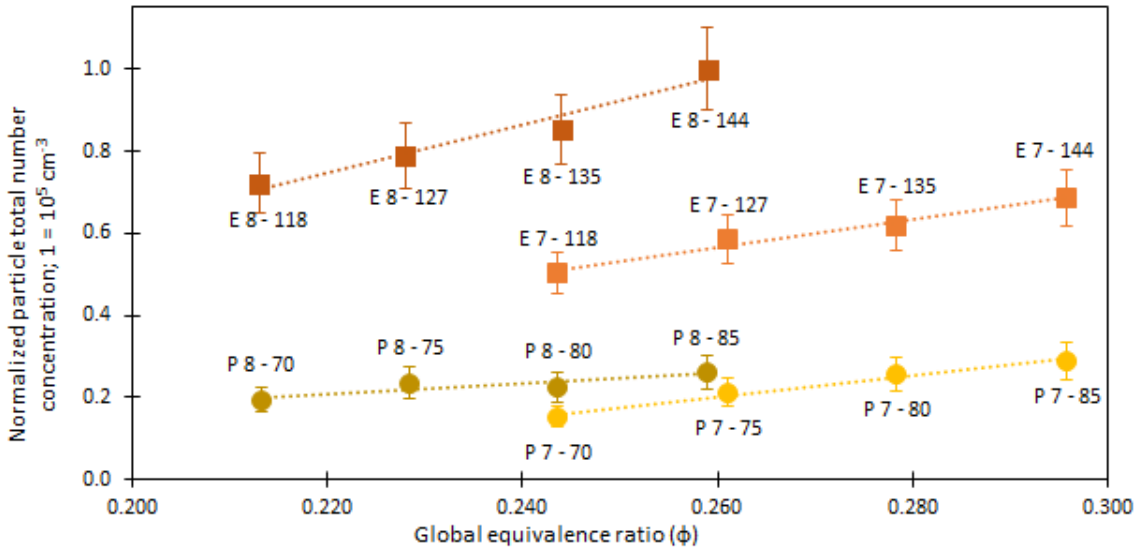

Figure 3.3: Particle number concentration vs. global equivalence ratio. Values are normalized to the highest of the whole set. Each point is labelled by E or P (ethylene or propane) and a pair of numbers indicating air and fuel flow, respectively in lpm an mlpm. Lines aim to facilitate the reader eye.

A similar representation is adopted to particle mode diameters, as shown in Fig. 3.4. Particle mode diameters resulted quite constant for ethylene and slightly increasing with air flow for propane (at fixed fuel flow). In addition, at fixed global equivalence ratio, MISG produced bigger particles when fuelled with propane. The mode diameters was about 180 nm for ethylene while ranged from 210 and 260 nm for propane.

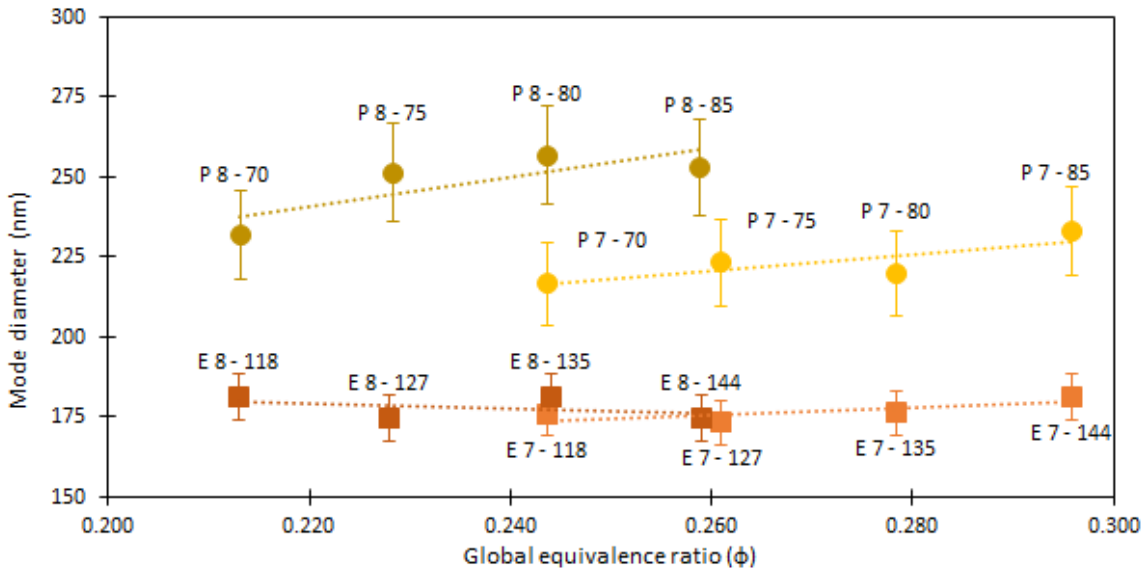

Figure 3.4: Particle mode diameter in function of global equivalence ratio. Each point is indicated by E or P (ethylene or propane) and a pair of numbers indicating air and fuel flow rate, respectively in lpm and mlpm. Lines aim to facilitate the reader eye.

Significant differences between the two fuels emerged when considering the super-micrometric range (i.e., diameter > 1 µm) of generated soot particles, measured by OPS: a number of big particles, likely super-aggregates, were produced by ethylene combustion. This behaviour was not observed with propane combustion. Results on particle number concentration, normalized to the total particle number concentration, are shown in Fig. 3.5.a. The super-micrometric fraction of total number particle concentration resulted to be about 3 % with ethylene and 0.2 % with propane. Particles larger than 4 µm were about 2 % with ethylene, and totally negligible with propane.

Considering the particle mass distribution (Fig. 3.5.b), the difference was enhanced: the super-micrometric fraction resulted about 99 % of total mass concentration for ethylene and only 9 % for propane. Particles larger than 4 µm were 98 % and 1 % of total mass (and hence of the soot concentration), for ethylene and propane respectively.

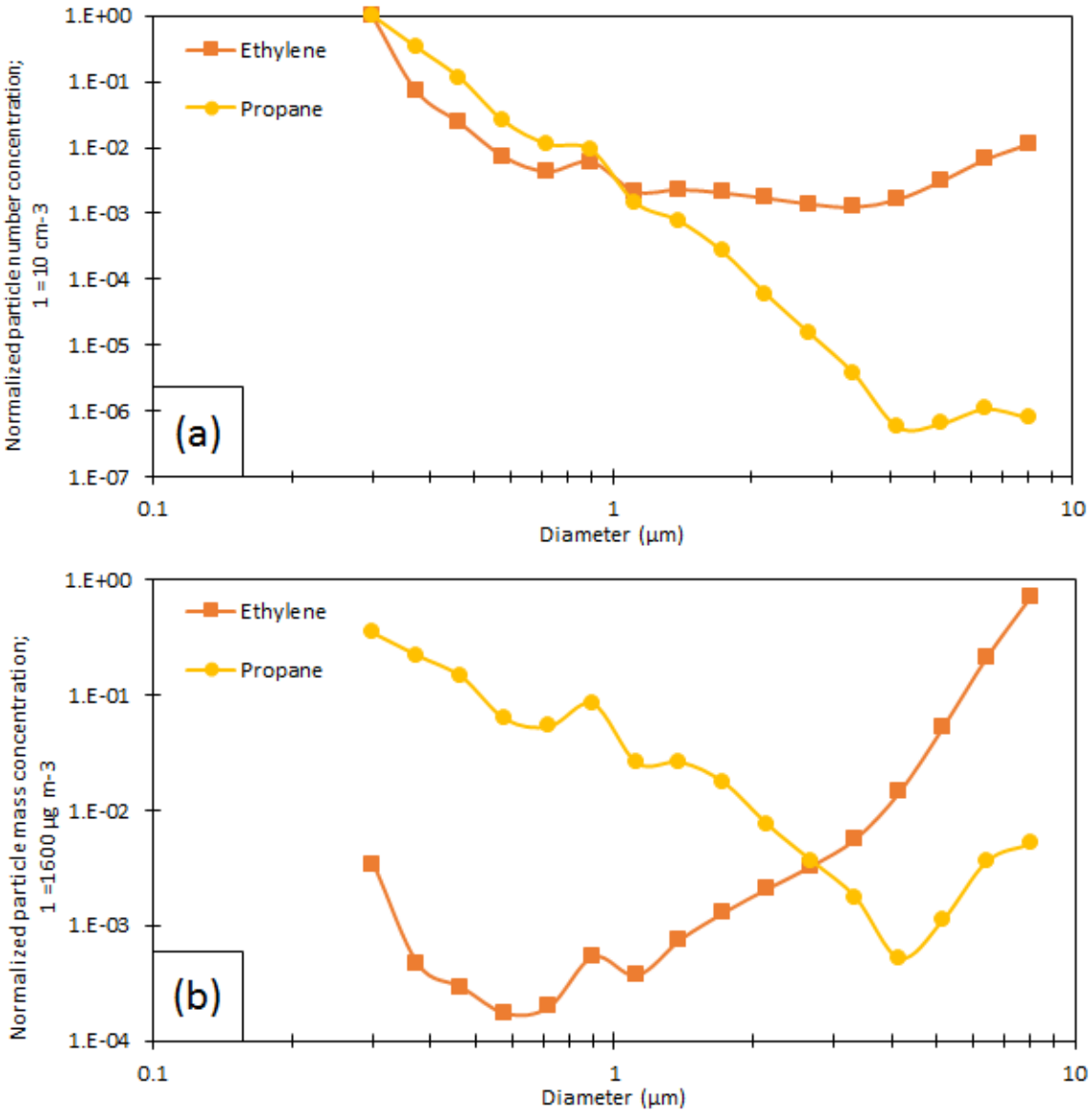

Figure 3.5: Particle concentration normalized to the total vs. particle diameter, measured by OPS, panel (a) shows number distribution, panel (b) shows mass distribution. MISG was fuelled with 7 lpm of air and 75 mlpm of fuel during propane experiment and 127 mlpm of fuel during ethylene experiment. No cyclone.

The super-aggregates probably formed in the stagnation plane at the bottom part of the combustion cell of the soot generator (Chakrabarty et al., 2012). In an up-side-down flame system, a stagnation plane formed at the lower end of the flame due to the buoyancy effect. Buoyant forces opposed to the flow forces creating a zero-acceleration plane of stagnation downstream from the flame zone (Bedat and Cheng, 1995). The aggregate residence time is enhanced in the stagnation plane thus enhancing the growth mechanism of the aggregates (Jullien and Botet, 1987). The hypothesis of the super-aggregates formation in the stagnation plane was confirmed by dedicated experiments, performed

only for ethylene, with the setup specifically modified and fuelling the soot generator with the same flows used in Fig. 3.5 (i.e., 7 lpm of air and 127 mlpm of ethylene). Three different line lengths were used to connect the MISG to ChAMBRe; the "normal" line (i.e., the same used in Fig. 3.5) was 65 cm, "long" line was about 5 meters and "short" line was 30 cm. In addition, with the "normal" line, MISG exhaust was diluted just after the outlet of the generator, by adding an extra air flow; the ratio between dilution air and MISG generator was 4:1. Only the experiment with the longest line showed a significant decrease in particle concentration, probably due to the losses inside the pipe (see Fig. 3.6).

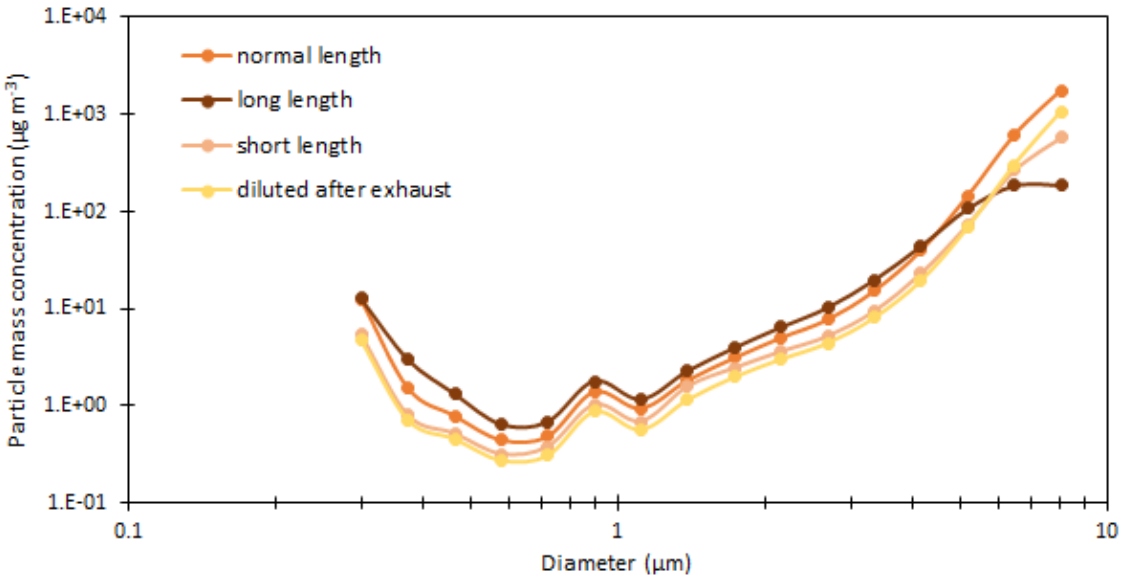

Figure 3.6: Comparison between mass size distributions measured by OPS. The MISG was fuelled with 7 lpm of air and 127 mlpm of ethylene.

Anyway, super-aggregates formation by ethylene combustion can be partly reduced by using lower air and fuel flow rates (see Fig. 3.7 for example).

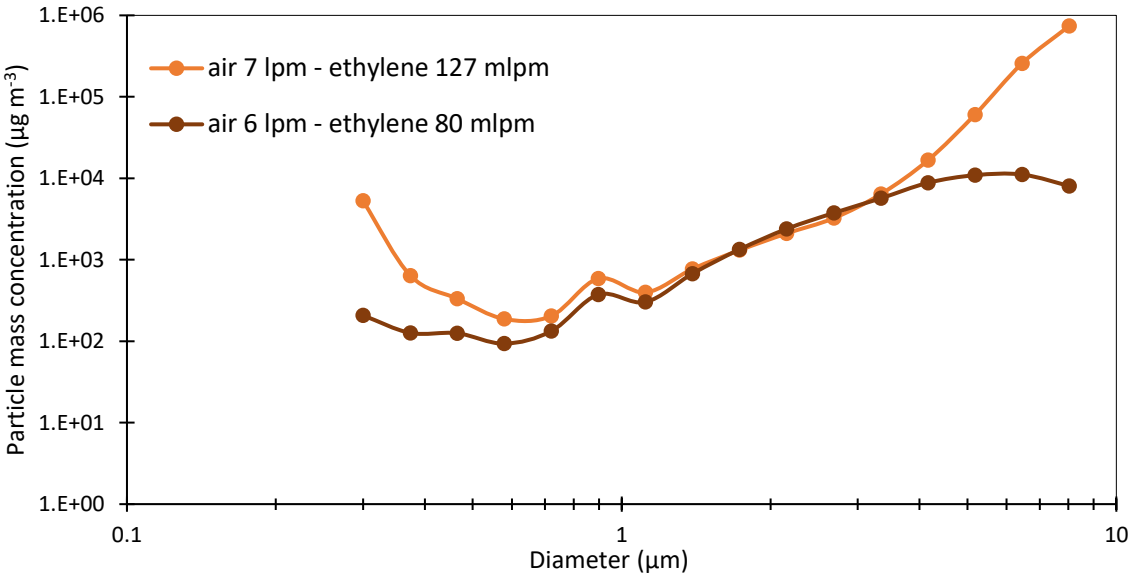

Figure 3.7: Comparison between mass size distributions measured by OPS.

The obtained results were compared with literature, in particular with (Kazemimanesh et al., 2019) for ethylene and (Bischof et al., 2019; Moallemi et al., 2019) for propane.

All the quoted works observed that particle number concentration increases, at equal air flow, with fuel flow. Even if they considered a lower range of global equivalence ratio, the behaviour was the same here reported. Both works reported, (Bischof et al., 2019) for propane and (Kazemimanesh et al., 2019) for ethylene, that particle mode diameter did not depend on the global equivalence ratio, this is congruent with ChAMBRe observations. However, (Moallemi et al., 2019) reported an opposite behaviour as they found that higher air flow, at fixed fuel flow, led to a slight decrease of the mode diameter. Lastly, (Bischof et al., 2019) and (Moallemi et al., 2019) obtained smaller particles than those observed in this work, in particular with a diameter smaller than 200 nm. This discrepancy could depend on differences in combustion conditions, since the experiments quoted in the literature works were performed at lower global equivalence ratios. (Kazemimanesh et al., 2019) observed super-aggregates formation but with smaller size (i.e., about 2 µm) than the observed in this work.

It should be noted that particles generated by both the fuels were larger than the typical exhausts of modern engines, such as aircraft and diesel vehicle engines, which emit ultrafine soot particles. In addition, soot concentrations inside the chamber were higher than the limit of atmospheric PM (Standards - Air Quality - Environment - European

Commission) of about ten times. Smaller particles and lower concentration will have to be used to better mimic real conditions.

Lifetime evaluation

Reaction time of atmospheric processes varies from few seconds up to several days, depending on kinetics. With experiments in an atmospheric simulation chamber is necessary that aerosols remain suspended for a long enough time to allow the chemical or biological interactions under investigation to occur. Lifetime inside chambers depends on a combination of several factors, among them diffusion and mixing processes, wall losses by adsorption or deposition, gravitational settling and obviously particle properties. Inside ChAMBRe, lifetime of particles with diameters from few hundreds of nm to few μm varies from 2 to 10 hours (Massabò et al., 2018).

Some experiments to evaluate soot particles lifetime (i.e., time after which concentration is half reduced) were performed, by using SMPS to monitor both particle size and concentration. Injected particles were left into ChAMBRe overnight. Soot particle lifetime was determined for the size of mode diameter (i.e., about 200 nm), fitting the respective concentration decay curve with a simple first order exponential law. Dilution caused by sample flow through instruments connected to the chamber volume was considered and corrected. The first time interval after each injection, when coagulation could take place, was excluded in the analysis, thus considering the concentration values smaller than 10^4 particle cm^{-3} only. The lifetime observed for the soot particles was of 2 hours, according to the wall deposition model described in (Lai and Nazaroff, 2000) and observations in (Massabò et al., 2018). The comparison of obtained lifetime with those in literature is shown in Fig. 3.8, reported also in terms of particle loss rate coefficient (β) that is the opposite of the lifetime.

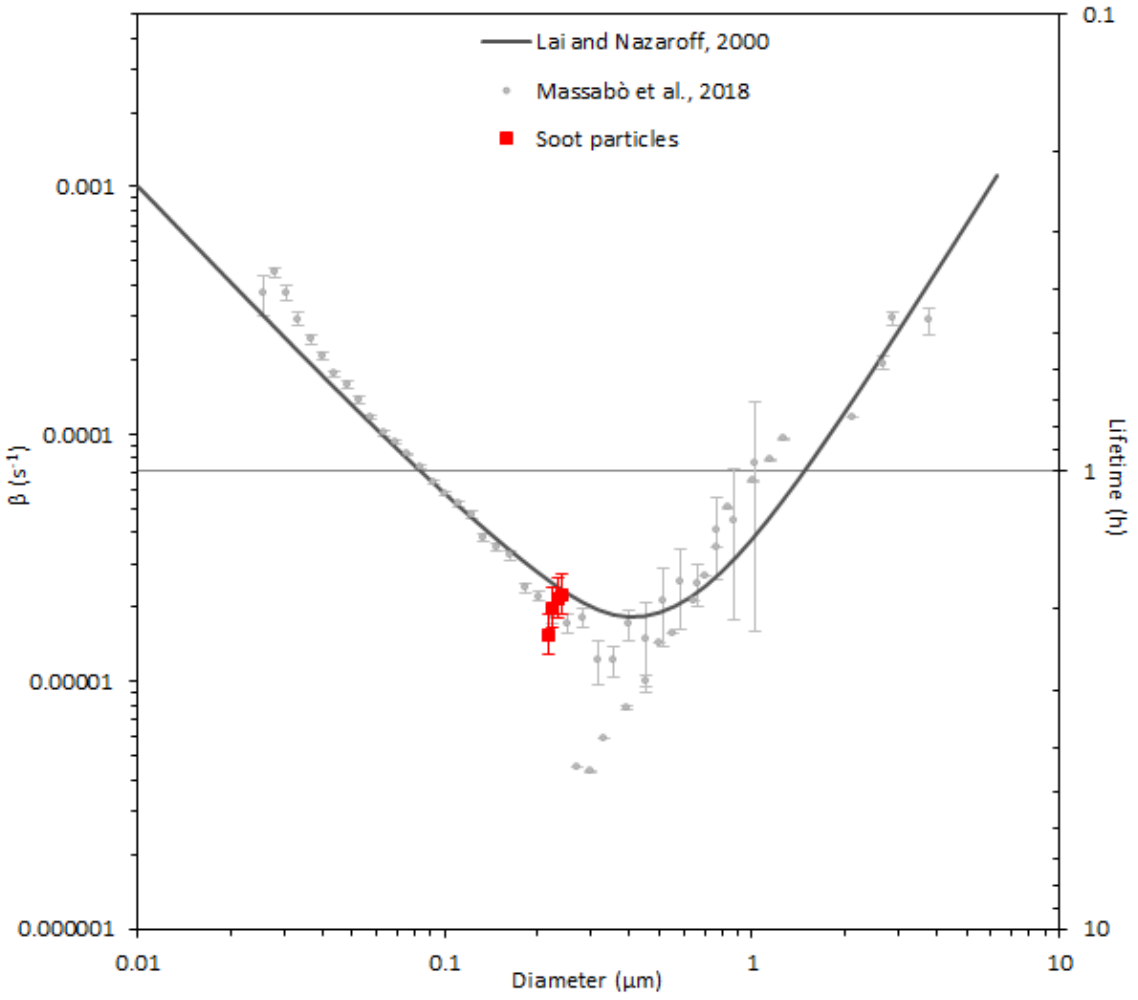

Figure 3.8: Particle loss rate coefficient (β) and lifetime (secondary vertical axis), vs. particle size measured in ChAMBRe.

3.2.2 Gaseous exhausts

Several gas monitors were connected to ChAMBRe (see Par. 2.2.1), however focus of gaseous exhausts was on CO_2 and NO, since they were the most abundantly emitted gas species. CO_2 is a typical gaseous product of combustion processes while NO emission seems to be typical of MISG, since it is not a typical combustion product.

As for size distribution, reproducibility was determined for gas concentration. Variability of CO_2 and NO production was about 2 % and 3 %, respectively with propane and ethylene. Comparison of gas concentration produced by ethylene and propane combustion was performed as the same way of total particle concentration, which means by normalizing to the maximum value recorded during the whole set of tests. Results are shown in Fig. 3.9 for CO_2 and Fig. 3.10 for NO. Both gases showed a similar behaviour: at fixed air flow,

gas concentration increased with the fuel flow; at fixed fuel flow, no significant change in gas emission was observed when varying the air flow. At equal operative conditions (i.e., same combustion conditions, injection time and time from the injection), gaseous emissions were higher with ethylene than with propane. CO_2 concentration values were similar for both ethylene and propane while NO concentration values were generally higher for ethylene. Maximum values were 360 ppm and 980 ppb, respectively for CO_2 and NO, after 3 minutes of soot injection, generated by 144 mlpm of ethylene and 8 lpm of air.

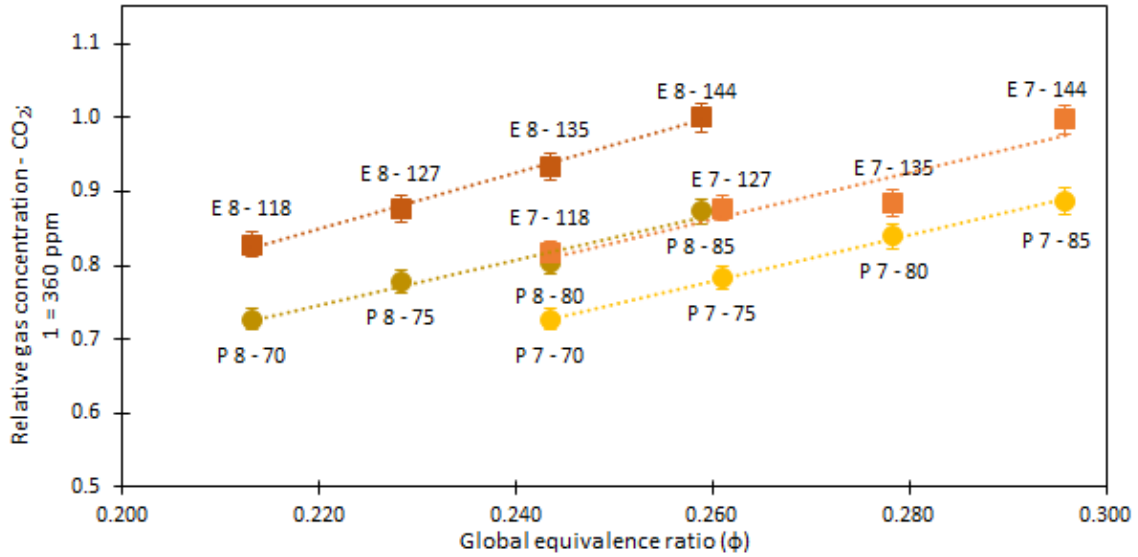

Figure 3.9: CO_2 concentration vs. global equivalence ratio. Each value is normalized to the highest of the whole set. Data points are labelled by E or P (ethylene or propane) and a pair of numbers indicating air and fuel flow, respectively in lpm and mlpm. Lines aim to facilitate the reader eye.

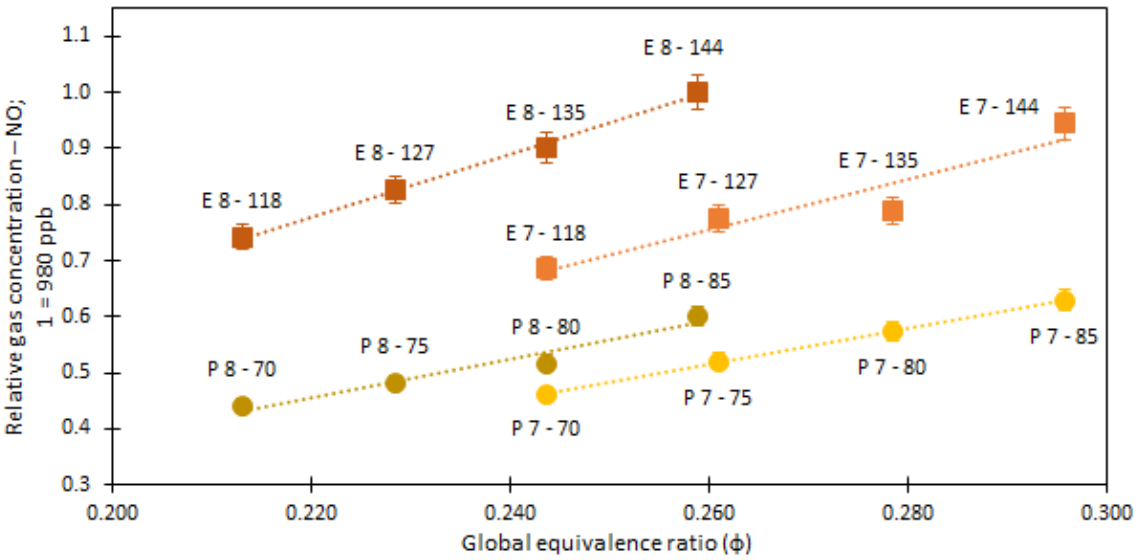

Figure 3.10: NO concentration vs. global equivalence ratio. Each value is normalized to the highest of the whole set. Data points are labelled by E or P (ethylene or propane) and a pair of numbers indicating air and fuel flow, respectively in lpm and mlpm. Lines aim to facilitate the reader eye.

3.2.3 EC/OC quantification

Elemental Carbon and Organic Carbon concentration values were determined by a thermal-optical analysis, performed by the Sunset EC/OC analyzer (see Par. 2.5.3) on soot particles collected on filters (see Par. 2.5). Reported data are the mean of measurements on three filters with different volumes of sampled air, opportunely normalized to the sampling volume.

The highest EC concentration was EC = 3517 µg m^{-3}: it was measured fuelling the MISG with 144 mlpm of ethylene and 7 lpm of air. EC concentration values were normalized to the highest value measured in the whole set of experiments, the resulting EC quantification is shown in Fig. 3.11. EC production was higher for ethylene than for propane combustion; it increased with fuel flow (at fixed air flow), for both ethylene and propane. Some differences between the two fuels appeared keeping fixed fuel flow: air flow rate variations did not seem to alter the relative EC concentration for propane (i.e., EC variation of about 10 %), while concentrations increased by decreasing air flow rate for ethylene (i.e., EC variation of about 40 %).

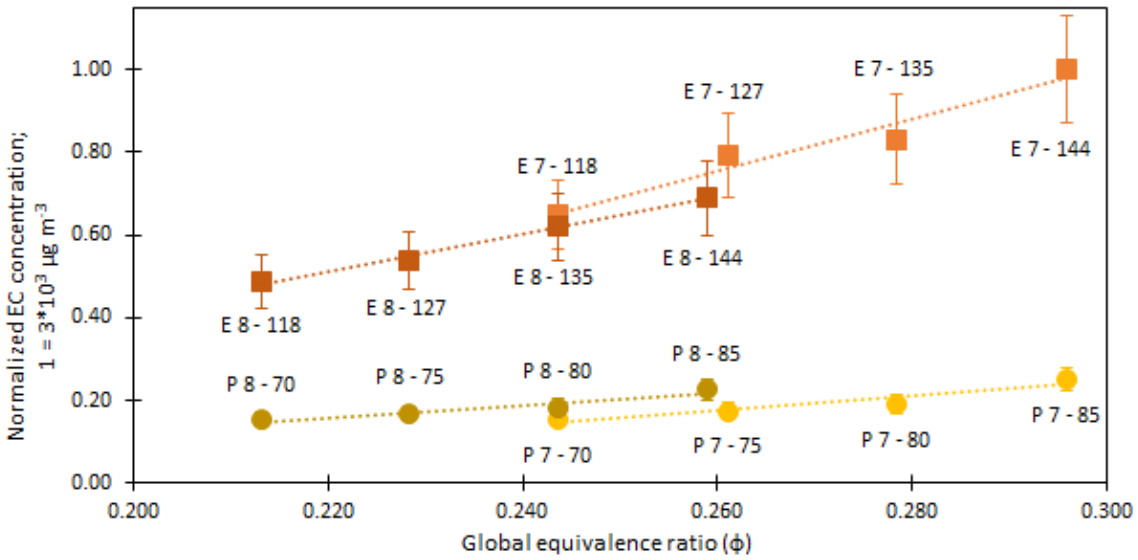

Figure 3.11: EC mass concentration vs. global equivalence ratio, each value was normalized to the highest of the whole set. Each point is labelled by E or P (ethylene or propane) and a pair of numbers indicating air and fuel flow rate, respectively in lpm and mlpm. Lines aim to facilitate the reader eye.

The EC:TC concentration ratio is reported in Table 3.3 for the four sets of experiments: in all the explored working conditions the MISG delivered a very high EC output.

Table 3.3: EC:TC ratio; mean values for experimental series without cyclone.

FUEL	AIR	
	7 lpm	8 lpm
PROPANE	0.69 ± 0.10	0.78 ± 0.05
ETHYLENE	0.89 ± 0.03	0.89 ± 0.07

The soot sampling was repeated inserting a cyclone unit upstream with respect to the filter: in this way only particles with diameter smaller than 1 µm were collected. In this configuration, the highest EC concentration, measured fuelling the MISG with 85 mlpm of propane and 8 lpm of air, was of 1480 µg m^{-3}. The whole set of EC concentration values, again normalized to the maximum value, are reported in Fig. 3.12. With the same combustion conditions (i.e., air flow and global equivalence ratio), EC concentrations were higher for propane than for ethylene, the opposite of the results obtained without cyclone.

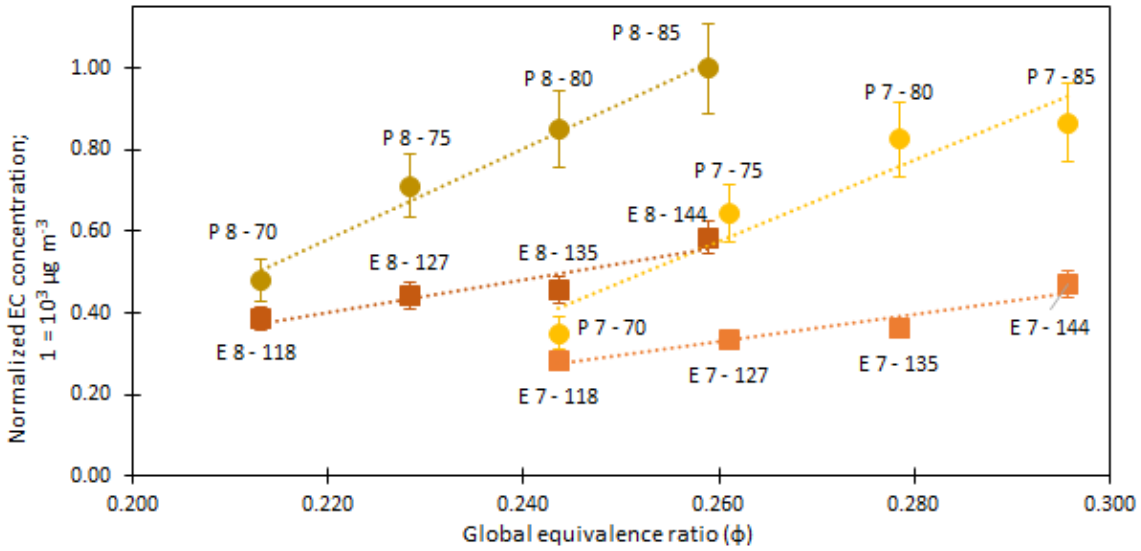

Figure 3.12: EC mass concentration vs. global equivalence ratio, each value was normalized to the highest of the whole set. Each point is labelled by E or P (ethylene or propane) and a pair of numbers indicating air and fuel flow rate, respectively in lpm and mlpm. Experiments were performed with cyclone, which removed super-micrometric particles. Lines aim to facilitate the reader eye.

The EC:TC ratio also showed some variations caused by the cyclone cut, as shown in Table 3.4. Values were around 0.8 with both fuels.

Table 3.4: EC:TC ratio; mean values for experimental series with cyclone.

FUEL	AIR	
	7 lpm	8 lpm
PROPANE	0.82 ± 0.07	0.85 ± 0.04
ETHYLENE	0.78 ± 0.05	0.82 ± 0.03

Actually, with ethylene about 40 % of the EC concentration was associated with particles larger than 1 µm. With both fuels, the EC:OC ratio increased with the global equivalence ratios whether the cyclone was present or not, in agreement with (Kazemimanesh et al., 2019) and (Moallemi et al., 2019).

In all the experiments, the OC:EC ratio varied between 0.1 and 0.3. It is noteworthy that the maximum OC:EC ratio always corresponded to the lowest fuel flow rate (i.e., 70 lpm with propane and 118 lpm with ethylene). Actually flames generated with low fuel flows were *Partially Open tip*, with a reduced production of soot particles, and hence EC, with

respect to *Open tip* flames. The OC:EC trend turned out to be in agreement with the observations of (Kazemimanesh et al., 2019; Moallemi et al., 2019).

Investigations on the volatile fraction of OC were performed by adding a backup filter behind the main filter during sampling. OC concentration on backup filters resulted compatible with organic contamination of not-sampled filters. Mean OC concentration for backup filters was 0.6 ± 0.2 μg cm^{-2}; mean OC concentration for 13 blank filters was 0.5 ± 0.2 μg cm^{-2}.

3.2.4 Optical properties

Optical properties of soot particles were determined in terms of absorption coefficient (b_abs). Measurements were performed both on-line inside ChAMBRe by PAXs (see Par. 2.4.1) and on sampled filters by MWAA analysis (see Par. 2.5.2).

Online analysis

Absorption coefficient values provided by PAXs with the cyclone impactor upstream were normalized to the total particle concentration measured inside ChAMBRe by SMPS during each experiment. Each b_abs value resulted from the average of 1-second data recorded for a specific time interval (i.e., 4 to 10 minutes). The normalized b_abs values are plotted in Fig. 3.13 vs the global equivalence ratio, for the three PAX units (i.e., λ = 870, 532 and 405 nm). The trend was similar for all the three wavelengths and for both the fuels. Absorption coefficient values did not show any dependence on global equivalence ratio, resulting almost constant. Soot particles produced by propane combustion were more absorptive than particles produced by ethylene. The picture was not so different when PAX data recorded removing the cyclone impactor were considered: particles from propane generation were still more absorptive, with a smaller gap from ethylene. Optical properties such as absorption depend on several parameters, mainly composition, mixing state, aging, and size. Considering all the experiments reported in this work, no differences in composition can be expected, since only EC particles were present: this means that differences in absorption cannot depend on particle composition. Also mixing state and aging cannot explain this difference: soot inside the chamber was fresh. We can explain the higher light absorbing capability of propane by considering differences in: size

distributions (see Figs. 3.1 – 3.4) and morphology/density of the particles produced by the burning of the two different fuels.

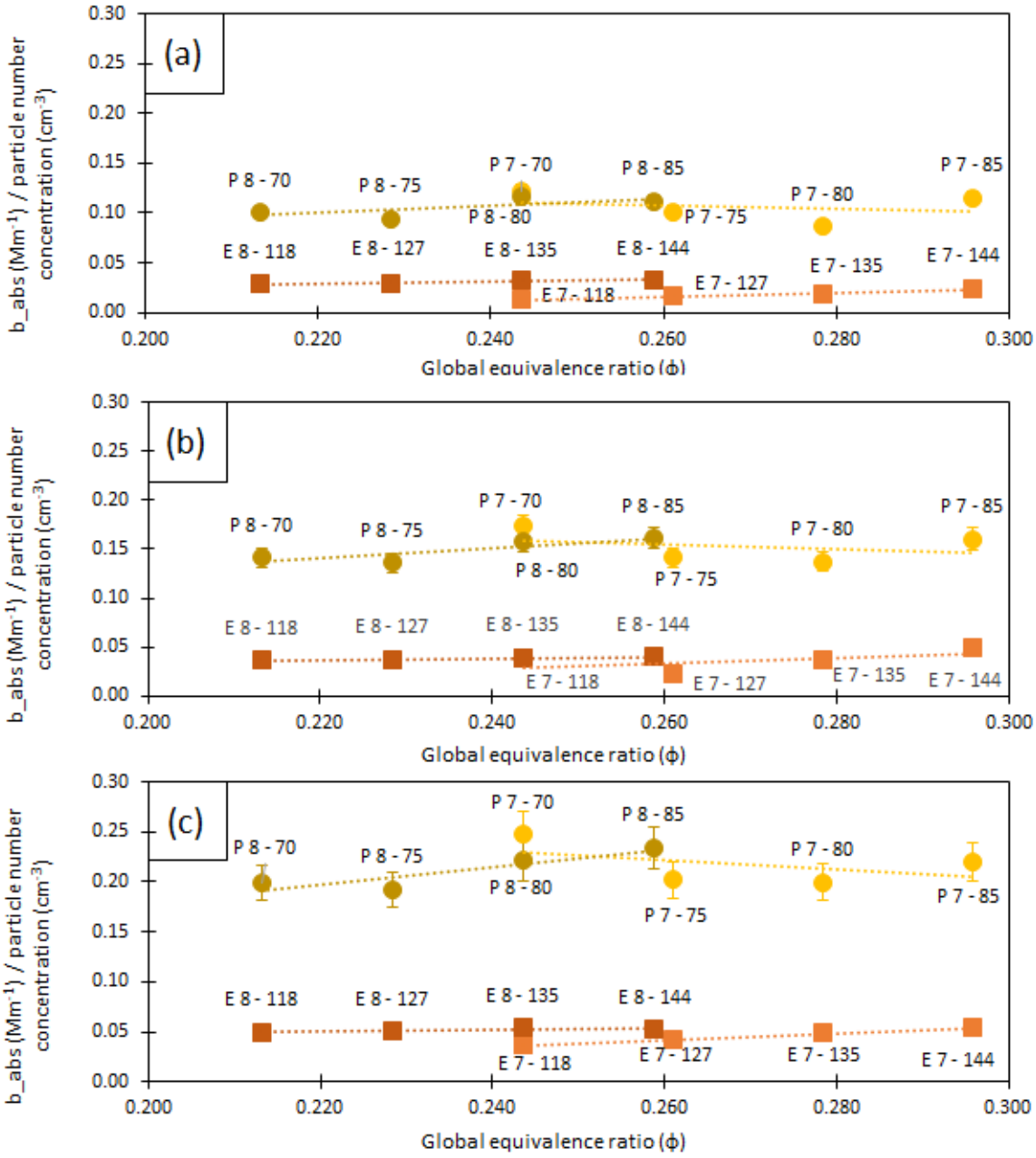

Figure 3.13: Absorption coefficient at λ = 870 (a), 532 (b) and 405 (c) nm, measured by PAXs vs. global equivalence ratio. b_abs values are normalized to total particle number concentration measured by SMPS in each experiment. Each point is labelled by E or P (ethylene or propane) and a pair of numbers indicating air and fuel flow, respectively in lpm and mlpm. Data refer to PM1. Lines aim to facilitate the reader eye.

About propane combustion emissions of MISG, in the literature are reported data for the IR-PAX in terms of Single Scattering Albedo (SSA). SSA values measured in this work varied

from 0.15 to 0.18, in agreement with those obtained by (Moallemi et al., 2019), which ranged from 0.15 to 0.25.

Mass Absorption Coefficient

The b_abs and EC data can be used to determine the MAC of the produced aerosol (see Par. 2.4). Such analysis can be performed both with the PAXS and MWAA b_abs values. Results of the MWAA are reported in Fig. 3.14, separately for propane and ethylene, in both cases without cyclone impactor upstream the filter. At all wavelengths, MAC values were higher for propane than for ethylene. MAC values were compatible with those previously reported in the literature for soot (Bond and Bergstrom, 2006).

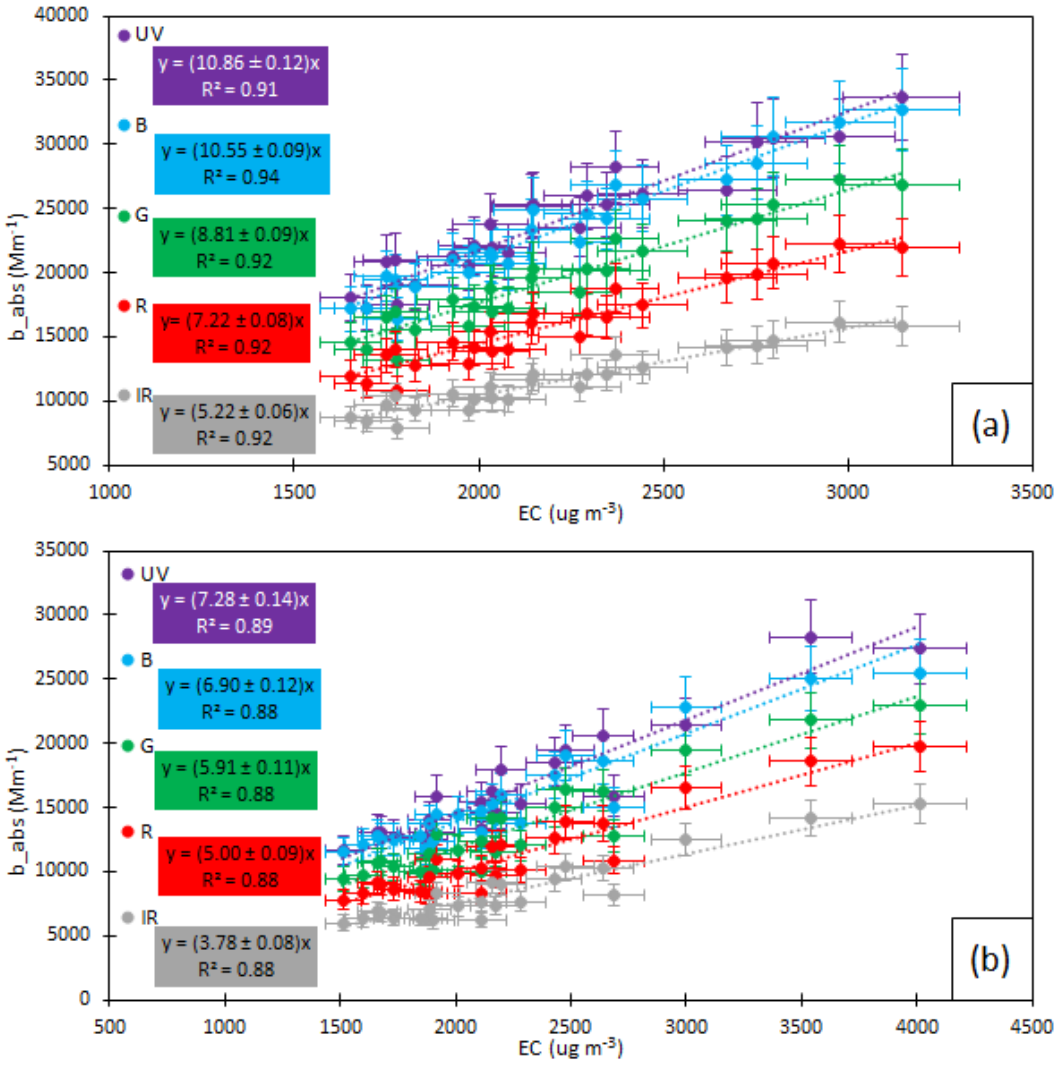

Figure 3.14: Absorption coefficient measured by MWAA vs. EC concentration measured by Sunset, for (a) propane and (b) ethylene. The slope of each fit corresponds to the Mass Absorption Coefficient, in $m^2\ g^{-1}$.

MWAA results with cyclone selection upstream the filter are reported in Fig. 3.15, separately for propane and ethylene. MAC values did not show any significant differences depending on the fuel.

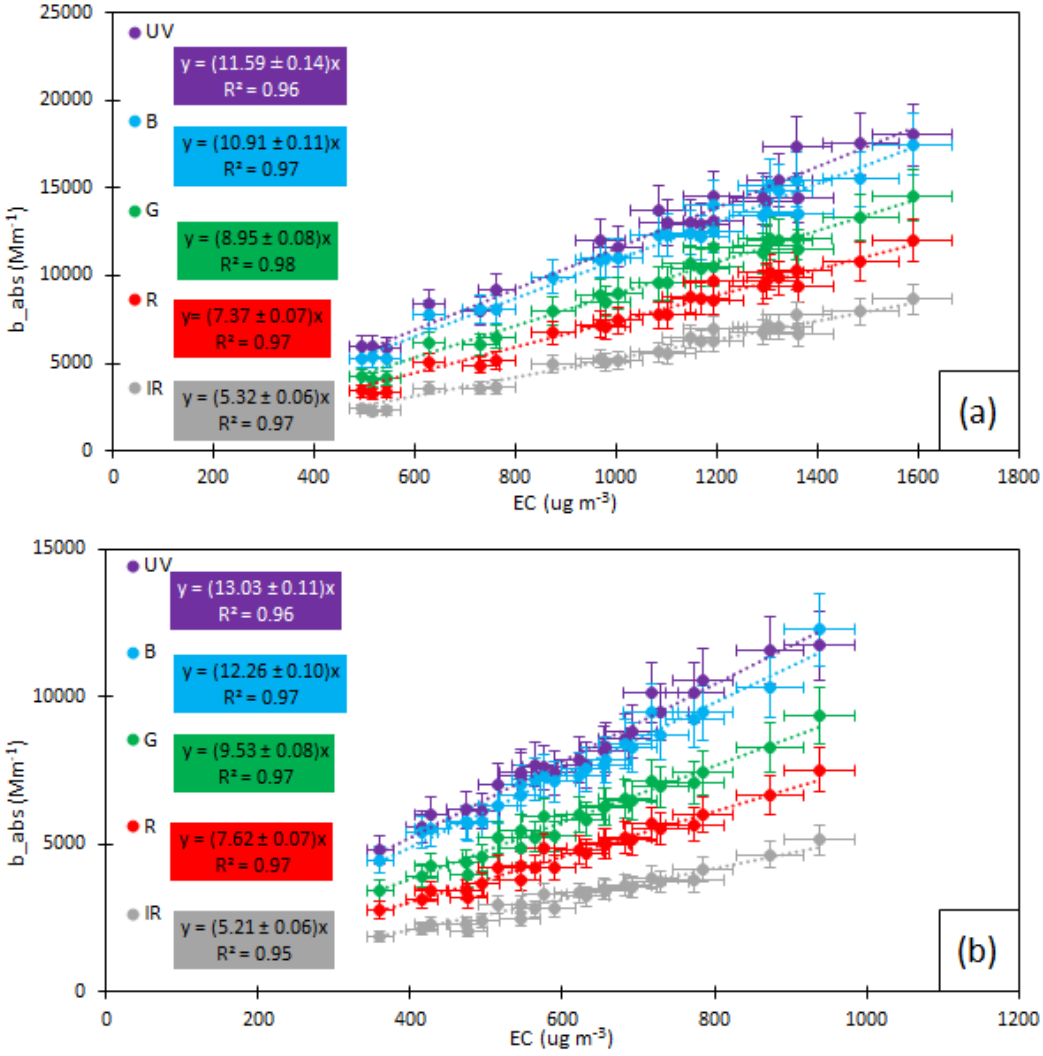

Figure 3.157: Absorption coefficient measured by MWAA vs. EC concentration measured by Sunset, for (a) propane and (b) ethylene. The slope of each fit corresponds to the Mass Absorption Coefficient, in $m^2\ g^{-1}$.

A summary of all the measured MAC values is given in Table 3.5. MAC values obtained with and without the cyclone selection were in substantial agreement except for those retrieved from data collected in ethylene experiments without cyclone. With both the fuels, MAC values increased when super-micrometric particles were removed by the cyclone. Lower MAC values were probably due to the presence of super-aggregates in the

atmospheric simulation chamber, because with equal mass, larger particles are less absorptive.

Table 3.5: Summary of MWAA measured Mass Absorption Coefficient values, in $m^2 g^{-1}$.

FUEL	MWAA				
	850 nm	635 nm	532 nm	405 nm	375 nm
PROPANE	5.22 ± 0.06	7.22 ± 0.09	8.81 ± 0.09	10.55 ± 0.09	10.86 ± 0.12
PROPANE with cyclone	5.32 ± 0.06	7.37 ± 0.07	8.95 ± 0.08	10.91 ± 0.11	11.59 ± 0.14
ETHYLENE	3.78 ± 0.08	5.00 ± 0.09	5.91 ± 0.11	6.90 ± 0.12	7.28 ± 0.14
ETHYLENE with cyclone	5.21 ± 0.06	7.62 ± 0.07	9.53 ± 0.08	12.26 ± 0.10	13.03 ± 0.11

Results of the PAXs are summarized in Table 3.6, for both the fuels and with/without cyclone. MAC values turned out higher in the series with cyclone and the ethylene series without cyclone showed the lowest MAC values for each wavelength, as observed with the MWAA analysis. PAXs data showed a higher variability in MAC values, especially depending on the use of the cyclone: MAC values measured by PAXs varied of about 35 % while those measured by MWAA of about 19 %. This was likely due to a higher PAXs sensitivity to particle size than filter based MWAA analysis.

Table 3.6: Summary of PAXs measured Mass Absorption Coefficient values, in $m^2 g^{-1}$.

FUEL	PAX		
	870 nm	532 nm	405 nm
PROPANE	5.30 ± 0.06	8.35 ± 0.08	10.55 ± 0.11
PROPANE with cyclone	6.27 ± 0.06	10.26 ± 0.06	13.48 ± 0.08
ETHYLENE	3.28 ± 0.15	4.92 ± 0.19	5.89 ± 0.20
ETHYLENE with cyclone	5.41 ± 0.08	10.42 ± 0.12	15.74 ± 0.15

Discrepancies between MAC values obtained from PAXs and MWAA, for the same experiment, were compatible with the differences of measured b_abs values discussed below.

PAXs and MWAA comparison

The b_abs values measured by PAXs and MWAA are directly compared in Fig. 3.16. Only the three wavelengths shared by PAXs and MWAA (λ = 870/850, 532 and 405 nm) were

considered. The agreement between the two analytical techniques ranges from 1 % to 7 % and from 14 % to 25 %, without and with cyclone respectively.

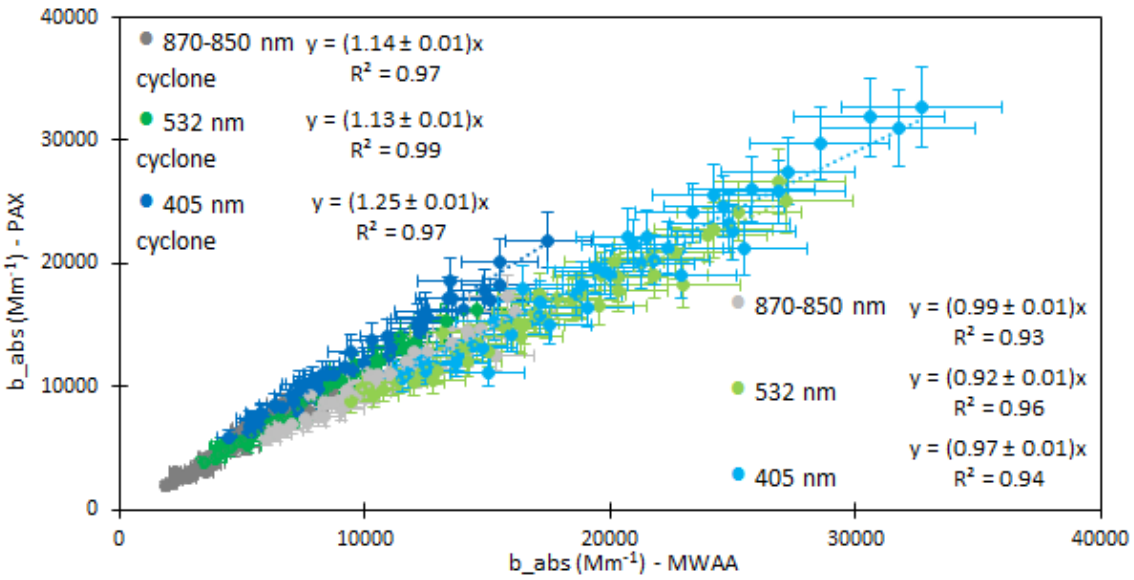

Figure 3.16: Correlation study between absorption coefficients measured by PAX and MWAA.

<u>Ångström Absorption Exponent</u>

Spectral dependence of b_abs and consequently the Ångström Absorption Exponent (see Par. 2.5.2) were determined, both for PAXs and MWAA datasets. The averages of the resulting AAEs for the different experimental conditions are reported in Table 3.7. The AAE values measured in this work for the MISG exhausts were generally close to 1.0, according to literature (Harrison et al., 2013), higher values were observed for the cyclone-selected aerosol. AAE values from ethylene showed a certain variability, depending on the presence of cyclone, while AAE values from propane were similar more stable.

Discrepancies between AAE values retrieved for PAXs and MWAA were compatible with the differences of b_abs values measured by the two analytical techniques.

Table 3.7: AAE values obtained in different experimental conditions by the analysis of PAXs and MWAA raw data.

EXPERIMENTAL CONDITIONS	AAE - PAX	AAE - MWAA
PROPANE 70 to 85 mlpm - AIR 7 lpm	0.88 ± 0.06	0.92 ± 0.04
PROPANE 70 to 85 mlpm - AIR 8 lpm	0.92 ± 0.06	0.91 ± 0.05
PROPANE 70 to 85 mlpm - AIR 7 lpm - cyclone	0.98 ± 0.09	0.99 ± 0.10
PROPANE 70 to 85 mlpm - AIR 8 lpm - cyclone	1.05 ± 0.04	0.97 ± 0.09
ETHYLENE 118 to 144 mlpm - AIR 7 lpm	0.93 ± 0.28	0.84 ± 0.08
ETHYLENE 118 to 144 mlpm - AIR 8 lpm	0.76 ± 0.04	0.81 ± 0.06
ETHYLENE 118 to 144 mlpm - AIR 7 lpm - cyclone	1.40 ± 0.05	1.19 ± 0.09
ETHYLENE 118 to 144 mlpm - AIR 8 lpm - cyclone	1.39 ± 0.04	1.08 ± 0.05

CHAPTER 4

Results

The soot characterization opens to various kinds of experiments in ASCs. Particles with well-known properties can be used to investigate the possible interactions between soot and other atmospheric pollutants (e.g., gaseous pollutants or bio-aerosol), the effects of meteorological variables (e.g., temperature and relative humidity) on soot properties and the oxidative and toxicological potential of soot particles.

To explore the potentiality of the coupling of soot generator with an atmospheric simulation chamber, preliminary experiments on the soot oxidative potential and toxicological effects as well on the interactions between soot particles and bacteria viability were performed.

4.1 Soot particles oxidative potential and toxicological effects

Characterized soot particles were collected on filters to be analysed for retrieving information on their oxidative potential and toxicological effects (see Par. 1.6). OP and toxicological analysis were performed at the Department of Pharmacological and Biomolecular Sciences of University of Milan and at the Chemistry Department of Sapienza University of Rome.

Four series of samples were produced and analysed:

- Soot particles generated by propane combustion and exposed to a clean atmosphere condition in ChAMBRe, that means no other pollutants introduced in the chamber volume. This is considered the *standard* condition. In the following, this series is referred as *P-std*.
- Soot particles generated by propane combustion and exposed to a condition in ChAMBRe of relative humidity in the range 80 – 90 %RH and ozone concentration ranging between 150 – 690 ppb. This is defined the *polluted* condition. In the following, this series is referred as *P-poll*.
- Soot particles generated by ethylene combustion and exposed to standard conditions. In the following, this series is referred as *E-std*.

- Soot particles generated by ethylene combustion and exposed to polluted conditions. In the following, this series is referred as *E-poll*.

Ozone has oxidant properties and it is responsible of atmospheric processing of several species (Li et al., 2005); previous studies reported the effects of ozonisation on soot physicochemical and toxicological properties (Daly and Horn, 2009; Han et al., 2012; Q. Li et al., 2013; Liu et al., 2010; Niranjan and Thakur, 2017), even if interaction mechanisms are still unclear (Zhu et al., 2019).

During both standard and polluted experiments, soot was injected inside ChAMBRe following the procedure described in Par. 2.2.2, using an air flow rate of 7 lpm and a fuel flow rate of 70 mlpm for propane or 118 mlpm for ethylene. For each series, three filters with different volumes of sampled air were collected, by using the cyclone (i.e., only the aerosol fine fraction was collected). Mean particle number concentration and mode diameter (both measured by SMPS) and BC concentration values (mean value of the three PAXs measurements) inside the ChAMBRe volume during each experimental series are reported in Table 4.1 and Table 4.2, for samples subjected to cellular and chemical assays respectively. Within each subset of samples, no significant differences were observed in particle concentration and size, hence excluding any possible dependence of effects on particle size or concentration. BC concentration values were used to determine BC mass on each sampled filter, multiplying the concentration itself by the sampled air volume.

Table 4.1: Mean particle number concentration, mode diameter and BC concentration values inside ChAMBRe during the experiments to produce samples submitted to cellular assays.

SERIES	PARTICLE NUMBER CONCENTRATION	MODE DIAMETER	BC CONCENTRATION
	# cm^{-3}	nm	ug m^{-3}
P-std	1.2E+05 ± 2.3E+04	179 ± 8	669 ± 71
P-poll	2.0E+05 ± 7.6E+04	169 ± 16	635 ± 95
E-std	1.5E+05 ± 3.0E+04	171 ± 9	462 ± 41
E-poll	1.8E+05 ± 5.3E+04	183 ± 4	457 ± 49

Table 4.2: Mean particle number concentration, mode diameter and BC concentration values inside ChAMBRe during the experiments to produce samples submitted to chemical assays.

SERIES	PARTICLE NUMBER CONCENTRATION # cm^{-3}	MODE DIAMETER nm	BC CONCENTRATION ug m^{-3}
P-std	1.1E+05 ± 2.3E+04	175 ± 6	634 ± 88
P-poll	1.7E+05 ± 6.3E+04	177 ± 10	597 ± 100
E-std	1.3E+05 ± 2.9E+04	173 ± 9	437 ± 54
E-poll	1.5E+05 ± 4.8E+04	179 ± 4	428 ± 58

It is the first time that a similar study has been carried out in the laboratory that hosted my PhD work, and the OP-TOX laboratories had not performed the assays on similar soot particles before. Therefore it was a preliminary and exploratory investigation, which certainly need to be improved. The match of PM properties and toxicology is a multidisciplinary growing branch of science, yet to be consolidated. Since the results discussed below were exploratory, in agreement with whoever performed OP-TOX analysis, the information obtained have to be considered interlocutory and qualitative.

4.1.1 Cellular assays

Three cellular assays were performed to evaluate oxidative stress (DCFH assay), cytotoxicity (MTT assay) and genotoxicity (MN assay) of soot particles (see Par. 1.6) on *BEAS-2B* cells (ATCC® CRL-9609™). *BEAS-2B* are epithelial cells of bronchial tract, extracted from a situation of no disease, this implies that they are representative of typical physiological responses. Results of all the assays are reported relative to a Control value (*C-value*) that is the assay response of cell not exposed to the pollutant agents (in this case the soot particles). No normalization for the volume of sampled air is applied.

Results disclosed below showed high variability among samples, and the interpretation is not so clear. It is known that these assays have many limitations and suffer of artifacts that produce false positives or false negatives (Holder et al., 2012; Le Hégarat et al., 2014). Some typical mechanisms of interfering are connected to the particle optical properties that can alter light absorption or fluorescence detection system (Pope and Dockery, 2006), as in MTT and DCFH assay. Even reactions between particles and assay compounds can be responsible for artifacts (Lighty et al., 2000). Since soot particles are strong light

absorber, they can induce artifacts confounding the results of the assays (Holder et al., 2012). Hence in view of this, caution is required in data discussion, in order to avoid any false cause-effect relation.

DCFH assay

DCFH assay is a marker of the oxidative stress induced by the exposure of cell to the pollutants. Cells were exposed to the soot for 30 minutes and for 1 hour. Response values higher than the C-value indicate a cell stress. The high variability of responses among samples could depend on the time delay between sampling and analysis. ROS are reactive and short-live components could be decayed before analysis (Bates et al., 2019; Fuller et al., 2014; Zhang et al., 2021).

After 30 minutes (Fig. 4.1.a) both the propane series showed a certain percentage of extra ROS production, without a dependence on the BC mass collected on filter. In particular, P-std series resulted in higher values than P-poll, suggesting that the ozonisation of soot particles reduced their ability to induce ROS production. For ethylene the scenario was apparently confused: the majority of the samples had responses lower than the C-value, suggesting that they did not induce any oxidative stress, however some values higher than the Control also appeared. E-std(27) sample showed the highest response, since it was significantly higher than the others, the presence of some artifacts was hypothesized. E-poll(56) was the only ethylene sample that induced ROS production, it shall be further investigated whether this is indicative of a BC-quantity threshold inducing oxidative stress on cell.

After 1 hour of cell exposure to soot particles (Fig. 4.1.b), the level of ROS production was decreased overall, if compared with the exposure of 30 minutes. This was because after a certain time the damaging effects pass to other targets, such as cell viability or DNA. The stress caused by the prolonged and/or high level of ROS exposure, typically induces blocks of the cell cycle progression (Gartel and Radhakrishnan, 2005) or apoptosis mechanisms (i.e., a form of programmed cell death) (Held, 2021). P-poll and E-std series responses were all lower than C-value, thus no extra ROS production was induced by soot particle exposure. P-std and E-poll values were correlated with the values of BC mass on filter, suggesting a dose-response relationship with a threshold value. Since this trend was observed only in certain situations, it needs to be further investigated.

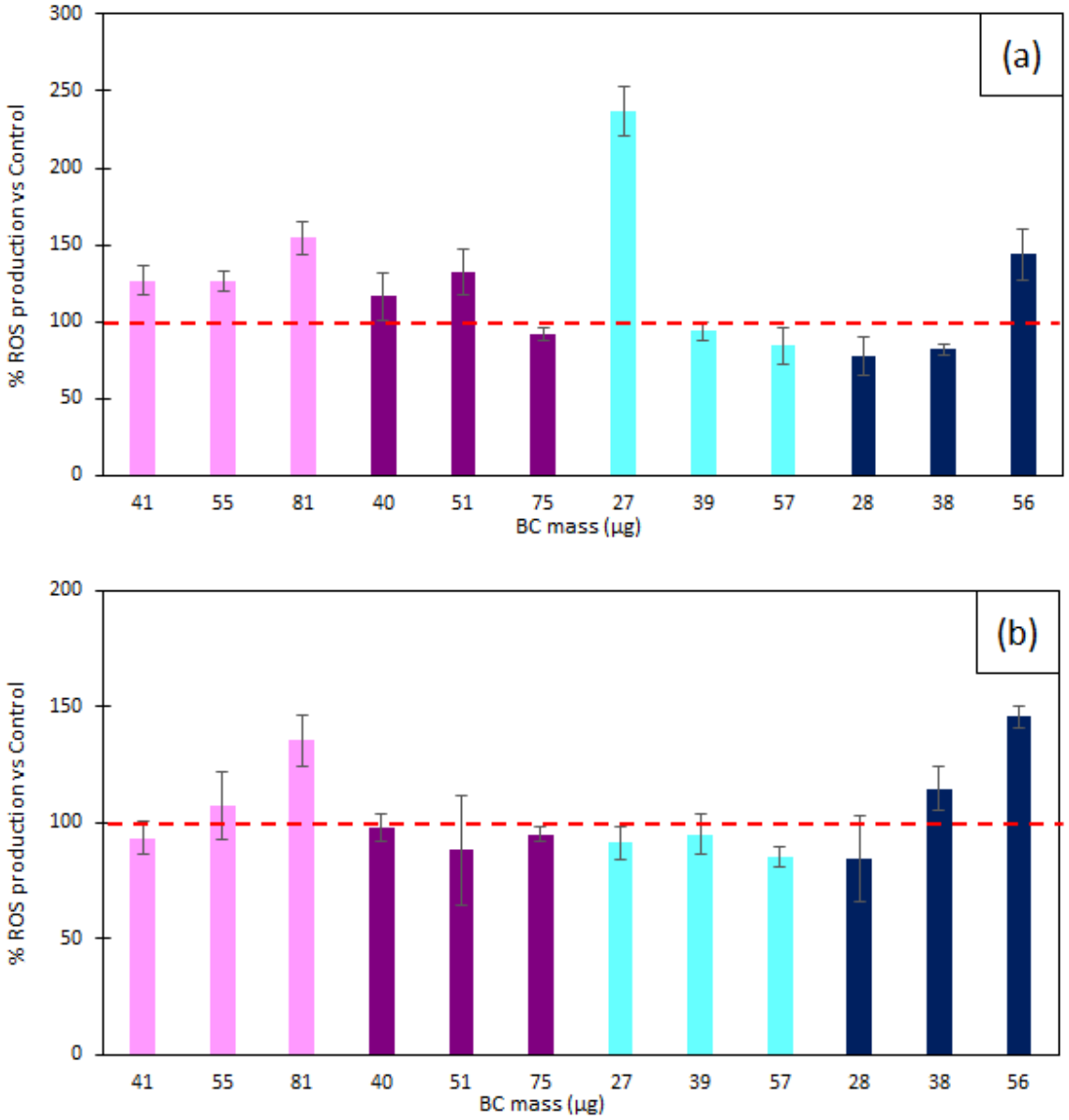

Figure 4.1: ROS production % vs. BC mass on filter. The red line indicates the Control value. Pink is for P-std series, purple for P-poll, cyan for E-std and blue for E-poll. Exposition time was 30 and 60 minutes, respectively for data in Panel (a) and (b).

MTT assay

MTT assay provides information on cell viability (i.e., cytotoxicity), cells were exposed to the soot for 24 hours (Fig. 4.2). Only P-std results were compatible with the C-value, while the other series showed a decrease in cell viability. Anyway, since the cell viability was still higher than the 80 % of C-value, the reduction is not so large to imply huge damages. With equal atmospheric conditions (i.e., standard or polluted), ethylene series showed a larger

decrease in cell viability despite lower values of BC mass on filters, so ethylene was supposed to generate more toxic particles than propane. Comparing standard and polluted series for the same fuel, the oxidised soot particles caused higher decrease of cell viability. Within each series, viability was not dependent on the BC mass collected on filter.

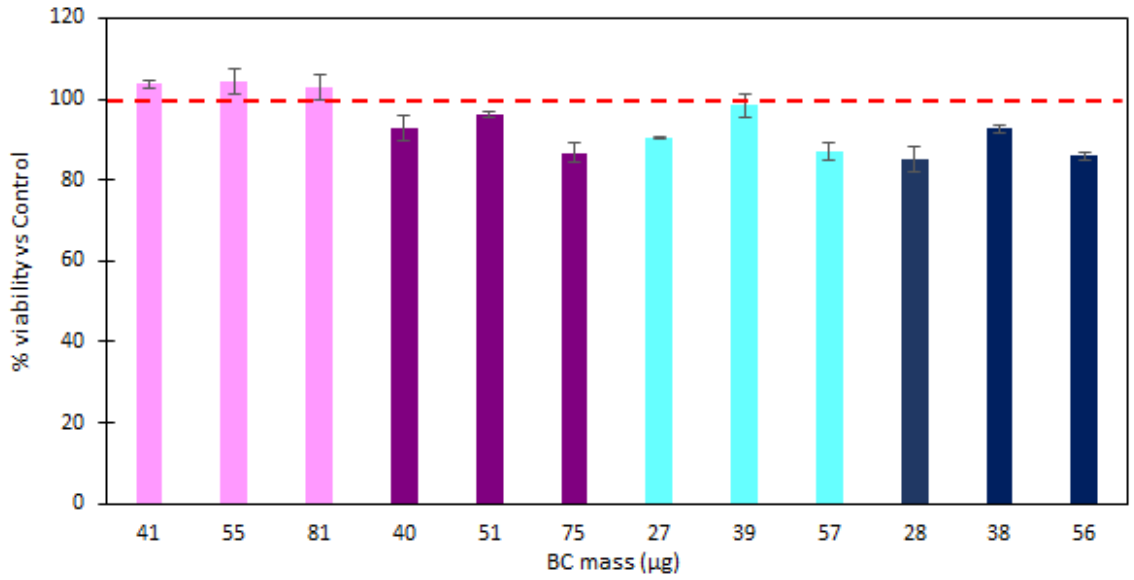

Figure 4.2: cell viability % vs. BC mass on filter. The red line indicates the Control value. Pink is for P-std series, purple for P-poll, cyan for E-std and blue for E-poll.

MN assay

MN assay evaluated genotoxicity (i.e., DNA damages) of pollutants, by counting micronucleous (i.e., extranuclear corpuscles generated by asymmetric cellular division due to DNA damages). Cells were exposed to the soot for 24 hours. DNA damages are more dangerous than oxidative and cytoxycal effects because they are transmitted with cellular reproduction without any possibility of being repaired by the cell. Response higher than C-value implies damages, even small increases have to be considered significant due to the dangerousness of DNA damages. Samples cannot be compared among them because they could have differences in cell viability, as depicted by MTT assay. This means that different responses to the MN assay can depend on real effects but also on the fact that the target was made of a different number of cells (i.e., cells could not respond to the assay because they were already dead).

All the samples showed a substantial formation of micronucleous (Fig. 4.3) suggesting that both ethylene and propane generated particle, ozonised or not, were able to induce DNA damages. Anyway, (Phillips and Arlt, 2009) reported that genotoxicity should be assessed by a certain number of tests, because no single assay can detect all genotoxic agents (Kirkland et al., 2003).

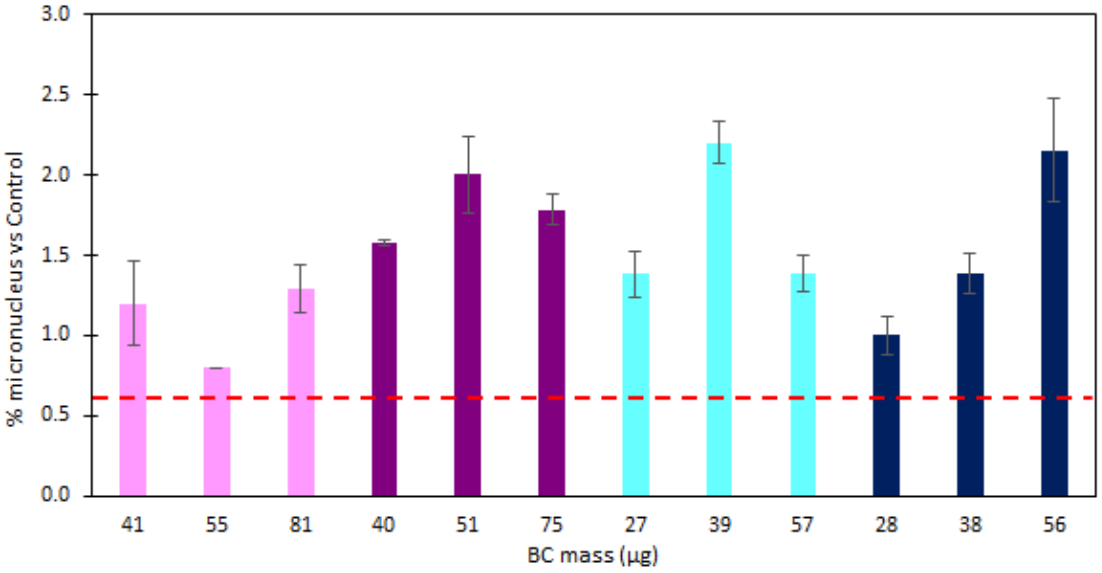

Figure 4.3: Percent of micronucleus within cells vs. BC mass on filter. The red line indicates the Control value. Pink is for P-std series, purple for P-poll, cyan for E-std and blue for E-poll.

The MN assay was the only test showing a significant response for all the samples (i.e., all the samples suggested an effect), this results suggests that soot particles generally could be responsible for direct than for indirect effects. Effects are defined as direct if exerted directly on DNA, affecting the cell ability of replication properly, or inducing alteration in the information carried by the DNA molecule. Effects are indirect if they manifest themselves as ROS production, inflammatory mediators or other mechanisms that not necessarily damage the DNA.

4.1.2 Chemical assays

Three chemical assays were performed to evaluate the oxidative potential of soot particles (see Par. 1.6): DTT, AA and DCFH are complementary assays since they are sensitive to different species but all them are marker of the same oxidative stress. DTT

and AA responses are expressed in terms of reagent depletion rate due to oxidation while DCFH data refer to concentration of H_2O_2, a typical ROS species. Higher assay responses correspond to higher oxidative stress effects.

Data obtained and here reported showed high variability among samples, probably due to the storage and delivery operations. Standardized experimental procedures are not yet available and several operating conditions influence responses of assays. Among them, sample storage time and conditions were confirmed to be a very critical issue (Frezzini et al., 2022). Another potential factor altering OP measurements is the time delay between filter sampling and OP analyses, that seems to induce an underestimation of particles OP, caused by a possible decomposition and/or chemical transformation of sampled PM (Campbell et al., 2019; Fuller et al., 2014; Hedayat et al., 2015). The high variability among samples made the results of difficult interpretation. No normalization for the volume of sampled air is applied.

DTT assay results are depicted in (Fig. 4.4.a). The sample P-std(52) showed a very different response respect the other samples of the same series, in particular it resulted compatible with zero. This let reasonably assume that some analytical issue occurred. It was not possible to repeat the measurement because the signal is time dependent and the retrieved result would not have been comparable with the others previously obtained. Therefore the sample P-std(52) was excluded from the data discussion. Anyway, E-std series resulted in higher OP than E-poll and the same behaviour was shown by propane series, suggesting a decrease of OP due to the particle ozonisation. Comparing equal exposure conditions (i.e., standard or polluted), soot generated by propane led to an higher ROS generation. It is noteworthy that BC mass on filters of the propane series were higher than those of ethylene series, on average. It shall be verified if the differences in DTT response depended on the BC amount or on particle properties.

Response to AA assay (Fig. 4.4.b) resulted very low and often compatible with zero. AA assay is particle-size dependent, with higher responses for the coarse fraction of PM (Perrone et al., 2019). Sampled particles involved in this work, belong to the fine fraction and this is probably why assay responses were so low.

In DCFH assay (Fig. 4.4.c), both propane and ethylene generated soot showed higher values for polluted than standard series, suggesting that soot ozonisation increased the OP. This result is the opposite of the DTT assay, the difference probably depended on the

different species sensitivity of the assays but it shall be deeper investigated. No significant differences were shown by propane and ethylene if the same exposure condition was considered.

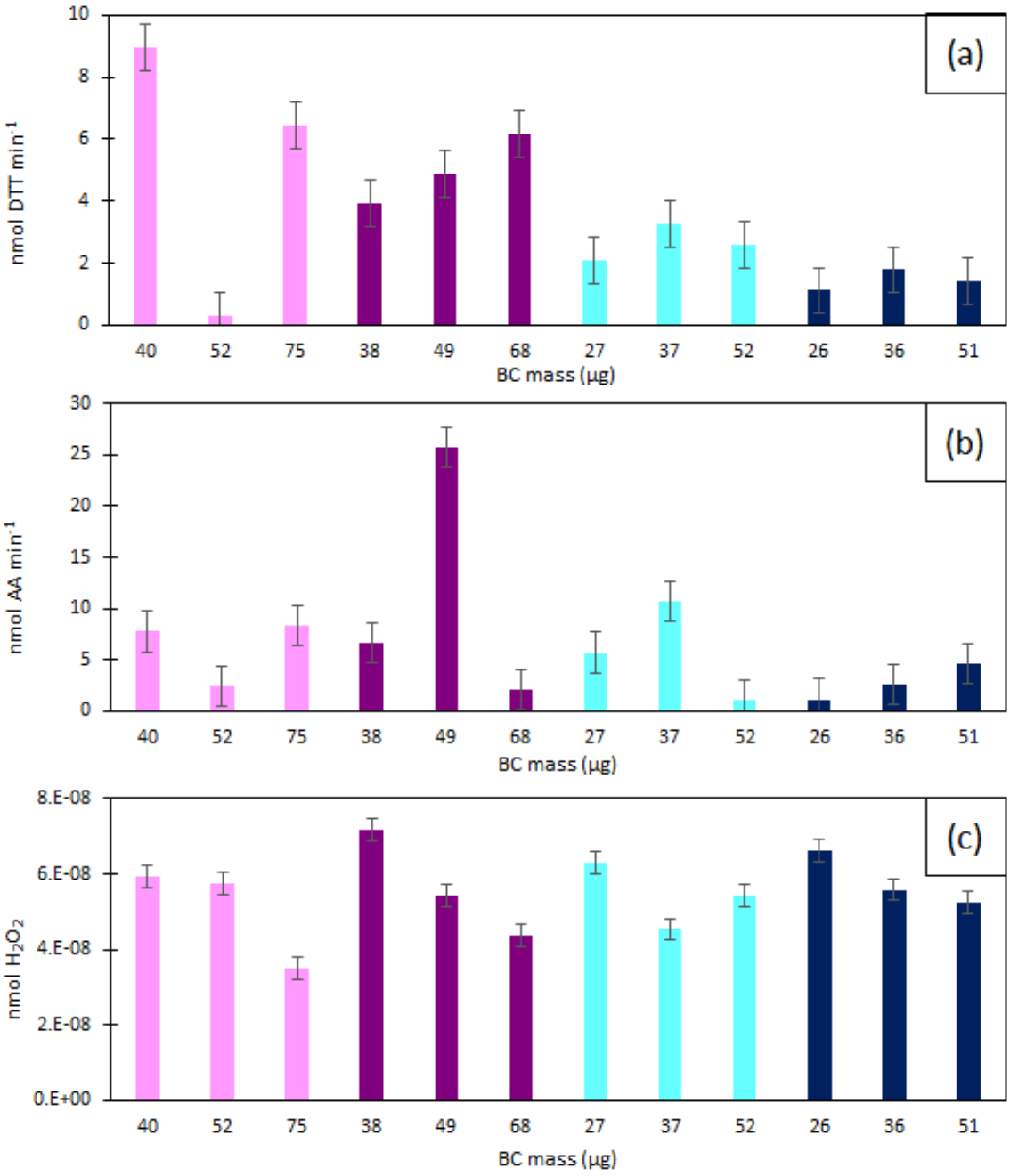

Figure 4.4: Results of DTT (a), AA (b) and DCFH (c) assays vs. BC mass on filter. Pink is for P-std series, purple for P-poll, cyan for E-std and blue for E-poll.

4.2 Soot particles and bacteria viability

It is reported in literature (Noda et al., 2021, 2019) that soot particles can have a primary toxic effects on bacteria, affecting their viability. The external layer of bacteria structure consists of a complex mixture of several compounds. Soot particle affinity for bacteria depends on the properties of this layer, leading to a specific selectivity (Noda et al., 2021). In this work, possible effects on bacteria viability due to the exposure to propane generated soot particles were investigated (see Par. 2.6).

Results are discussed in terms of bacteria viability changes in comparison with a set of "baseline experiments". During baseline experiments, bacteria were not exposed to pollutants, thus their viability depended on their characteristics and experimental procedures only. The baseline was retrieved by fitting results of several reproducibility experiments. Viability was determined by comparing the number of CFUs counted on the petri dishes and the concentration of bacteria injected inside chamber measured by WIBS (see Par. 2.6).

BC concentration values (average value of 1-second data recorded for 1 minute, starting 3 minutes after the injection, by IR-PAX) inside the ChAMBRe volume during experiments to evaluate the effects of soot on *E. Coli* viability are reported in Table 4.3.

Table 4.3: Mean BC concentration values inside ChAMBRe during the experiments to evaluate the effects of soot on E. Coli viability.

EXPERIMENT	BC CONCENTRATION ug m^{-3}
A	394 ± 1
B	529 ± 8
C	563 ± 7

E. Coli (Fig. 4.5) counts were comparable with the baseline values, suggesting that soot exposure did not affect their viability.

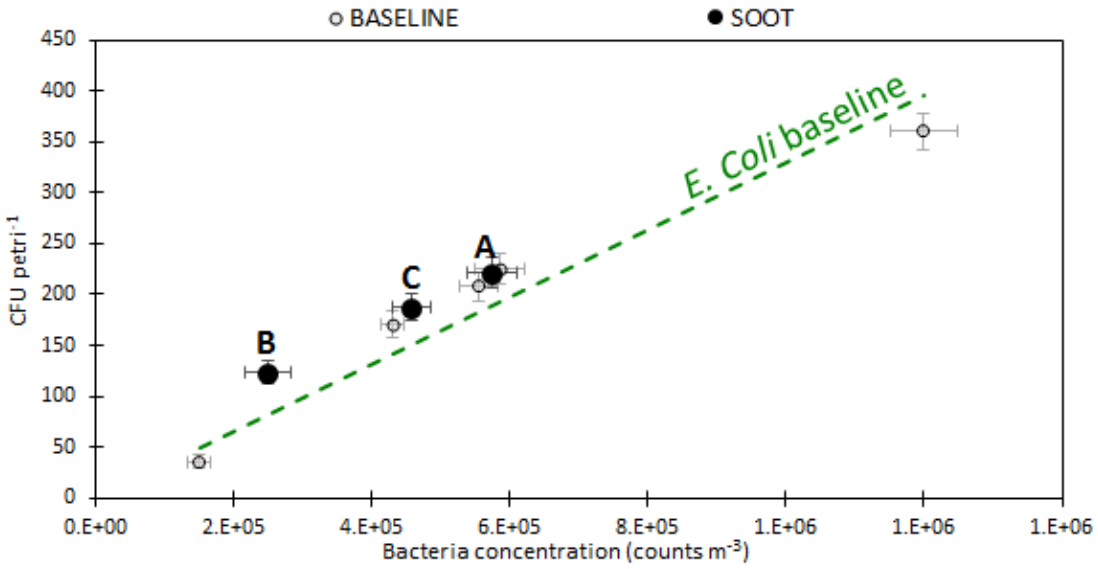

Figure 4.5: E. Coli CFUs collected on petri comparing with bacteria concentration inside ChAMBRe. The green line indicates baseline experiments, the letter indicates the experiment.

BC concentration values inside the ChAMBRe volume during the experiments to evaluate the effects of soot on *B. Subtilis* viability are reported in Table 4.4.

Table 4.4: Mean BC concentration values inside ChAMBRe during the experiments to evaluate the effects of soot on B. Subtilis viability.

EXPERIMENT	BC CONCENTRATION ug m^{-3}
A	420 ± 15
B	533 ± 8
C	553 ± 9
D	562 ± 7
E	588 ± 10
F	659 ± 10

B. Subtilis (Fig. 4.6) showed a more complex scenario, bacteria viability generally decreased even if data compatible with the baseline, or higher, also existed. Since most of the results were lower than the baseline values, a toxic effect on bacteria viability by soot can be reasonably supposed. However, data did not show any clear correlation between BC concentration and impact on bacteria viability.

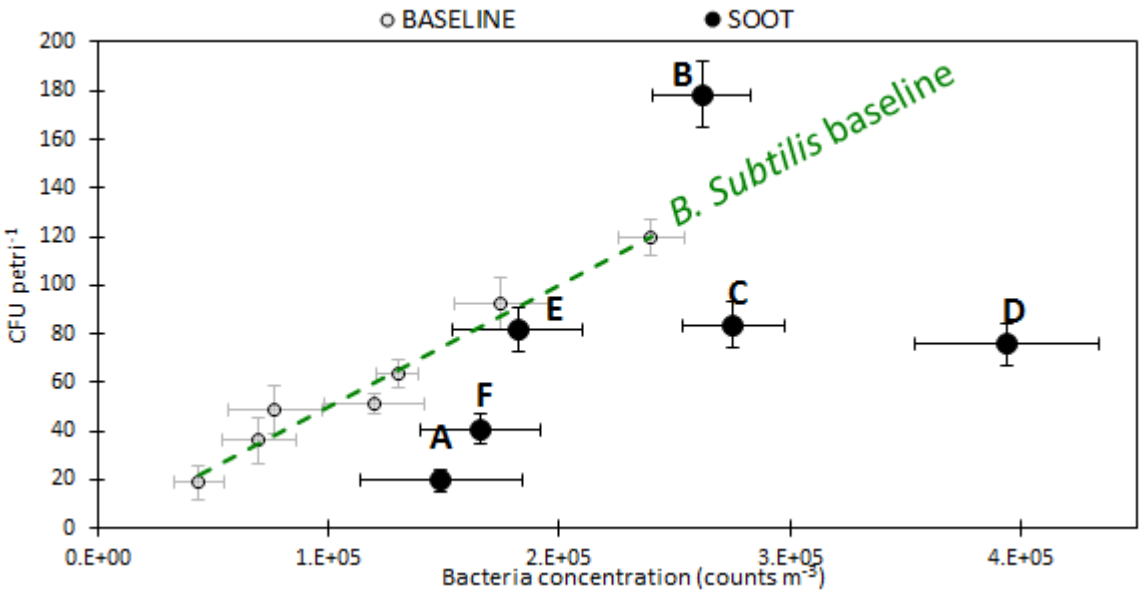

Figure 4.6: B. Subtilis CFUs collected on petri comparing with bacteria concentration inside ChAMBRe. The green line indicates baseline experiments, the letter indicates the experiment.

Soot generation also produces gaseous pollutants, in particular NO (see Par. 3.2.2), that can be responsible of the variations in viability. So, it will be necessary to determine if the negative effects are due to soot particles, to gases or to a combination of both the pollutants.

Differences in response between the two bacteria strains could be explained by their different Gram classification. Bacteria are classified as Gram-positive and Gram-negative depending on their response to the Gram staining procedure. Gram-positive bacteria retain Gram's stain while Gram-negative bacteria do not. The response to the test depends on the structural composition of the cell envelope, which is a complex multi-layered structure aiming to protect bacteria from the surrounding environment. The most relevant difference between the two groups is the presence of the outer membrane in the Gram-negative bacteria. The membrane is not present in Gram-positive bacteria, but they have thicker peptidoglycan layers (Silhavy et al., 2010). Both the structures are schematized in Fig. 4.7. The outer membrane is crucial to protect Gram-negative bacteria from external species; thus, Gram-negative bacteria are generally more resistant than Gram-positive bacteria (Breijyeh et al., 2020). *E.Coli* belongs to the Gram-negative group and *B. Subtilis* is Gram-positive. This could justify why *E. Coli* seems to be not affected by the exposure to soot particles while *B. Subtilis* results in viability variations.

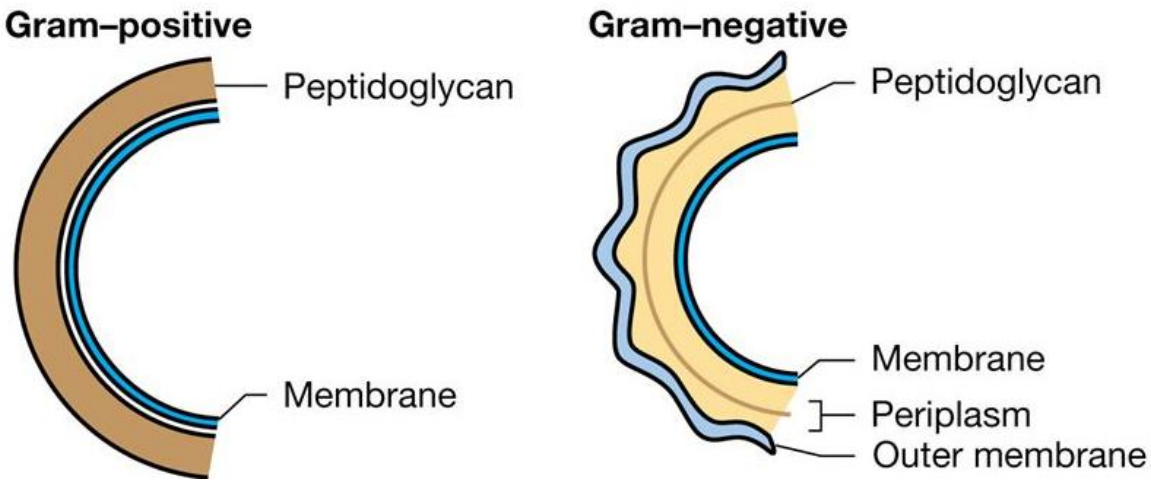

Figure 4.7: Layering of Gram-positive and Gram-negative cell envelopes.

In conclusion, these preliminary experiments led to interlocutory information, but potentially interesting, so it is clear the need of a deeper and systematic study. In addition, in this work the effects of fresh (i.e., just generated) soot particles were only investigated. Aging (i.e., oxidant) processes could make soot more reactive and thus with a different toxicity on bacteria viability. Effects of aged soot particles have to be considered for further studies.

Conclusions

The main objective of this thesis was to implement a setup and experimental procedures to perform systematic studies on/with soot particles by using a soot generator in conjunction with an atmospheric simulation chamber. In this context, a stable source of soot particles, the MISG, and the instruments to characterize them were identified. The methodological classification of combustion conditions led to the determination of the most interesting operative parameters. A dedicated protocol for systematic experiments in ChAMBRe was established and the soot generator was fuelled both with ethylene and propane and with different fuel-air ratios. Thus, MISG exhausts were characterized to determine their properties and highlight differences between the two fuels. The understanding of properties and behaviours of soot particles inside ChAMBRe paved the way to new and more complex experiments. For example, soot particles could be exposed and maintained in different atmospheric conditions to observe whether their properties encounter variations. In addition, effects on and interactions with other atmospheric pollutants could be investigated.

In this thesis work, two possible applications of MISG-generated soot particles were explored. In particular, soot particles exposed to different atmospheric conditions were used in preliminary studies on toxicological effects and dose-response assessment. In addition, a few experiments on the effect of soot particles on bacteria viability were also performed. Both the experiments gave interesting but interlocutory results that will require more in-depth analysis and systematic studies to be also designed as complement of in-field experiments.

In conclusion, this thesis work led to a substantial methodological development which made possible, within atmospheric simulation chambers, a new generation of experiments on carbonaceous aerosols and their effects.

Bibliography

Aammi, S., Karaca, F., Petek, M., 2017. A toxicological and genotoxicological indexing study of ambient aerosols (PM2.5-10) using in vitro bioassays. Chemosphere 174, 490–498. https://doi.org/10.1016/j.chemosphere.2017.01.141

Abbas, I., Garçon, G., Saint-Georges, F., Andre, V., Gosset, P., Billet, S., Goff, J.L., Verdin, A., Mulliez, P., Sichel, F., Shirali, P., 2013. Polycyclic aromatic hydrocarbons within airborne particulate matter (PM2.5) produced DNA bulky stable adducts in a human lung cell coculture model. Journal of Applied Toxicology 33, 109–119. https://doi.org/10.1002/jat.1722

Ackerman, A., Toon, O., Stevens, D., Heymsfield, A., Ramanathan, V., Welton, E., 2000. Reduction of Tropical Cloudiness by Soot. Science (New York, N.Y.) 288, 1042–7. https://doi.org/10.1126/science.288.5468.1042

Al-Abadleh, H.A., Grassian, V.H., 2000. Heterogeneous reaction of NO2 on hexane soot: A Knudsen cell and FT-IR study. Journal of Physical Chemistry A 104, 11926–11933. https://doi.org/10.1021/jp002918i

Amato, P., Joly, M., Schaupp, C., Attard, E., Möhler, O., Morris, C.E., Brunet, Y., Delort, A.-M., 2015. Survival and ice nucleation activity of bacteria as aerosols in a cloud simulation chamber. Atmospheric Chemistry and Physics 15, 6455–6465. https://doi.org/10.5194/acp-15-6455-2015

André, V., Billet, S., Pottier, D., Le Goff, J., Pottier, I., Garçon, G., Shirali, P., Sichel, F., 2011. Mutagenicity and genotoxicity of PM2.5 issued from an urbano-industrialized area of Dunkerque (France). Journal of Applied Toxicology 31, 131–138. https://doi.org/10.1002/jat.1572

Andreae, M.O., Gelencsér, A., 2006. Black carbon or brown carbon? The nature of light-absorbing carbonaceous aerosols. Atmospheric Chemistry and Physics 6, 3131–3148. https://doi.org/10.5194/acp-6-3131-2006

Anenberg, S., Horowitz, L., Tong, D., West, J., 2010. An Estimate of the Global Burden of Anthropogenic Ozone and Fine Particulate Matter on Premature Human Mortality Using Atmospheric Modeling. Environmental health perspectives 118, 1189–95. https://doi.org/10.1289/ehp.0901220

Ångström, A., 1964. The parameters of atmospheric turbidity. Tellus 16, 64–75. https://doi.org/10.1111/j.2153-3490.1964.tb00144.x

Antiñolo, M., Willis, M.D., Zhou, S., Abbatt, J.P.D., 2015. Connecting the oxidation of soot to its redox cycling abilities. Nature Communications 6. https://doi.org/10.1038/ncomms7812

Argonaut Scientific, 2017. Mini Inverted Soot Generator [WWW Document]. URL https://www.argonautscientific.com

Aydogdu, H., Asan, A., Tatman Otkun, M., 2010. Indoor and outdoor airborne bacteria in child day-care centers in Edirne City (Turkey), seasonal distribution and influence of meteorological factors. Environ Monit Assess 164, 53–66. https://doi.org/10.1007/s10661-009-0874-0

Ayres, J.G., Borm, P., Cassee, F.R., Castranova, V., Donaldson, K., Ghio, A., Harrison, R.M., Hider, R., Kelly, F., Kooter, I.M., Marano, F., Maynard, R.L., Mudway, I., Nel, A., Sioutas, C., Smith, S., Baeza-Squiban, A., Cho, A., Duggan, S., Froines, J., 2008. Evaluating the Toxicity of Airborne Particulate Matter and Nanoparticles by Measuring Oxidative Stress Potential—A Workshop Report and Consensus Statement. Inhalation Toxicology 20, 75–99. https://doi.org/10.1080/08958370701665517

Badyda, A.J., Dabrowiecki, P., Lubinski, W., Czechowski, P.O., Majewski, G., 2013. Exposure to traffic-related air pollutants as a risk of airway obstruction. Adv Exp Med Biol 755, 35–45. https://doi.org/10.1007/978-94-007-4546-9_5

Bates, J.T., Fang, T., Verma, V., Zeng, L., Weber, R.J., Tolbert, P.E., Abrams, J.Y., Sarnat, S.E., Klein, M., Mulholland, J.A., Russell, A.G., 2019. Review of Acellular Assays of Ambient Particulate Matter Oxidative Potential: Methods and Relationships with Composition, Sources, and Health Effects. Environ Sci Technol 53, 4003–4019. https://doi.org/10.1021/acs.est.8b03430

Bauer, H., Giebl, H., Hitzenberger, R., Kasper-Giebl, A., Reischl, G., Zibuschka, F., Puxbaum, H., 2003. Airborne bacteria as cloud condensation nuclei. Journal of Geophysical Research: Atmospheres 108. https://doi.org/10.1029/2003JD003545

Bedat, B., Cheng, R.K., 1995. Effects of buoyancy on premixed flame stabilization [WWW Document]. Fall meeting of the Western States Section of the Combustion Institute, Stanford, CA (United States), 30-31 Oct 1995. URL https://digital.library.unt.edu/ark:/67531/metadc625854/ (accessed 3.14.22).

Behndig, A.F., Mudway, I.S., Brown, J.L., Stenfors, N., Helleday, R., Duggan, S.T., Wilson, S.J., Boman, C., Cassee, F.R., Frew, A.J., Kelly, F.J., Sandström, T., Blomberg, A., 2006. Airway antioxidant and inflammatory responses to diesel exhaust exposure

in healthy humans. Eur Respir J 27, 359–365. https://doi.org/10.1183/09031936.06.00136904

Behrens, I., Pena, A.I.V., Alonso, M.J., Kissel, T., 2002. Comparative Uptake Studies of Bioadhesive and Non-Bioadhesive Nanoparticles in Human Intestinal Cell Lines and Rats: The Effect of Mucus on Particle Adsorption and Transport. Pharm Res 19, 1185–1193. https://doi.org/10.1023/A:1019854327540

Benbough, J.E., 1967. Death Mechanisms in Airborne Escherichia coli. Journal of General Microbiology 47, 325–333. https://doi.org/10.1099/00221287-47-3-325

Bernstein, J.A., Alexis, N., Barnes, C., Bernstein, I.L., Bernstein, J.A., Nel, A., Peden, D., Diaz-Sanchez, D., Tarlo, S.M., Williams, P.B., 2004. Health effects of air pollution. J Allergy Clin Immunol 114, 1116–1123. https://doi.org/10.1016/j.jaci.2004.08.030

Billet, S., Garçon, G., Dagher, Z., Verdin, A., Ledoux, F., Cazier, F., Courcot, D., Aboukais, A., Shirali, P., 2007. Ambient particulate matter (PM2.5): physicochemical characterization and metabolic activation of the organic fraction in human lung epithelial cells (A549). Environ Res 105, 212–223. https://doi.org/10.1016/j.envres.2007.03.001

Birch, M.E., Cary, R.A., 1996. Elemental carbon-based method for occupational monitoring of particulate diesel exhaust: methodology and exposure issues. Analyst 121, 1183–1190. https://doi.org/10.1039/an9962101183

Bischof, O., Weber, P., Bundke, U., Petzold, A., Kiendler-Scharr, A., 2019. Characterization of the Miniaturized Inverted Flame Burner as a Combustion Source to Generate a Nanoparticle Calibration Aerosol 37–46. https://doi.org/10.1007/s40825-019-00147-w

Bockhorn, H., 1994. Soot Formation in Combustion: Mechanisms and Models, Springer Series in Chemical Physics. Springer, Berlin, Heidelberg. https://doi.org/10.1007/978-3-642-85167-4_1

Bond, T.C., Bergstrom, R.W., 2006. Light Absorption by Carbonaceous Particles: An Investigative Review. Aerosol Science and Technology 40, 27–67. https://doi.org/10.1080/02786820500421521

Bond, T.C., Doherty, S.J., Fahey, D.W., Forster, P.M., Berntsen, T., DeAngelo, B.J., Flanner, M.G., Ghan, S., Kärcher, B., Koch, D., Kinne, S., Kondo, Y., Quinn, P.K., Sarofim, M.C., Schultz, M.G., Schulz, M., Venkataraman, C., Zhang, H., Zhang, S., Bellouin, N., Guttikunda, S.K., Hopke, P.K., Jacobson, M.Z., Kaiser, J.W., Klimont, Z., Lohmann, U., Schwarz, J.P., Shindell, D., Storelvmo, T., Warren, S.G., Zender, C.S.,

2013. Bounding the role of black carbon in the climate system: A scientific assessment. Journal of Geophysical Research: Atmospheres 118, 5380–5552. https://doi.org/10.1002/jgrd.50171

Boublil, L., Assémat, E., Borot, M.-C., Boland, S., Martinon, L., Sciare, J., Baeza-Squiban, A., 2012. Development of a repeated exposure protocol of human bronchial epithelium in vitro to study the long-term effects of atmospheric particles. Toxicology in vitro : an international journal published in association with BIBRA 27. https://doi.org/10.1016/j.tiv.2012.11.008

Bowers, R.M., McLetchie, S., Knight, R., Fierer, N., 2011. Spatial variability in airborne bacterial communities across land-use types and their relationship to the bacterial communities of potential source environments. ISME J 5, 601–612. https://doi.org/10.1038/ismej.2010.167

Breijyeh, Z., Jubeh, B., Karaman, R., 2020. Resistance of Gram-Negative Bacteria to Current Antibacterial Agents and Approaches to Resolve It. Molecules 25, E1340. https://doi.org/10.3390/molecules25061340

Brotto, P., Repetto, B., Formenti, P., Pangui, E., Livet, A., Bousserrhine, N., Martini, I., Varnier, O., Doussin, J.F., Prati, P., 2015. Use of an atmospheric simulation chamber for bioaerosol investigation: a feasibility study. Aerobiologia 31, 445–455. https://doi.org/10.1007/s10453-015-9378-2

Brown, J.S., Gordon, T., Price, O., Asgharian, B., 2013. Thoracic and respirable particle definitions for human health risk assessment. Part Fibre Toxicol 10, 12. https://doi.org/10.1186/1743-8977-10-12

Browne, E.C., Franklin, J.P., Canagaratna, M.R., Massoli, P., Kirchstetter, T.W., Worsnop, D.R., Wilson, K.R., Kroll, J.H., 2015. Changes to the Chemical Composition of Soot from Heterogeneous Oxidation Reactions. J. Phys. Chem. A 119, 1154–1163. https://doi.org/10.1021/jp511507d

Burrows, S.M., Elbert, W., Lawrence, M.G., Pöschl, U., 2009. Bacteria in the global atmosphere – Part 1: Review and synthesis of literature data for different ecosystems. Atmospheric Chemistry and Physics 9, 9263–9280. https://doi.org/10.5194/acp-9-9263-2009

Calcote, H.F., 1981. Mechanisms of soot nucleation in flames—A critical review. Combustion and Flame 42, 215–242. https://doi.org/10.1016/0010-2180(81)90159-0

Campbell, S.J., Utinger, B., Lienhard, D.M., Paulson, S.E., Shen, J., Griffiths, P.T., Stell, A.C., Kalberer, M., 2019. Development of a Physiologically Relevant Online Chemical Assay To Quantify Aerosol Oxidative Potential. Anal. Chem. 91, 13088–13095. https://doi.org/10.1021/acs.analchem.9b03282

Cassee, F.R., Héroux, M.-E., Gerlofs-Nijland, M.E., Kelly, F.J., 2013. Particulate matter beyond mass: recent health evidence on the role of fractions, chemical constituents and sources of emission. Inhalation Toxicology 25, 802–812. https://doi.org/10.3109/08958378.2013.850127

Cavalli, F., Viana, M., Yttri, K.E., Genberg, J., Putaud, J.-P., 2010. Toward a standardised thermal-optical protocol for measuring atmospheric organic and elemental carbon: the EUSAAR protocol. Atmospheric Measurement Techniques 3, 79–89. https://doi.org/10.5194/amt-3-79-2010

Chakrabarty, R.K., Moosmüller, H., Garro, M.A., Stipe, C.B., 2012. Observation of Superaggregates from a Reversed Gravity Low-Sooting Flame. Aerosol Science and Technology 46, i–iii. https://doi.org/10.1080/02786826.2011.608389

Chen, Q., Wang, M., Wang, Y., Zhang, L., Li, Y., Han, Y., 2019. Oxidative Potential of Water-Soluble Matter Associated with Chromophoric Substances in PM2.5 over Xi'an, China. Environ. Sci. Technol. 53, 8574–8584. https://doi.org/10.1021/acs.est.9b01976

Chow, J., Watson, J., Pritchett, L.C., Pierson, W., Frazier, C., Purcell, R., 1993. The dri thermal/optical reflectance carbon analysis system: description, evaluation and applications in U.S. Air quality studies. https://doi.org/10.1016/0960-1686(93)90245-T

Chow, J.C., Yu, J.Z., Watson, J.G., Hang Ho, S.S., Bohannan, T.L., Hays, M.D., Fung, K.K., 2007. The application of thermal methods for determining chemical composition of carbonaceous aerosols: A review. Journal of Environmental Science and Health, Part A 42, 1521–1541. https://doi.org/10.1080/10934520701513365

Chuang, H.-C., BéruBé, K., Lung, S.-C.C., Bai, K.-J., Jones, T., 2013. Investigation into the oxidative potential generated by the formation of particulate matter from incense combustion. J Hazard Mater 244–245, 142–150. https://doi.org/10.1016/j.jhazmat.2012.11.034

Costabile, F., Alas, H., Aufderheide, M., Avino, P., Amato, F., Argentini, S., Barnaba, F., Berico, M., Bernardoni, V., Biondi, R., Casasanta, G., Ciampichetti, S., Calzolai, G., Canepari, S., Conidi, A., Cordelli, E., Di Ianni, A., Di Liberto, L., Facchini, M.C., Facci,

A., Frasca, D., Gilardoni, S., Grollino, M.G., Gualtieri, M., Lucarelli, F., Malaguti, A., Manigrasso, M., Montagnoli, M., Nava, S., Perrino, C., Padoan, E., Petenko, I., Querol, X., Simonetti, G., Tranfo, G., Ubertini, S., Valli, G., Valentini, S., Vecchi, R., Volpi, F., Weinhold, K., Wiedensohler, A., Zanini, G., Gobbi, G.P., Petralia, E., 2017. First Results of the "Carbonaceous Aerosol in Rome and Environs (CARE)" Experiment: Beyond Current Standards for PM10. Atmosphere 8, 249. https://doi.org/10.3390/atmos8120249

Cox, C.S., 1966. The Survival of Escherichia coli sprayed into Air and into Nitrogen from Distilled Water and from Solutions of Protecting Agents, as a Function of Relative Humidity. Journal of General Microbiology 43, 383–399. https://doi.org/10.1099/00221287-43-3-383

Daly, H.M., Horn, A.B., 2009. Heterogeneous chemistry of toluene, kerosene and diesel soots. Phys. Chem. Chem. Phys. 11, 1069–1076. https://doi.org/10.1039/B815400G

Danelli, S.G., Brunoldi, M., Massabò, D., Parodi, F., Vernocchi, V., Prati, P., 2021. Comparative characterization of the performance of bio-aerosol nebulizers in connection with atmospheric simulation chambers. Atmospheric Measurement Techniques 14, 4461–4470. https://doi.org/10.5194/amt-14-4461-2021

Daniel, L.N., Mao, Y., Williams, A.O., Saffiotti, U., 1995. Direct interaction between crystalline silica and DNA - a proposed model for silica carcinogenesis. Scand J Work Environ Health 21 Suppl 2, 22–26.

Deguillaume, L., Leriche, M., Amato, P., Ariya, P.A., Delort, A.M., Pöschl, U., Chaumerliac, N., Bauer, H., Flossmann, A., Morris, C.E., 2008. Microbiology and atmospheric processes: chemical interactions of Primary Biological Aerosols 31.

Delfino, R.J., Staimer, N., Tjoa, T., Gillen, D.L., Schauer, J.J., Shafer, M.M., 2013. Airway inflammation and oxidative potential of air pollutant particles in a pediatric asthma panel. J Expo Sci Environ Epidemiol 23, 466–473. https://doi.org/10.1038/jes.2013.25

Dergham, M., Lepers, C., Verdin, A., Billet, S., Cazier, F., Courcot, D., Shirali, P., Garçon, G., 2012. Prooxidant and Proinflammatory Potency of Air Pollution Particulate Matter (PM2.5–0.3) Produced in Rural, Urban, or Industrial Surroundings in Human Bronchial Epithelial Cells (BEAS-2B). Chem. Res. Toxicol. 25, 904–919. https://doi.org/10.1021/tx200529v

Després, VivianeR., Huffman, J.A., Burrows, S.M., Hoose, C., Safatov, AleksandrS., Buryak, G., Fröhlich-Nowoisky, J., Elbert, W., Andreae, MeinratO., Pöschl, U., Jaenicke, R., 2012. Primary biological aerosol particles in the atmosphere: a review. Tellus B: Chemical and Physical Meteorology 64, 15598. https://doi.org/10.3402/tellusb.v64i0.15598

Dhawan, A., Bajpayee, M., Parmar, D., 2009. Comet assay: a reliable tool for the assessment of DNA damage in different models. Cell Biol Toxicol 28.

Dieme, D., Cabral-Ndior, M., Garçon, G., Verdin, A., Billet, S., Cazier, F., Courcot, D., Diouf, A., Shirali, P., 2012. Relationship between physicochemical characterization and toxicity of fine particulate matter (PM2.5) collected in Dakar city (Senegal). Environ. Res. 113, 1–13.

DOE, 2006. Basic Research Needs for Clean and Efficient Combustion of 21st Century Transportation Fuels.

Droplet Measurement Technologies, LLC, 2020. Photoacoustic Extinctiometer [WWW Document]. URL https://www.dropletmeasurement.com/product/photoacoustic-extinctiometer/

Dunklin, E.W., Puck, T.T., 1948. The lethal effect of relative humidity on air-borne bacteria. Journal of Experimental Medicine 87, 87–101. https://doi.org/10.1084/jem.87.2.87

Earl, A.M., Losick, R., Kolter, R., 2008. Ecology and genomics of Bacillus subtilis. Trends Microbiol 16, 269. https://doi.org/10.1016/j.tim.2008.03.004

Favez, O., El Haddad, I., Piot, C., Boréave, A., Abidi, E., Marchand, N., Jaffrezo, J.-L., Besombes, J.-L., Personnaz, M.-B., Sciare, J., Wortham, H., George, C., D'Anna, B., 2010. Inter-comparison of source apportionment models for the estimation of wood burning aerosols during wintertime in an Alpine city (Grenoble, France). Atmospheric Chemistry and Physics 10, 5295–5314. https://doi.org/10.5194/acp-10-5295-2010

Fenech, M., 2000. The in vitro micronucleus technique. Mutat Res 455, 81–95. https://doi.org/10.1016/s0027-5107(00)00065-8

Finlayson-Pitts, B.J., Pitts, J.N., Jr., 2000. Chemistry of the upper and lower atmosphere: Theory, experiments and applications. Academic Press, San Diego, CA.

Forbe, T., García, M., Gonzalez, E., 2011. Potencial risks of nanoparticles. Ciênc. Tecnol. Aliment. 31, 835–842. https://doi.org/10.1590/S0101-20612011000400002

Frenklach, M., 2002. Reaction mechanism of soot formation in flames. Phys. Chem. Chem. Phys. 4, 2028–2037. https://doi.org/10.1039/B110045A

Frezzini, M.A., Castellani, F., De Francesco, N., Ristorini, M., Canepari, S., 2019. Application of DPPH Assay for Assessment of Particulate Matter Reducing Properties. Atmosphere 10, 816. https://doi.org/10.3390/atmos10120816

Frezzini, M.A., De Francesco, N., Massimi, L., Canepari, S., 2022. Effects of operating conditions on PM oxidative potential assays. Atmospheric Environment 268, 118802. https://doi.org/10.1016/j.atmosenv.2021.118802

Fröhlich-Nowoisky, J., Kampf, C.J., Weber, B., Huffman, J.A., Pöhlker, C., Andreae, M.O., Lang-Yona, N., Burrows, S.M., Gunthe, S.S., Elbert, W., Su, H., Hoor, P., Thines, E., Hoffmann, T., Després, V.R., Pöschl, U., 2016. Bioaerosols in the Earth system: Climate, health, and ecosystem interactions. Atmospheric Research 182, 346–376. https://doi.org/10.1016/j.atmosres.2016.07.018

Fuller, K., Malm, W., Kreidenweis, S., 1999. Effects of mixing on extinction by carbonaceous particles. Journal of Geophysical Research 104, 15941–15954. https://doi.org/10.1029/1998JD100069

Fuller, S.J., Wragg, F.P.H., Nutter, J., Kalberer, M., 2014. Comparison of on-line and off-line methods to quantify reactive oxygen species (ROS) in atmospheric aerosols. Atmospheric Environment 92, 97–103. https://doi.org/10.1016/j.atmosenv.2014.04.006

Fuzzi, S., Baltensperger, U., Carslaw, K., Decesari, S., Denier van der Gon, H., Facchini, M.C., Fowler, D., Koren, I., Langford, B., Lohmann, U., Nemitz, E., Pandis, S., Riipinen, I., Rudich, Y., Schaap, M., Slowik, J.G., Spracklen, D.V., Vignati, E., Wild, M., Williams, M., Gilardoni, S., 2015. Particulate matter, air quality and climate: lessons learned and future needs. Atmos. Chem. Phys. 15, 8217–8299. https://doi.org/10.5194/acp-15-8217-2015

Gan, W.Q., Koehoorn, M., Davies, H.W., Demers, P.A., Tamburic, L., Brauer, M., 2011. Long-Term Exposure to Traffic-Related Air Pollution and the Risk of Coronary Heart Disease Hospitalization and Mortality. Environmental Health Perspectives 119, 501–507. https://doi.org/10.1289/ehp.1002511

Gandolfi, I., Bertolini, V., Ambrosini, R., Bestetti, G., Franzetti, A., 2013. Unravelling the bacterial diversity in the atmosphere. Appl Microbiol Biotechnol 97, 4727–4736. https://doi.org/10.1007/s00253-013-4901-2

Garçon, G., Dagher, Z., Zerimech, F., Ledoux, F., Courcot, D., Aboukais, A., Puskaric, E., Shirali, P., 2006. Dunkerque City air pollution particulate matter-induced cytotoxicity, oxidative stress and inflammation in human epithelial lung cells (L132) in culture. Toxicology in Vitro 20, 519–528. https://doi.org/10.1016/j.tiv.2005.09.012

Gartel, A.L., Radhakrishnan, S.K., 2005. Lost in Transcription: p21 Repression, Mechanisms, and Consequences. Cancer Res 65, 3980–3985. https://doi.org/10.1158/0008-5472.CAN-04-3995

Gauderman, W.J., Avol, E., Gilliland, F., Vora, H., Thomas, D., Berhane, K., McConnell, R., Kuenzli, N., Lurmann, F., Rappaport, E., Margolis, H., Bates, D., Peters, J., 2004. The Effect of Air Pollution on Lung Development from 10 to 18 Years of Age. New England Journal of Medicine 351, 1057–1067. https://doi.org/10.1056/NEJMoa040610

Gelencsér, A. (Ed.), 2004. Carbonaceous Aerosol, in: Carbonaceous Aerosol, Atmospheric And Oceanographic Sciences Library. Springer Netherlands, Dordrecht, pp. 1–5. https://doi.org/10.1007/978-1-4020-2887-8_1

Ghosh, B., Lal, H., Srivastava, A., 2015. Review of bioaerosols in indoor environment with special reference to sampling, analysis and control mechanisms. Environment International 85, 254–272. https://doi.org/10.1016/j.envint.2015.09.018

Gilmour, P.S., Ziesenis, A., Morrison, E.R., Vickers, M.A., Drost, E.M., Ford, I., Karg, E., Mossa, C., Schroeppel, A., Ferron, G.A., Heyder, J., Greaves, M., MacNee, W., Donaldson, K., 2004. Pulmonary and systemic effects of short-term inhalation exposure to ultrafine carbon black particles. Toxicology and Applied Pharmacology 195, 35–44. https://doi.org/10.1016/j.taap.2003.10.003

Grela, E., Kozłowska, J., Grabowiecka, A., 2018. Current methodology of MTT assay in bacteria – A review. Acta Histochemica 120, 303–311. https://doi.org/10.1016/j.acthis.2018.03.007

Gussman, R.A., Kenny, L.C., Labickas, M., Norton, P., 2002. Design, Calibration, and Field Test of a Cyclone for PM 1 Ambient Air Sampling. Aerosol Science and Technology 36, 361–365. https://doi.org/10.1080/027868202753504461

Hagens, W.I., Oomen, A.G., de Jong, W.H., Cassee, F.R., Sips, A.J.A.M., 2007. What do we (need to) know about the kinetic properties of nanoparticles in the body? Regulatory Toxicology and Pharmacology 49, 217–229. https://doi.org/10.1016/j.yrtph.2007.07.006

Hamanaka, R.B., Mutlu, G.M., 2018. Particulate Matter Air Pollution: Effects on the Cardiovascular System. Front Endocrinol (Lausanne) 9, 680. https://doi.org/10.3389/fendo.2018.00680

Han, C., Liu, Y., Ma, J., He, H., 2012. Effect of soot microstructure on its ozonization reactivity. J. Chem. Phys. 137, 084507. https://doi.org/10.1063/1.4747190

Hänel, G., 1994. Optical properties of atmospheric particles: complete parameter sets obtained through polar photometry and an improved inversion technique. Appl. Opt., AO 33, 7187–7199. https://doi.org/10.1364/AO.33.007187

Hänel, G., 1987. Radiation budget of the boundary layer: Part II. Simultaneous measurement of mean solar volume absorption and extinction coefficients of particles, in: Beiträge Zur Physik Der Atmosphäre.

Harrison, R.M., Beddows, D.C.S., Jones, A.M., Calvo, A., Alves, C., Pio, C., 2013. An evaluation of some issues regarding the use of aethalometers to measure woodsmoke concentrations. Atmospheric Environment 80, 540–548. https://doi.org/10.1016/j.atmosenv.2013.08.026

Hedayat, F., Stevanovic, S., Miljevic, B., Bottle, S., Ristovski, Z.D., 2015. Review-evaluating the molecular assays for measuring the oxidative potential of particulate matter. Chemical Industry and Chemical Engineering Quarterly 21, 201–210.

Held, P., 2021. An Introduction to Reactive Oxygen Species Measurement of ROS in Cells. J. biol. chem.

Henning, S., Rosenørn, T., D'Anna, B., Gola, A.A., Svenningsson, B., Bilde, M., 2005. Cloud droplet activation and surface tension of mixtures of slightly soluble organics and inorganic salt. Atmospheric Chemistry and Physics 5, 575–582. https://doi.org/10.5194/acp-5-575-2005

Hernandez, M., Perring, A.E., McCabe, K., Kok, G., Granger, G., Baumgardner, D., 2016. Chamber catalogues of optical and fluorescent signatures distinguish bioaerosol classes. Atmospheric Measurement Techniques 9, 3283–3292. https://doi.org/10.5194/amt-9-3283-2016

Hoffer, A., Gelencsér, A., Guyon, P., Kiss, G., Schmid, O., Frank, G.P., Artaxo, P., Andreae, M.O., 2006. Optical properties of humic-like substances (HULIS) in biomass-burning aerosols. Atmospheric Chemistry and Physics 6, 3563–3570. https://doi.org/10.5194/acp-6-3563-2006

Holder, A.L., Goth-Goldstein, R., Lucas, D., Koshland, C.P., 2012. Particle-Induced Artifacts in the MTT and LDH Viability Assays. Chem. Res. Toxicol. 25, 1885–1892. https://doi.org/10.1021/tx3001708

Homann, K.-H., 1998. Fullerenes and soot formation - New pathways to large particles in flames. Angewandte Chemie - International Edition 37, 2434–2451. https://doi.org/10.1002/(SICI)1521-3773(19981002)37:18<2434::AID-ANIE2434>3.0.CO;2-L

Horvath, H., 1993. Atmospheric light absorption—A review. Atmospheric Environment. Part A. General Topics, First Ibero-American Conference on the Atmospheric Environment, CIAMAA91/ACAE91 27, 293–317. https://doi.org/10.1016/0960-1686(93)90104-7

Houghton, J.E.T., Ding, Y., Griggs, D., Noguer, M., van der Linden, P., Dai, X., Maskell, M., Johnson, C., 2001. Climate Change 2001: The Scientific Basis, in: Contribution of Working Group I to the Third Assessment Report of the Intergovernmental Panel on Climate Change (IPCC). p. 881.

Huntzicker, J.J., Johnson, R.L., Shah, J.J., Cary, R.A., 1982. Analysis of Organic and Elemental Carbon in Ambient Aerosols by a Thermal-Optical Method, in: Wolff, G.T., Klimisch, R.L. (Eds.), Particulate Carbon: Atmospheric Life Cycle. Springer US, Boston, MA, pp. 79–88. https://doi.org/10.1007/978-1-4684-4154-3_6

Hussey, Shane.J.K., Purves, J., Allcock, N., Fernandes, V.E., Monks, P.S., Ketley, J.M., Andrew, P.W., Morrissey, J.A., 2017. Air pollution alters Staphylococcus aureus and Streptococcus pneumoniae biofilms, antibiotic tolerance and colonisation. Environmental Microbiology 19, 1868–1880. https://doi.org/10.1111/1462-2920.13686

Janssen, N.A., Gerlofs-Nijland, M.E., Lanki, T., Salonen, R.O., Cassee, F., Hoek, G., Fischer, P., Brunekreef, B., Krzyzanowski, M., 2012. Health Effects of Black Carbon (Res. Rep.). World Health Organization, Regional Office for Europe, Copenaghen, Denmark.

Johansson, S.A.E., Campbell, J.L., Malmqvists, K.G., 1995. Particle-Induced X-Ray Emission Spectrometry. John Wiley and Sons.

Jones, A.M., Harrison, R.M., 2004. The effects of meteorological factors on atmospheric bioaerosol concentrations—a review. Science of The Total Environment 326, 151–180. https://doi.org/10.1016/j.scitotenv.2003.11.021

Jullien, R., Botet, R., 1987. Aggregation and fractal aggregates. World Scientific, Singapore.

Kanakidou, M., Seinfeld, J.H., Pandis, S.N., Barnes, I., Dentener, F.J., Facchini, M.C., Van Dingenen, R., Ervens, B., Nenes, A., Nielsen, C.J., Swietlicki, E., Putaud, J.P., Balkanski, Y., Fuzzi, S., Horth, J., Moortgat, G.K., Winterhalter, R., Myhre, C.E.L., Tsigaridis, K., Vignati, E., Stephanou, E.G., Wilson, J., 2005. Organic aerosol and global climate modelling: a review. Atmospheric Chemistry and Physics 5, 1053–1123. https://doi.org/10.5194/acp-5-1053-2005

Kazemimanesh, M., Moallemi, A., Thomson, K., Smallwood, G., Lobo, P., Olfert, J., 2019. A novel miniature inverted-flame burner for the generation of soot nanoparticles. Aerosol Science and Technology. https://doi.org/10.1080/02786826.2018.1556774

Keady, P.B., Quant, F.R., Sem, G.J., 1986. A Condensation Nucleus Counter for Clean Rooms, Annual Technical Mtg. Proc. Institute of Environmental Sci.

Kellogg, C., Griffin, D., 2006. Aerobiology and the global transport of desert dust. Trends in ecology & evolution 21, 638–44. https://doi.org/10.1016/j.tree.2006.07.004

Kelly, C., 2016. Scientists discuss complexities of studying tiny particles that have a big impact on climate 3.

Kelly, F.J., Tetley, T.D., 1997. Nitrogen dioxide depletes uric acid and ascorbic acid but not glutathione from lung lining fluid. Biochem J 325 (Pt 1), 95–99. https://doi.org/10.1042/bj3250095

Kirchner, U., Scheer, V., Vogt, R., 2000. FTIR spectroscopic investigation of the mechanism and kinetics of the heterogeneous reactions of NO2 and HNO3 with soot. Journal of Physical Chemistry A 104, 8908–8915. https://doi.org/10.1021/jp0005322

Kirchstetter, T.W., Novakov, T., 2007. Controlled generation of black carbon particles from a diffusion flame and applications in evaluating black carbon measurement methods. Atmospheric Environment 41, 1874–1888. https://doi.org/10.1016/j.atmosenv.2006.10.067

Kirchstetter, T.W., Novakov, T., Hobbs, P.V., 2004. Evidence that the spectral dependence of light absorption by aerosols is affected by organic carbon. Journal of Geophysical Research: Atmospheres 109. https://doi.org/10.1029/2004JD004999

Kirkland, D.J., Hayashi, M., MacGregor, J.T., Müller, L., Schechtman, L.M., Sofuni, T., 2003. Summary of major conclusions. Mutation Research/Genetic Toxicology and Environmental Mutagenesis 540, 123–125. https://doi.org/10.1016/j.mrgentox.2003.07.002

Kirsch-Volders, M., Sofuni, T., Aardema, M., Albertini, S., Eastmond, D., Fenech, M., Ishidate, M., Kirchner, S., Lorge, E., Morita, T., Norppa, H., Surrallés, J., Vanhauwaert, A., Wakata, A., 2003. Report from the in vitro micronucleus assay working group. Mutation Research/Genetic Toxicology and Environmental Mutagenesis, International Workshop on Genotoxicity Testing (IWGT) 540, 153–163. https://doi.org/10.1016/j.mrgentox.2003.07.005

Kirsch-Volders, M., Vanhauwaert, A., De Boeck, M., Decordier, I., 2002. Importance of detecting numerical versus structural chromosome aberrations. Mutat Res 504, 137–148. https://doi.org/10.1016/s0027-5107(02)00087-8

Koehler, B.G., Nicholson, V.T., Roe, H.G., Whitney, E.S., 1999. A Fourier transform infrared study of the adsorption of SO2 on n-hexane soot from -130° to -40°C. Journal of Geophysical Research Atmospheres 104, 5507–5514. https://doi.org/10.1029/1998JD100081

Kulmala, M., Suni, T., Lehtinen, K.E.J., Dal Maso, M., Boy, M., Reissell, A., Rannik, Ü., Aalto, P., Keronen, P., Hakola, H., Bäck, J., Hoffmann, T., Vesala, T., Hari, P., 2004. A new feedback mechanism linking forests, aerosols, and climate. Atmospheric Chemistry and Physics 4, 557–562. https://doi.org/10.5194/acp-4-557-2004

Lai, A.C., Nazaroff, W.W., 2000. Modeling indoor particle deposition from turbulent flow onto smooth surfaces. Journal of Aerosol Science 31, 463–476. https://doi.org/10.1016/S0021-8502(99)00536-4

Le Hégarat, L.L., Mourot, A., Huet, S., Vasseur, L., Camus, S., Chesné, C., Fessard, V., 2014. Performance of Comet and Micronucleus Assays in Metabolic Competent HepaRG Cells to Predict In Vivo Genotoxicity. Toxicological Sciences 138, 300–309. https://doi.org/10.1093/toxsci/kfu004

Lee, B.U., Kim, S.H., Kim, S.S., 2002. Hygroscopic growth of E. coli and B. subtilis bioaerosols. Journal of Aerosol Science 33, 1721–1723. https://doi.org/10.1016/S0021-8502(02)00114-3

Lelieveld, J., Evans, J.S., Fnais, M., Giannadaki, D., Pozzer, A., 2015. The contribution of outdoor air pollution sources to premature mortality on a global scale. Nature 525, 367–371. https://doi.org/10.1038/nature15371

Lelièvre, S., Bedjanian, Y., Pouvesle, N., Delfau, J.-L., Vovelle, C., Le Bras, G., 2004. Heterogeneous reaction of ozone with hydrocarbon flame soot. Physical Chemistry Chemical Physics 1181–1191. https://doi.org/10.1039/b316895f

Leni, Z., Künzi, L., Geiser, M., 2020. Air pollution causing oxidative stress. Current Opinion in Toxicology, Oxidative Toxicology 20–21, 1–8. https://doi.org/10.1016/j.cotox.2020.02.006

Lepers, C., André, V., Dergham, M., Billet, S., Verdin, A., Garçon, G., Dewaele, D., Cazier, F., Sichel, F., Shirali, P., 2014. Xenobiotic metabolism induction and bulky DNA adducts generated by particulate matter pollution in BEAS-2B cell line: geographical and seasonal influence. Journal of Applied Toxicology 34, 703–713. https://doi.org/10.1002/jat.2931

Li, G., Zhang, R., Fan, J., Tie, X., 2005. Impacts of black carbon aerosol on photolysis and ozone. Journal of Geophysical Research: Atmospheres 110. https://doi.org/10.1029/2005JD005898

Li, Q., Shang, J., Zhu, T., 2013. Physicochemical characteristics and toxic effects of ozone-oxidized black carbon particles. Atmospheric Environment 81, 68–75. https://doi.org/10.1016/j.atmosenv.2013.08.043

Li, X., Wang, Yuesi, Guo, X., Wang, Yingfeng, 2013. Seasonal variation and source apportionment of organic and inorganic compounds in PM2.5 and PM10 particulates in Beijing, China. J Environ Sci (China) 25, 741–750. https://doi.org/10.1016/s1001-0742(12)60121-1

Lighthart, B., 2000. Mini-review of the concentration variations found inthe alfresco atmospheric bacterial populations. Aerobiologia 16, 7–16. https://doi.org/10.1023/A:1007694618888

Lighty, J.S., Veranth, J.M., Sarofim, A.F., 2000. Combustion Aerosols: Factors Governing Their Size and Composition and Implications to Human Health. Journal of the Air & Waste Management Association 50, 1565–1618. https://doi.org/10.1080/10473289.2000.10464197

Lim, C.C., Thurston, G.D., 2019. Air Pollution, Oxidative Stress, and Diabetes: a Life Course Epidemiologic Perspective. Curr Diab Rep 19, 58. https://doi.org/10.1007/s11892-019-1181-y

Lin, M., Yu, J.Z., 2020. Assessment of Interactions between Transition Metals and Atmospheric Organics: Ascorbic Acid Depletion and Hydroxyl Radical Formation in Organic-Metal Mixtures. Environ. Sci. Technol. 54, 1431–1442. https://doi.org/10.1021/acs.est.9b07478

Lindberg, J.D., Douglass, R.E., Garvey, D.M., 1993. Carbon and the optical properties of atmospheric dust. Appl. Opt., AO 32, 6077–6081. https://doi.org/10.1364/AO.32.006077

Lionetto, M.G., Caricato, R., Giordano, M.E., 2019. Pollution Biomarkers in Environmental and Human Biomonitoring. The Open Biomarkers Journal 9. https://doi.org/10.2174/1875318301909010001

Liu, B.Y.H., Pui, D.Y.H., 1974. Equilibrium bipolar charge distribution of aerosols. Journal of Colloid and Interface Science 49, 305–312. https://doi.org/10.1016/0021-9797(74)90366-X

Liu, Y., Liu, C., Ma, J., Ma, Q., He, H., 2010. Structural and hygroscopic changes of soot during heterogeneous reaction with O3. Phys. Chem. Chem. Phys. 12, 10896–10903. https://doi.org/10.1039/C0CP00402B

Lodovici, M., Bigagli, E., 2011. Oxidative Stress and Air Pollution Exposure. Journal of Toxicology 2011, 1–9. https://doi.org/10.1155/2011/487074

Mamakos, A., Khalek, I., Giannelli, B., Spears, M., 2013. Characterization of Combustion Aerosol Produced by a Mini-CAST and Treated in a Catalytic Stripper. Aerosol Science and Technology 47, 927–936. https://doi.org/10.1080/02786826.2013.802762

Manigrasso, M., Simonetti, G., Astolfi, M.L., Perrino, C., Canepari, S., Protano, C., Antonucci, A., Avino, P., Vitali, M., 2020. Oxidative potential associated with urban aerosol deposited into the respiratory system and relevant elemental and ionic fraction contributions. Atmosphere 11. https://doi.org/10.3390/ATMOS11010006

Marple, V., Willeke, K., 1976. Impactor design. Atmospheric Environment.

Massabò, D., Altomari, A., Vernocchi, V., Prati, P., 2019. Two-wavelength thermal–optical determination of light-absorbing carbon in atmospheric aerosols. Atmos. Meas. Tech. 12, 3173–3182. https://doi.org/10.5194/amt-12-3173-2019

Massabò, D., Bernardoni, V., Bove, M., Brunengo, A., Cuccia, E., Piazzalunga, A., Prati, P., Valli, G., Vecchi, R., 2013. A multi-wavelength optical set-up for the characterization of carbonaceous particulate matter. Journal of Aerosol Science 60, 34–46. https://doi.org/10.1016/j.jaerosci.2013.02.006

Massabò, D., Caponi, L., Bernardoni, V., Bove, M.C., Brotto, P., Calzolai, G., Cassola, F., Chiari, M., Fedi, M.E., Fermo, P., Giannoni, M., Lucarelli, F., Nava, S., Piazzalunga, A., Valli, G., Vecchi, R., Prati, P., 2015. Multi-wavelength optical determination of

black and brown carbon in atmospheric aerosols. Atmospheric Environment 108, 1–12. https://doi.org/10.1016/j.atmosenv.2015.02.058

Massabò, D., Danelli, S.G., Brotto, P., Comite, A., Costa, C., Di Cesare, A., Doussin, J.F., Ferraro, F., Formenti, P., Gatta, E., Negretti, L., Oliva, M., Parodi, F., Vezzulli, L., Prati, P., 2018. ChAMBRe: a new atmospheric simulation chamber for aerosol modelling and bio-aerosol research. Atmospheric Measurement Techniques 11, 5885–5900. https://doi.org/10.5194/amt-11-5885-2018

Massabò, D., Prati, P., 2021. An overview of optical and thermal methods for the characterization of carbonaceous aerosol. Riv. Nuovo Cim. 44, 145–192. https://doi.org/10.1007/s40766-021-00017-8

Maynard, R.L., Howard, V., 1999. Particulate matter: properties and effects upon health. BIOS Scientific Pub. ; Springer, Oxford; New York.

McEnally, C.S., Pfefferle, L.D., Atakan, B., Kohse-Höinghaus, K., 2006. Studies of aromatic hydrocarbon formation mechanisms in flames: Progress towards closing the fuel gap. Progress in Energy and Combustion Science 32, 247–294. https://doi.org/10.1016/j.pecs.2005.11.003

Megaridis, C.M., 1989. Comparison of soot growth and oxidation in smoking and non-smoking ethylene diffusion flames. Combustion Science and Technology 66, 1–16. https://doi.org/10.1080/00102208908947136

Menon, S., Hansen, J., Nazarenko, L., Luo, Y., 2002. Climate effects of black carbon aerosols in China and India. Science 297, 2250–2253. https://doi.org/10.1126/science.1075159

Mesa Labs, 2001. PM1 Sharp Cut Cyclone (SCC 2.229).

Michelsen, H.A., 2017. Probing soot formation, chemical and physical evolution, and oxidation: A review of in situ diagnostic techniques and needs. Proceedings of the Combustion Institute 36, 717–735. https://doi.org/10.1016/j.proci.2016.08.027

Michelsen, H.A., Colket, M.B., Bengtsson, P.-E., D'Anna, A., Desgroux, P., Haynes, B.S., Miller, J.H., Nathan, G.J., Pitsch, H., Wang, H., 2020. A Review of Terminology Used to Describe Soot Formation and Evolution under Combustion and Pyrolytic Conditions. ACS Nano 14, 12470–12490. https://doi.org/10.1021/acsnano.0c06226

Moallemi, A., Kazemimanesh, M., Corbin, J.C., Thomson, K., Smallwood, G., Olfert, J.S., Lobo, P., 2019. Characterization of black carbon particles generated by a propane-

fueled miniature inverted soot generator. Journal of Aerosol Science 135, 46–57. https://doi.org/10.1016/j.jaerosci.2019.05.004

Moore, R.H., Ziemba, L.D., Dutcher, D., Beyersdorf, A.J., Chan, K., Crumeyrolle, S., Raymond, T.M., Thornhill, K.L., Winstead, E.L., Anderson, B.E., 2014. Mapping the Operation of the Miniature Combustion Aerosol Standard (Mini-CAST) Soot Generator. Aerosol Science and Technology 48, 467–479. https://doi.org/10.1080/02786826.2014.890694

Moosmuller, H., Chakrabarty, R., Arnott, W., 2009. Aerosol light absorption and its measurement: A review. Journal of Quantitative Spectroscopy and Radiative Transfer 110, 844–878. https://doi.org/10.1016/j.jqsrt.2009.02.035

National Institute for Occupational Safety and Health: NIOSH, 1999. NIOSH Method 5040 Issue 3 (Interim): Elemental Carbon (diesel exhaust) (Technical), NIOSH Manual of Analytical Methods. National Institute for Occupational Safety and Health, Cincinnati, OH.

Nel, A., Xia, T., Mädler, L., Li, N., 2006. Toxic Potential of Materials at the Nanolevel 311, 7.

Nemmar, A., Hoet, P.H.M., Vanquickenborne, B., Dinsdale, D., Thomeer, M., Hoylaerts, M.F., Vanbilloen, H., Mortelmans, L., Nemery, B., 2002. Passage of inhaled particles into the blood circulation in humans. Circulation 105, 411–414. https://doi.org/10.1161/hc0402.104118

Nienow, A.M., Roberts, J.T., 2006. Heterogeneous Chemistry of Carbon Aerosols. Annual Review of Physical Chemistry 57, 105–128. https://doi.org/10.1146/annurev.physchem.57.032905.104525

Niranjan, R., Thakur, A.K., 2017. The Toxicological Mechanisms of Environmental Soot (Black Carbon) and Carbon Black: Focus on Oxidative Stress and Inflammatory Pathways. Frontiers in Immunology 8, 763. https://doi.org/10.3389/fimmu.2017.00763

Noda, J., Tomizawa, S., Hoshino, B., Munkhjargal, E., Kawai, K., Kai, K., 2019. Atmospheric dust as a possible survival factor for bioaerosols. E3S Web Conf. 99, 04007. https://doi.org/10.1051/e3sconf/20199904007

Noda, J., Tomizawa, S., Takahashi, K., Morimoto, K., Mitarai, S., 2021. Air pollution and airborne infection with mycobacterial bioaerosols: a potential attribution of soot. Int. J. Environ. Sci. Technol. https://doi.org/10.1007/s13762-021-03203-7

Nordmann, S., Birmili, W., Weinhold, K., Müller, K., Spindler, G., Wiedensohler, A., 2013. Measurements of the mass absorption cross section of atmospheric soot particles using Raman spectroscopy. Journal of Geophysical Research: Atmospheres 118, 12,075-12,085. https://doi.org/10.1002/2013JD020021

Oberdörster, G., Ferin, J., Lehnert, B.E., 1994. Correlation between particle size, in vivo particle persistence, and lung injury. Environmental Health Perspectives 102, 173–179. https://doi.org/10.1289/ehp.102-1567252

Oberdörster, G., Oberdörster, E., Oberdörster, J., 2005. Nanotoxicology: An Emerging Discipline Evolving from Studies of Ultrafine Particles. Environmental Health Perspectives 113, 823–839. https://doi.org/10.1289/ehp.7339

Oberdörster, G., Sharp, Z., Atudorei, V., Elder, A., Gelein, R., Kreyling, W., Cox, C., 2004. Translocation of Inhaled Ultrafine Particles to the Brain. Inhalation Toxicology 16, 437–445. https://doi.org/10.1080/08958370490439597

Oh, S.M., Kim, H.R., Park, Y.J., Lee, S.Y., Chung, K.H., 2011. Organic extracts of urban air pollution particulate matter (PM2.5)-induced genotoxicity and oxidative stress in human lung bronchial epithelial cells (BEAS-2B cells). Mutat Res 723, 142–151. https://doi.org/10.1016/j.mrgentox.2011.04.003

Olstrup, H., Johansson, C., Forsberg, B., 2016. The Use of Carbonaceous Particle Exposure Metrics in Health Impact Calculations. International Journal of Environmental Research and Public Health 13, 249. https://doi.org/10.3390/ijerph13030249

Øvrevik, J., 2019. Oxidative Potential Versus Biological Effects: A Review on the Relevance of Cell-Free/Abiotic Assays as Predictors of Toxicity from Airborne Particulate Matter. Int J Mol Sci 20, E4772. https://doi.org/10.3390/ijms20194772

Peacock, J.L., Anderson, H.R., Bremner, S.A., Marston, L., Seemungal, T.A., Strachan, D.P., Wedzicha, J.A., 2011. Outdoor air pollution and respiratory health in patients with COPD. Thorax 66, 591–596. https://doi.org/10.1136/thx.2010.155358

Pearson, C., Littlewood, E., Douglas, P., Robertson, S., Gant, T.W., Hansell, A.L., 2015. Exposures and Health Outcomes in Relation to Bioaerosol Emissions From Composting Facilities: A Systematic Review of Occupational and Community Studies. Journal of Toxicology and Environmental Health, Part B 18, 43–69. https://doi.org/10.1080/10937404.2015.1009961

Perrone, M.R., Bertoli, I., Romano, S., Russo, M., Rispoli, G., Pietrogrande, M.C., 2019. PM2.5 and PM10 oxidative potential at a Central Mediterranean Site: Contrasts between dithiothreitol- and ascorbic acid-measured values in relation with

particle size and chemical composition. Atmospheric Environment 210, 143–155. https://doi.org/10.1016/j.atmosenv.2019.04.047

Peterson, M.R., Richards, M.H., 2002. Thermal-Optical-Transmittance Analysis for Organic, Elemental, Carbonate, Total Carbon, and OCX2 in PM2.5 by the EPA/NIOSH Method- #83.

Petzold, A., Ogren, J.A., Fiebig, M., Laj, P., Li, S.-M., Baltensperger, U., Holzer-Popp, T., Kinne, S., Pappalardo, G., Sugimoto, N., Wehrli, C., Wiedensohler, A., Zhang, X.-Y., 2013. Recommendations for reporting "black carbon" measurements. Atmospheric Chemistry and Physics 13, 8365–8379. https://doi.org/10.5194/acp-13-8365-2013

Petzold, A., Schönlinner, M., 2004. Multi-angle absorption photometry—a new method for the measurement of aerosol light absorption and atmospheric black carbon. Journal of Aerosol Science 35, 421–441. https://doi.org/10.1016/j.jaerosci.2003.09.005

Phillips, D.H., Arlt, V.M., 2009. Genotoxicity: damage to DNA and its consequences. Molecular, Clinical and Environmental Toxicology 1, 87–110.

Pope, C.A., Burnett, R.T., Thun, M.J., Calle, E.E., Krewski, D., Ito, K., Thurston, G.D., 2002. Lung cancer, cardiopulmonary mortality, and long-term exposure to fine particulate air pollution. JAMA 287, 1132–1141. https://doi.org/10.1001/jama.287.9.1132

Pope, C.A., Burnett, R.T., Thurston, G.D., Thun, M.J., Calle, E.E., Krewski, D., Godleski, J.J., 2004. Cardiovascular mortality and long-term exposure to particulate air pollution: epidemiological evidence of general pathophysiological pathways of disease. Circulation 109, 71–77. https://doi.org/10.1161/01.CIR.0000108927.80044.7F

Pope, C.A., Dockery, D.W., 2006. Health Effects of Fine Particulate Air Pollution: Lines that Connect. Journal of the Air & Waste Management Association 56, 709–742. https://doi.org/10.1080/10473289.2006.10464485

Pöschl, U., 2005. Atmospheric Aerosols: Composition, Transformation, Climate and Health Effects. Angewandte Chemie International Edition 44, 7520–7540. https://doi.org/10.1002/anie.200501122

Pöschl, U., 2003. Aerosol particle analysis: challenges and progress. Anal Bioanal Chem 375, 30–32. https://doi.org/10.1007/s00216-002-1611-5

Propulsion and Clean Energy Research Group, n.d. Scheme of soot formation.

Puri, R., Richardson, T.F., Santoro, R.J., Dobbins, R.A., 1993. Aerosol dynamic processes of soot aggregates in a laminar ethene diffusion flame. Combustion and Flame 92, 320–333. https://doi.org/10.1016/0010-2180(93)90043-3

Quinn, P.K., Bates, T.S., Baum, E., Doubleday, N., Fiore, A.M., Flanner, M., Fridlind, A., Garrett, T.J., Koch, D., Menon, S., Shindell, D., Stohl, A., Warren, S.G., 2008. Short-lived pollutants in the Arctic: their climate impact and possible mitigation strategies. Atmospheric Chemistry and Physics 8, 1723–1735. https://doi.org/10.5194/acp-8-1723-2008

Rajper, S.A., Ullah, S., Li, Z., 2018. Exposure to air pollution and self-reported effects on Chinese students: A case study of 13 megacities. PLOS ONE 13, e0194364. https://doi.org/10.1371/journal.pone.0194364

Ramanathan, V., Carmichael, G., 2008. Global and Regional Climate Changes Due to Black Carbon. Nat Geosci 1. https://doi.org/10.1038/ngeo156

Rao, L., Zhang, L., Wang, X., Xie, T., Zhou, S., Lu, S., Liu, X., Lu, H., Xiao, K., Wang, W., Wang, Q., 2020. Oxidative Potential Induced by Ambient Particulate Matters with Acellular Assays: A Review. Processes 8, 1410. https://doi.org/10.3390/pr8111410

Rao, X., Zhong, J., Brook, R.D., Rajagopalan, S., 2018. Effect of Particulate Matter Air Pollution on Cardiovascular Oxidative Stress Pathways. Antioxid Redox Signal 28, 797–818. https://doi.org/10.1089/ars.2017.7394

Reche, C., Querol, X., Alastuey, A., Viana, M., Pey, J., Moreno, T., Rodríguez, S., González, Y., Fernández-Camacho, R., de la Rosa, J., Dall'Osto, M., Prévôt, A.S.H., Hueglin, C., Harrison, R.M., Quincey, P., 2011. New considerations for PM, Black Carbon and particle number concentration for air quality monitoring across different European cities. Atmospheric Chemistry and Physics 11, 6207–6227. https://doi.org/10.5194/acp-11-6207-2011

Reischl, G.P., Mäkelä, J.M., Karch, R., Necid, J., 1996. Bipolar charging of ultrafine particles in the size range below 10 nm. Journal of Aerosol Science, Fuchs Memorial Issue 27, 931–949. https://doi.org/10.1016/0021-8502(96)00026-2

Richter, H., Howard, J.B., 2000. Formation of polycyclic aromatic hydrocarbons and their growth to soot—a review of chemical reaction pathways. Progress in Energy and Combustion Science 26, 565–608. https://doi.org/10.1016/S0360-1285(00)00009-5

Risom, L., Møller, P., Loft, S., 2005. Oxidative stress-induced DNA damage by particulate air pollution. Mutat Res 592, 119–137. https://doi.org/10.1016/j.mrfmmm.2005.06.012

Rosen, H., Hansen, A.D.A., Gundel, L., Novakov, T., 1978. Identification of the optically absorbing component in urban aerosols. Appl. Opt., AO 17, 3859–3861. https://doi.org/10.1364/AO.17.003859

Saarikoski, S., Timonen, H., Saarnio, K., Aurela, M., Järvi, L., Keronen, P., Kerminen, V.-M., Hillamo, R., 2008. Sources of organic carbon in fine particulate matter in northern European urban air. Atmospheric Chemistry and Physics 8, 6281–6295. https://doi.org/10.5194/acp-8-6281-2008

Sala Ferré, M.R., Arias, C., Oliva, J.M., Pedrol, A., García, M., Pellicer, T., Roura, P., Domínguez, A., 2008. A community outbreak of Legionnaires' disease associated with a cooling tower in Vic and Gurb, Catalonia (Spain) in 2005. Eur J Clin Microbiol Infect Dis 28, 153. https://doi.org/10.1007/s10096-008-0603-6

Samake, A., Uzu, G., Martins, J.M.F., Calas, A., Vince, E., Parat, S., Jaffrezo, J.L., 2017. The unexpected role of bioaerosols in the Oxidative Potential of PM. Sci Rep 7, 10978. https://doi.org/10.1038/s41598-017-11178-0

Samet, J., Wassel, R., Holmes, K.J., Abt, E., Bakshi, K., 2005. Research priorities for airborne particulate matter in the United States. Environ Sci Technol 39, 299A-304A. https://doi.org/10.1021/es053307c

Sandradewi, J., Prévôt, A.S.H., Szidat, S., Perron, N., Alfarra, M.R., Lanz, V.A., Weingartner, E., Baltensperger, U., 2008. Using Aerosol Light Absorption Measurements for the Quantitative Determination of Wood Burning and Traffic Emission Contributions to Particulate Matter. Environ. Sci. Technol. 42, 3316–3323. https://doi.org/10.1021/es702253m

Satsangi, D.P., Agarwal, A.K., 2019. Particulate Matter and Its Impact on Human Health in Urban Settings, in: Agarwal, A.K., Gautam, A., Sharma, N., Singh, A.P. (Eds.), Methanol and the Alternate Fuel Economy, Energy, Environment, and Sustainability. Springer, Singapore, pp. 213–231. https://doi.org/10.1007/978-981-13-3287-6_10

Schnaiter, M., Linke, C., Möhler, O., Naumann, K.-H., Saathoff, H., Wagner, R., Schurath, U., Wehner, B., 2005. Absorption amplification of black carbon internally mixed with secondary Organic Aerosol. Journal of Geophysical Research 110, D19204. https://doi.org/10.1029/2005JD006046

Segersson, D., Eneroth, K., Gidhagen, L., Johansson, C., Omstedt, G., Nylén, A.E., Forsberg, B., 2017. Health Impact of PM10, PM2.5 and Black Carbon Exposure Due to Different Source Sectors in Stockholm, Gothenburg and Umea, Sweden. International Journal of Environmental Research and Public Health 14, 742. https://doi.org/10.3390/ijerph14070742

Seinfeld, J.H., 1986. Atmospheric Chemistry and Physics of Air Pollution. Wiley, New York.

Seinfeld, J.H., Pandis, S.N., Noone, K., 1998. Atmospheric Chemistry and Physics: From Air Pollution to Climate Change. Physics Today 51, 88–90. https://doi.org/10.1063/1.882420

Silhavy, T.J., Kahne, D., Walker, S., 2010. The Bacterial Cell Envelope. Cold Spring Harb Perspect Biol 2, a000414. https://doi.org/10.1101/cshperspect.a000414

Singh, H.B., 1995. Composition Chemistry, and Climate of the Atmosphere | Wiley. John Wiley and Sons, New York.

Skiles, S.M., Flanner, M., Cook, J.M., Dumont, M., Painter, T.H., 2018. Radiative forcing by light-absorbing particles in snow. Nature Clim Change 8, 964–971. https://doi.org/10.1038/s41558-018-0296-5

Slezakova, K., Morais, S., Pereira, M. do C., 2013. Atmospheric Nanoparticles and Their Impacts on Public Health, Current Topics in Public Health. IntechOpen. https://doi.org/10.5772/54775

Standards - Air Quality - Environment - European Commission [WWW Document], n.d. URL https://ec.europa.eu/environment/air/quality/standards.htm (accessed 3.14.22).

Stanmore, B.R., Tschamber, V., Brilhac, J.-F., 2008. Oxidation of carbon by NOx, with particular reference to NO2 and N2O. Fuel 87, 131–146. https://doi.org/10.1016/j.fuel.2007.04.012

Stipe, C.B., Higgins, B.S., Lucas, D., Koshland, C.P., Sawyer, R.F., 2005. Inverted co-flow diffusion flame for producing soot. Review of Scientific Instruments 76, 023908. https://doi.org/10.1063/1.1851492

Sun, H., Shamy, M., Kluz, T., Muñoz, A.B., Zhong, M., Laulicht, F., Alghamdi, M.A., Khoder, M.I., Chen, L.-C., Costa, M., 2012. Gene expression profiling and pathway analysis of human bronchial epithelial cells exposed to airborne particulate matter collected from Saudi Arabia. Toxicol Appl Pharmacol 265, 147–157. https://doi.org/10.1016/j.taap.2012.10.008

Tang, J.W., 2009. The effect of environmental parameters on the survival of airborne infectious agents. Journal of The Royal Society Interface 6, S737–S746. https://doi.org/10.1098/rsif.2009.0227.focus

Tran, C.L., Buchanan, D., Cullen, R.T., Searl, A., Jones, A.D., Donaldson, K., 2000. Inhalation of Poorly Soluble Particles. Ii. Influence of Particle Surface Area on Inflammation and Clearance. Inhalation Toxicology 12, 1113–1126. https://doi.org/10.1080/08958370050166796

Traversi, D., Festa, E., Pignata, C., Gilli, G., 2015. Aero-dispersed mutagenicity attributed to particulate and semi volatile phase in an urban environment. Chemosphere 124, 163–169. https://doi.org/10.1016/j.chemosphere.2014.12.033

TSI Inc., 2019. Water-based Condensation Particle Counter Model 3789 Operation Manual.

TSI Inc., 2011. OPS model 3330 operation and service manual.

TSI Inc., 2009. Series 3080 Electrostatic Classifiers Operation and Service Manual.

Venkatachari, P., Hopke, P.K., Grover, B.D., Eatough, D.J., 2005. Measurement of Particle-Bound Reactive Oxygen Species in Rubidoux Aerosols. J Atmos Chem 50, 49–58. https://doi.org/10.1007/s10874-005-1662-z

Vernocchi, V., Brunoldi, M., Danelli, S.G., Parodi, F., Prati, P., Massabò, D., 2021. Characterization of the MISG soot generator with an atmospheric simulation chamber. Atmospheric Measurement Techniques Discussions 1–27. https://doi.org/10.5194/amt-2021-345

von der Weiden, S.-L., Drewnick, F., Borrmann, S., 2009. Particle Loss Calculator – a new software tool for the assessment of the performance of aerosol inlet systems. Atmospheric Measurement Techniques 2, 479–494. https://doi.org/10.5194/amt-2-479-2009

Wang, C., Friedlander, S.K., Mädler, L., 2005. Nanoparticle aerosol science and technology: an overview. China Particuology 3, 243–254. https://doi.org/10.1016/S1672-2515(07)60196-1

Wang, H., 2011. Formation of nascent soot and other condensed-phase materials in flames. Proceedings of the Combustion Institute 33, 41–67. https://doi.org/10.1016/j.proci.2010.09.009

Wang, J., Hu, Z., Chen, Y., Chen, Z., Xu, S., 2013. Contamination characteristics and possible sources of PM10 and PM2.5 in different functional areas of Shanghai, China. Atmospheric Environment Complete, 221–229. https://doi.org/10.1016/j.atmosenv.2012.10.070

Weber, S., Uzu, G., Calas, A., Chevrier, F., Besombes, J.-L., Charron, A., Salameh, D., Ježek, I., Močnik, G., Jaffrezo, J.-L., 2018. An apportionment method for the oxidative potential of atmospheric particulate matter sources: application to a one-year study in Chamonix, France. Atmospheric Chemistry and Physics 18, 9617–9629. https://doi.org/10.5194/acp-18-9617-2018

Weichenthal, S., Lavigne, E., Evans, G., Pollitt, K., Burnett, R.T., 2016. Ambient PM2.5 and risk of emergency room visits for myocardial infarction: impact of regional PM2.5 oxidative potential: a case-crossover study. Environmental Health 15, 46. https://doi.org/10.1186/s12940-016-0129-9

Weijers, E.P., Schaap, M., Nguyen, L., Matthijsen, J., Denier van der Gon, H. a. C., ten Brink, H.M., Hoogerbrugge, R., 2011. Anthropogenic and natural constituents in particulate matter in the Netherlands. Atmospheric Chemistry and Physics 11, 2281–2294. https://doi.org/10.5194/acp-11-2281-2011

Whitby, K.T., Cantrell, B.K., 1976. Atmospheric aerosols - characteristics and measurements. Presented at the International Conference on Environmental Sensing and Assessment (ICESA), Insititute of Electrical and Electronic Engineers (IEEE), Las Vegas, NV.

Xiong, Q., Yu, H., Wang, R., Wei, J., Verma, V., 2017. Rethinking Dithiothreitol-Based Particulate Matter Oxidative Potential: Measuring Dithiothreitol Consumption versus Reactive Oxygen Species Generation. Environ. Sci. Technol. 51, 6507–6514. https://doi.org/10.1021/acs.est.7b01272

Xu, Z., Yao, M., 2011. Analysis of Culturable Bacterial and Fungal Aerosol Diversity Obtained Using Different Samplers and Culturing Methods. Aerosol Science and Technology 45, 1143–1153. https://doi.org/10.1080/02786826.2011.582195

Yang, A., Jedynska, A., Hellack, B., Kooter, I., Hoek, G., Brunekreef, B., Kuhlbusch, T.A.J., Cassee, F.R., Janssen, N.A.H., 2014. Measurement of the oxidative potential of PM2.5 and its constituents: The effect of extraction solvent and filter type. Atmospheric Environment 83, 35–42. https://doi.org/10.1016/j.atmosenv.2013.10.049

Yang, M., Howell, S.G., Zhuang, J., Huebert, B.J., 2009. Attribution of aerosol light absorption to black carbon, brown carbon, and dust in China – interpretations of atmospheric measurements during EAST-AIRE. Atmospheric Chemistry and Physics 9, 2035–2050. https://doi.org/10.5194/acp-9-2035-2009

Zhang, Z.-H., Hartner, E., Utinger, B., Gfeller, B., Paul, A., Sklorz, M., Czech, H., Yang, B.X., Su, X.Y., Jakobi, G., Orasche, J., Schnelle-Kreis, J., Jeong, S., Gröger, T., Pardo, M., Hohaus, T., Adam, T., Kiendler-Scharr, A., Rudich, Y., Zimmermann, R., Kalberer, M., 2021. Are reactive oxygen species (ROS) a suitable metric to predict toxicity of carbonaceous aerosol particles? (preprint). Aerosols/Laboratory Studies/Troposphere/Chemistry (chemical composition and reactions). https://doi.org/10.5194/acp-2021-666

Zhu, J., Chen, Y., Shang, J., Zhu, T., 2019. Effects of air/fuel ratio and ozone aging on physicochemical properties and oxidative potential of soot particles. Chemosphere 220, 883–891. https://doi.org/10.1016/j.chemosphere.2018.12.107

Acknowledgments

This project/work has received funding by the European Union's Horizon 2020 research and innovation program through the EUROCHAMP-2020 Infrastructure Activity under grant agreement No 730997. This project/work has received funding by MIUR through the PON project PIR_00015 "Per ACTRIS IT" whose recipient is INFN.

Candidate publications

Vernocchi, V., Brunoldi, M., Danelli, S. G., Parodi, F., Prati, P., Massabò, D., 2021. Characterization of the MISG soot generator with an atmospheric simulation chamber, Atmos. Meas. Tech. Discuss. [preprint], https://doi.org/10.5194/amt-2021-345, in review.

Danelli, S.G., Brunoldi, M., Massabò, D., Parodi, F., Vernocchi, V., Prati, P., 2021. Comparative characterization of the performance of bio-aerosol nebulizers in connection with atmospheric simulation chambers. Atmospheric Measurement Techniques 14, 4461–4470. https://doi.org/10.5194/amt-14-4461-2021.

Massabò, D., Altomari, A., Vernocchi, V., Prati, P., 2019. Two-wavelength thermal–optical determination of light-absorbing carbon in atmospheric aerosols. Atmos. Meas. Tech. 12, 3173–3182. https://doi.org/10.5194/amt-12-3173-2019.